Towards synthesis of a novel chelator for zirconium-89

The University of Adelaide

School of Physical Sciences

Department of Chemistry

Submitted in fulfillment of the degree

Master of Philosophy (Chemical Sci)

Presented by

Padraig Lorcan Fyfe *B. Sc. (Adv)*

Supervisor(s): Prof. Andrew Abell,

Dr. Jinxiang Yu & Dr. William Tieu

July 2019

Towards synthesis of a novel chelator for zirconium-89

Towards synthesis of a novel chelator for zirconium-89

Abstract

The radioisotope zirconium-89 has attracted attention in recent years as a candidate for clinical use in positron emission tomography (PET), due to its favourable properties. Zirconium-89 has a long half-life of 78.4 hours, rendering it suitable for use in conjugation to monoclonal antibodies (mAB), therefore giving potential applications in personalised medicines. It also has favourable emission characteristics, such as low energy positron emissions. Furthermore, it can be produced at low cost. These factors combine to support zirconium-89 as a cheap and high-resolution radioisotope for PET imaging. The most widely used chelator of zirconium-89, desferrioxamine-B (DFO), forms an insufficiently stable complex with zirconium-89 and undergoes some demetallation *in vivo*, leading to ablation of zirconium-89 to bone tissues. While recent efforts have focussed on developing novel chelators with more stable properties, ^{89}Zr-DFO is the only complex which has been examined in a clinical setting, and novel zirconium chelators have required either difficult synthetic procedures or are insufficiently soluble. It is hypothesised that the ideal chelator for zirconium-89 will: bind via hydroxamate groups in an octadentate manner; be bifunctional; and be simple to synthesise. The novel chelators **8** and **10** were designed based on these criteria and to examine the feasibility of a zirconium-89 chelator incorporating α-amino acids.

Synthesis of both compounds was attempted via a modular solution-phase peptide synthesis. The molecular subunits **4a** and **4b** were synthesised with overall yields of 21% and 48% respectively. However, during the latter stages of the synthesis intramolecular degradation of compounds **7** and **8** resulted in the formation of an alternative product: compound **8.1**. Analytical evidence obtained through ^{1}HNMR and HRMS suggested this occurred by a mechanism akin to aspartimide formation, as seen in solid-phase peptide synthesis. To examine this hypothesis, an alternative chelator **14** was designed, incorporating β-alanine in place of glycine. This compound

Towards synthesis of a novel chelator for zirconium-89

was successfully synthesised via solid-phase peptide synthesis and identified with HRMS and
^{1}HNMR.

As the monohydroxamate compound **8.1** was isolated as a pure product, it was of interest to assess its binding affinity for the radiometals zirconium-89 and gallium-68. The chelator was compared to DFO and subject to challenge assays to assess resistance to competitive metal ions, transchelation by EDTA, and non-specific protein binding. While it was evident that compound **8.1** was inferior to DFO as a chelator of zirconium-89 under all conditions, it did display significantly increased stability than previously reported for monohydroxamate chelators. However, both compound **8.1** and DFO displayed low stability when complexed with gallium-68.

Originality Statement

I certify that this work contains no material which has been accepted for the award of any other degree or diploma in my name, in any university or other tertiary institution and, to the best of my knowledge and belief, contains no material previously published or written by another person, except where due reference has been made in the text. In addition, I certify that no part of this work will, in the future, be used in a submission in my name, for any other degree or diploma in any university or other tertiary institution without the prior approval of the University of Adelaide and where applicable, any partner institution responsible for the joint-award of this degree.

I give permission for the digital version of my thesis to be made available on the web, via the University's digital research repository, the Library Search and also through web search engines, unless permission has been granted by the University to restrict access for a period of time.

Padraig Fyfe

21/02/2020

Acknowledgments

Reflecting on the time I have spent working on this project and writing this document, it is necessary to thank the kind and thoughtful people around me, without whom I would certainly not have managed the task.

Firstly, I would like to acknowledge my principal supervisor, Professor Andrew Abell, for inspiring my interest in chemical research and for guiding me expertly through this process. I have gained far greater confidence, precision and resilience through your tutelage and I am thankful for your approachability. I would also like to thank my co-supervisors Dr. William Tieu and Dr. Jinxiang Yu for their efforts. Will was the source of the project, and my main resource in undertaking it. I was lucky to be able to draw on his considerable expertise while undergoing my work. Aside from the academic support, Will has been particularly supportive of me throughout my project in a personal level as well. Jin, meanwhile, has provided crucial overwatch of the project when required.

Thank you also to my parents Deb and Philip, who have always supported me through my studies and provided me with motivation, drive, food, and much more. It is difficult to feign interest in such esoteric work as this, but both of you managed with aplomb for the best part of two years. I would not have been able to finish this without your influence.

I would also like to extend my thanks to the rest of the Abell group for their support, both academic and personal, throughout my time in their ranks – in particular, but not exclusively, Georgina, Aimee, Pat, Kathryn, Damien, Jun, Rouven, Victoria and Dion. I am beyond lucky to have had access to an extremely talented quorum of peers who have helped motivate me, provide advice and answer theoretical questions, but most importantly to lend their solidarity and friendship (and

Abbreviations

ACN: acetonitrile; **AcOH**: acetic acid; **Boc:** *tert*-butoxycarbonyl protecting group; **Boc:** tert-Butyloxycarbonyl; **BSA:** bovine serum albumin; **CAM:** cerium ammonium molybdate**DCM:** dichloromethane; **DIPEA:** *N-N*-Diisopropylethylamine; **DMF:** N-N-dimethylformamide; **EDTA:** ethylenediaminetetraacetic acid; **EtOAc:** ethyl acetate; **Fmoc:** fluorenylmethyloxycarbonyl protecting group; **HATU:** 1-[Bis(dimethylamino)methylene]-1H-1,2,3-triazolo[4,5-b]pyridinium 3-oxid hexafluorophosphate; **HPLC:** High Performance Liquid Chromatography; **HRMS:** High Resolution Mass Spectrometry; **IPA:** Isopropyl alcohol; **LRMS:** Low Resolution Mass Spectrometry; **MeOH:** methanol; **NMR:** Nuclear Magnetic Resonance; **OBn:** Benzyl ether; **PBS:** Phosphate buffered saline; **TFA:** trifluoroacetic acid; **THF:** tetrahydrofuran.

Contents

1   New approaches to Positron Emission Tomography: ⁸⁹Zr and ⁶⁸Ga

1.1   Background: Modern Approaches to the Detection of Cancer

The treatment of cancer is one of the predominant medical issues of the modern day. In 2017, an estimated 134,174 cases of cancer were diagnosed, and an estimated 47,753 deaths were recorded as being a result of cancer in Australia. This comprised 19% of the total disease burden in Australia and cost upward of $4.25b.[1] The risk of developing cancer increases substantially with increasing age and considering Australia's aging national population, this burden of disease is only likely to increase. Cancer Australia has collected data pertaining to the diagnosis of the top 5 most common variants of cancer in Australia, with these being breast cancer, colorectal cancer, lung cancer, prostate cancer and malignant melanoma.[2] Of these, the majority of cases of melanoma, breast cancer and prostate cancer were diagnosed during the early stages of cancer – at stage 1, indicating no metastasis; or stage 2, indicating limited metastasis into surrounding tissue.[3] These cancer types had 5-year relative survival rates amongst the highest at 88%, 90% and 95% respectively.[1] Colorectal cancer was diagnosed at stages 1 and 2 only slightly more than at stages 3 and 4 (indicating greater metastasis of tumours), and had a lower 5-year survival rate of around 69%. Lung cancer was most commonly diagnosed at stage 4, and had one of the poorest 5-year prognoses of any cancer at 14% for males and 19% for females, indicating that the swift detection of cancers is crucial in providing effective and suitable treatment for the disease.[1-2] While early detection is reliant on a diverse range of factors, the accessibility of resources for detection is of utmost importance: people living more remotely are not more likely to develop cancer than those in cities, but they are more likely to die as a result.[1] Therefore, the availability of robust, reliable and easily-accessible detection methods is crucial for reducing mortality.

Advancing knowledge of the mechanisms of tumour proliferation has led to changes in treatment methods. While DNA alkylating agents such as *cis*-platin are still in wide use,[4] newer treatments are intended to target tumours with ever-increasing specificity. The targeting of cancer treatment carries several advantages: firstly, tumours which are resistant to traditional means of treatment can be better controlled; and secondly, damage to surrounding, healthy tissue is minimised while damage to tumorous tissue is maximised. Central to targeted therapy is the discovery of genetic or biological differences between tumour cells and healthy cells.[5] Genetic differences can manifest in the over- or under-expression of proteins by tumourous cells, which allows more specific targeting of these tumours. Such proteins are known as *biomarkers*; some examples include the prostate-specific membrane antigen, which is highly expressed in prostate cancers,[6] and human epidermal growth factor receptor 2, highly expressed in some breast cancers.[7] Membrane-expressed biomarkers are of particular interest, as they can be targeted and inhibited with exogenous ligands. Inhibitors of these biomarkers can also be used to detect the extent and severity of cancers through medical imaging.

The imaging methods of positron emission tomography (PET) and single photon emission computed tomography (SPECT) are regularly used for these purposes. Both methods require the injection of a radioisotope, known as a radiotracer. This radiotracer is intended to preferentially localise within tumours, the location and size of which can then be elucidated by the detection of radioactive emissions from the body. Naturally, in PET, a positron-emitting radioisotope is injected into the subject, while SPECT uses gamma-emitters. After emission, a positron collides with an electron and is annihilated, causing the generation of two identical photons with 511 kEV energy, which subsequently travel in opposite directions.[8-9] The subject is surrounded by a photon sensor; this sensor will detect the incident photons and calculate their single point of origin. The calculations based on the measurement of hundreds of thousands of said emissions can be used to generate an image of the subject. The resolution of PET sensors, and therefore the images, is

affected by several factors. Firstly, the energy of the positron affects the distance it travels before it is annihilated, which affects the accuracy of images. Similarly, residual kinetic motion at annihilation (Fermi motion, or translational motion) causes the angle between the photons to deviate from the original angle of 180°.[10] Lastly, the specificity with which the radionuclide is localised affects image resolution; greater tumour-to-background ratios result in clearer images. The effect of Fermi motion is largely affected by the diameter of the detector, while the energy of the positron is inherent to the decay pathway of specific radionuclides.[10] Radionuclide localisation however is dependent on the method of targeting. Even though PET is generally far more expensive than SPECT, the resolution obtained using the former is significantly better,[8] and during PET the number of emissions in each location can be quantified, which is advantageous for assessing *in vivo* targeting of the radionuclide.[11]

A variety of positron-emitters are utilised in PET, including carbon-11, nitrogen-13, oxygen-15, and fluorine-18. Less commonly, metals such as gallium-68 or copper-64 are used.[8] The advantage of the above non-metallic radioisotopes is their ease of incorporation into biological molecules such as glucose (fluorine-18 is incorporated as 2-fluoro-2-deoxy-D-glucose, or FDG), as the increased energy demands of rapidly growing cancer cells ensure radiolabelled glucose will accumulate more rapidly in tumours than healthy cells.[8] Alternatively, metallic radioisotopes require chelation to be transported into cells. This does, however, present the opportunity to target the radionuclide more specifically to cancer cells and lower background signals.

With the exception of copper-64 ($t_{1/2}$ = 12 h), each of the aforementioned radionuclides has quite a short half-life – 2 minutes for oxygen-15, 10 minutes for nitrogen-13, 20 minutes for carbon-11, 68 minutes for gallium-68, and 110 minutes for fluorine-18. These short half-lives make urgency paramount in the use of these radioisotopes; they must be produced on the day of use, and the chemical reaction to incorporate them into some biologically relevant molecule must happen

rapidly. In order to produce high-resolution images, the further processes of transportation, injection, and imaging must occur within a limited time. The setup of local cyclotrons or generators to reduce transport time can reduce the losses associated with short-lived radioisotopes, but the capital investment required to purchase and maintain a cyclotron is substantial. But there is a more pressing issue with the use of radioisotopes with short half-lives: a lack of specificity. As was previously mentioned, these radioisotopes are incorporated into biologically relevant molecules, such as glucose or water. These molecules are ubiquitous in living systems, and while tumours accumulate them at a greater rate than healthy tissue, they also readily incorporate into healthy tissues. This leads to increased background signals and causes lower image resolution.[8]

Another clinically proven approach to cancer detection and treatment is the use of monoclonal antibodies, or mAB. mAB are large proteins with highly specific cellular targets, a feature which can prove beneficial to both detection and treatment by lowering background noise and increasing radiochemical delivery.[11] In medical imaging, the use of mAB results in higher resolution images due to greater accumulation of the biomarker in cancerous tissue; in treatment, it should result in less collateral damage to healthy tissue. A further benefit is greater consistency between diagnostics and therapy. Such an incorporated approach to medicine is known as *theranostics*, a portmanteau of therapeutic and diagnostic.[12] Targeted treatment can also aid the staging and identification of cancer subtypes; for instance, imaging using the HER2 inhibitor trastuzumab as a vector will not only indicate the extent of the tumour, but will also indicate whether a suspected cancer is susceptible to treatment through that same pathway, permitting greater personalisation of treatment. The attachment of a radioisotope to mAB is known as conjugation, which can occur via substitution for non-metals or chelation for metals, as seen in Figure 1.
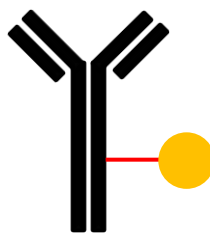
Figure 1: Diagram of a monoclonal antibody (mAB, black) with a conjugated radioisotope (yellow) connected by a linker (red).[7]

This approach, however, requires a departure from the use of short-lived isotopes. mAB have a lengthy period of circulation after injection of around 2-4 days which renders them unsuitable for use with short-lived radioisotopes such as gallium-68 or fluorine-18.[13] Even copper-64, with a half-life of 12 hours, is not ideal for this purpose. The use of alternative positron emitters with longer half-lives could therefore reduce waste during production and transportation and improve both resolution and the cost of PET procedures. Iodine-124 has been studied in this context due to its lengthy half-life of 4.18 days; however [124]I-mAB systems are vulnerable to dehalogenation *in vivo*, causing retention of iodine-124 in the blood.[14] Another positron emitter, zirconium-89, has been raised as a potential candidate for imaging procedures.

1.2   Zirconium-89

Zirconium-89 is a positron-emitting, neutron-deficient isotope of zirconium, with a half-life of 3.3 days.[15] Zirconium-89 decays firstly into the metastable [89m]Y by positron emission (22.7%) and electron capture (77.3%),[15] with the positron emission occurring at a relatively low average energy of 395 keV, and a maximum of 897 keV (Figure 2).[7] The annihilation of this positron results in the emission of two opposing gamma rays with 511 keV of energy.[15] The metastable [89m]Y further decays by a single gamma emission of 909 keV into stable yttrium-89. The gap between the 511 keV photon and the 909 keV gamma ray has little to no spectral overlap, giving two discrete peaks in the emission spectra.
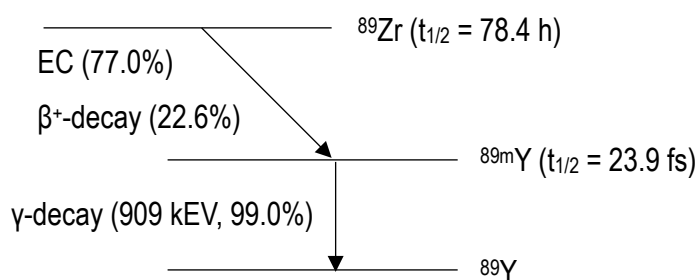

^{89}Zr (t$_{1/2}$ = 78.4 h)

EC (77.0%)

β$^+$-decay (22.6%)

^{89m}Y (t$_{1/2}$ = 23.9 fs)

γ-decay (909 kEV, 99.0%)

^{89}Y

Figure 2: Decay pathway of zirconium-89 to the stable ^{89}Y via the metastable ^{89m}Y.[16]

There is thus potential for zirconium-89 to carve out a therapeutic niche. The most attractive attribute of zirconium-89 is its extended half-life, which is well suited to conjugation to monoclonal antibodies, as these require a circulation time of approximately 2 - 4 days to facilitate sufficient uptake into cells for high-resolution imaging to occur.[15] As stated previously, the use of monoclonal antibodies as a targeting mechanism improves the resolution of images compared to biologically ubiquitous molecules such as glucose. It further provides a more accurate model for antibody-based radiotherapy, which is becoming increasingly more common; a number of monoclonal antibody-based radiotherapies utilising long-lived radionuclides such as lutetium-177 (half-life 6.7 days) to treat late-stage metastatic tumours have been successful in clinical trials.[17] Such a system benefits from an antibody-based method of imaging as this ensures consistency between imaging and treatment. Furthermore, the low average energy of the positron emitted by

zirconium-89 means the translational energy of the isotope after annihilation is low, further increasing the resolution of the images.[16, 18] To this end, there has been some interest in zirconium-89 since the 1980s.[19]

The standard production of high-purity zirconium-89 for therapeutic use was first reported by Meijs *et al.* in 1994,[20] and developed further by Holland *et al.* in 2009.[16] Yttrium-89 foil, naturally abundant as a single isotope, is placed into a shuttle and bombarded by a proton beam, converting it to zirconium-89 by the $^{89}Y(p,n)^{89}Zr$ transmutation reaction; controlling the energy of this bombardment is crucial so as not to promote the formation of zirconium-88. The threshold for formation of zirconium-89 occurs at 4.59 MeV, and the maximum average cross-section occurs at 13.80 MeV; the threshold for production of zirconium-88 is 13.30 MeV, suggesting the ideal proton energy is ~13 MeV.[16] Following bombardment, the target is cooled while the metastable ^{89m}Zr decays before dissolution of the foil in 6M hydrochloric acid. To separate zirconium-89 from impurities (particularly yttrium), the acidic solution is passed through a hydroxamate resin, which preferentially binds zirconium over yttrium. Washing this resin with hydrochloric acid removes the yttrium, after which zirconium-89 can be liberated from the resin by transchelation with 1M oxalic acid. This method yields zirconium-89 at a high radiochemical yield (>99.9%) as zirconium oxalate.[16] Oxalic acid is highly toxic and therefore must be removed before any radiopharmaceutical production; this is achieved typically by elution through an anion exchange resin flushed with water, and subsequent washing of the resin with 1M HCl will yield $^{89}ZrCl_4$.[16] Recent work has suggested that the published oxalic acid concentration can be further reduced without compromising the yield of zirconium-89.[21] The automated production of radiopure zirconium-89 was published by Lin *et al.* which improves safety and consistency of production.[22]

As this production method occurs with a relatively low-energy proton beam, it is possible to produce zirconium-89 with only a small medical cyclotron, reducing the costs of production.[16] The

advantages of zirconium-89-based imaging are therefore numerous compared to other long-lived radioisotopes: it can be produced relatively cheaply; it has a longer half-life than copper-64; and it has the potential to produce high-resolution images through precise targeting and its low-energy positron emissions. However, there are several challenges to overcome preceding its use in PET. The abundance of gamma radiation is of some concern; as previously mentioned, the decay of zirconium-89 to yttrium-89 occurs almost entirely by the emission of a 909keV gamma ray. This is a high energy emission which has a half-value of 10mm in lead and necessitates greater shielding than other isotopes, and could feasibly lead to mutation *in vivo*.[7] Furthermore, the behaviour of free zirconium-89 ions *in vivo* means that highly stable chelation is necessary for its use in radiopharmaceuticals; this will be addressed below.

Zirconium is a group IV metal which primarily exists in the Zr^{4+} form in solution, which has an ionic radius of 0.84 Å.[18] This ion is reduced at -1.4 – 1.5 V, which exceeds the reduction potential present in biological systems.[11] Zr^{4+} is a 'hard' Lewis acid which forms stable bonds with anionic oxygen or nitrogen donors, coordinating up to 8 ligands.
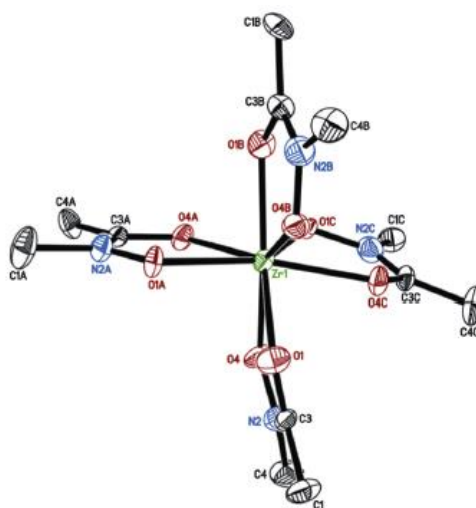

Figure 3: X-ray crystallographic structure of zirconium(N-methyl acetohydroxamic acid)$_4$ elucidated by Guérard et al.[23]The central zirconium ion (green) is coordinated by 4 hydroxamic acid subunits via the oxygen anions (red).

Guerard *et al*. have reported both computational and crystallographic structures for Zr^{4+} complexed to four free hydroxamic acid units (Figure 3). The average bond lengths were found to differ between the two structures: average bond lengths of 2.204 Å and 2.183 Å for the Zr-O-C and Zr-O-N bonds respectively were determined in the X-ray structure; meanwhile the calculated structure showed more disparate bond lengths of 2.324 Å and 2.199 Å respectively.[23] The difference between the two was rationalised as the existence of a second conformer, as the C-O and N-O groups are able to exchange positions. This study provides some insight into the necessary size and organisation of chelators intended for zirconium.

While zirconium is present in many animal tissues naturally in low quantities, little is known about the biological effects at these quantities.[24] Clearance of zirconium from the body greatly depends on the complex involved; while some complexes are rapidly cleared by the renal or hepatobiliary systems, some zirconium salts will precipitate and accumulate in the liver or spleen.[18] Free Zr^{4+} ions show a tendency to migrate to calcified tissue in the bones *in vivo*, which is problematic in the clinical use of zirconium-89; the incorporation of a long-lasting, gamma-emitting radioisotope into radiosensitive tissue adjoining the bone marrow could prove dangerous. Therefore, the use of chelators which form stable complexes at very low concentrations is paramount.

1.3   Chelation of zirconium-89

1.3.1   Desferrioxamine-B

The most widely studied and used chelator of zirconium-89 is presently the natural product desferrioxamine-B, also known as deferoxamine, desferal or DFO. DFO is a natural product that was first isolated from *Streptomyces pilosus* in the late 1950s,[25] with its structure elucidated in 1962 (Figure 4).[26] A succession of 3 hydroxamate groups are separated by a peptide-like backbone, providing 6 oxygen atoms for chelation to a donor. DFO is a type of natural product known as a "*siderophore*", classified as such due to its high affinity for Fe^{3+} compared to Fe^{2+}.[26] It is thought that microorganisms utilise DFO to shuttle the largely insoluble Fe(III) into cells in oxygen-rich environments where this state predominates. While DFO also displays strong affinity for Al^{3+} (K_f = 21.4), this is significantly lower than that for Fe^{3+} (K_f = 30.6).[26]
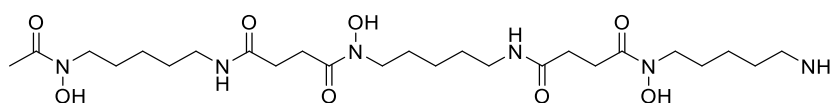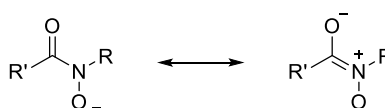

Figure 4: Desferrioxamine-B

Figure 5: Mesomerisation of the hydroxamate group.[26]

Hydroxamate groups have two resonance contributors (Figure 5), notably one in which the carbonyl oxygen becomes negatively charged, facilitating binding to donor atoms.[26] At neutral pH values, the dissociation of Fe^{3+} from DFO is extremely slow. As the redox potential of NADH exceeds that of hydroxamate-based chelators, the release of Fe(III) from DFO is suspected to generally proceed by reduction to Fe(II), which forms a substantially less stable ligand-donor complex with DFO (Figure 6).[26]
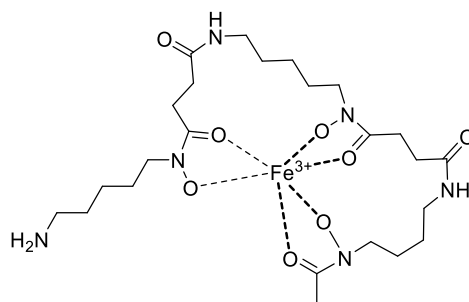
Figure 6: Desferrioxamine-B complexed with Fe(III) via hexadentate coordination.[18]

While another category of siderophores – the catecholates - have greater affinity for Fe(III), hydroxamate-based siderophores have a greater stability at lower pH than the catecholates.[26] The complexation of a catecholate to a donor requires the displacement of 6 protons, compared to 3 protons for the hydroxamate, increasing the influence of pH on catecholates.[26] This stability also renders natural hydroxamate-based siderophores more useful clinically.[26] Based on its particular affinity for Fe(III), DFO has been approved as a drug for the treatment of acute iron toxicity, marketed as Desferal.[15] Enterobactin (Figure 7), the most potent natural catecholate siderophore, is unsuitable for *in vivo* use due to rapid hydrolysis at physiological pH; however, more stable derivatives of it are widespread in clinical use in conjunction with gallium-68.[27]
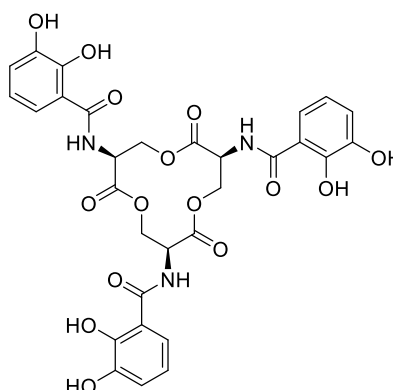
Figure 7: Enterobactin, a catecholate siderophore isolated from Salmonella typhimurium *and the siderophore with the greatest known affinity for Fe(III).[26]*

DFO has also been studied extensively as a chelator for a variety of radiopharmaceuticals, including gallium-68[28-31], and indium-111.[11] The remarkable stability of the Zr-DFO complex was first reported in 1992 by Meijs *et al.* based on the affinity between Zr^{4+} and monohydroxamate ligands.[19, 32] This landmark work proved that zirconium and DFO form a highly stable 1:1 complex,

undergoing only minor demetallation in human serum. The first *in vivo* assessment of the Zr-DFO

complex compared it with zirconium-89 citrate, chloride and oxalate salts. The use of the latter

three salts corresponded with increased uptake of zirconium-89 in the bones of subjects, however

Zr-DFO largely remained a stable complex and exhibited rapid clearance from the body.[33]

However, migration of zirconium-89 to bones is of great concern as it results in a long-lived,

gamma-emitting isotope being accumulated near the sensitive bone marrow tissue. More recent

research has elucidated the mechanism for Zr-DFO demetallation, with molecular modelling of

the complex indicating the simultaneous binding of two H_2O molecules in the remaining

coordination sites for zirconium-89 in a cis-conformation.[34] It is thought that these water

molecules may contribute to demetallation of the Zr-DFO complex by increasing complex lability.

As a result, *in vitro* assessments of chelators focus on conditions which might induce complex

dissociation: transchelation by other compounds, competition by other metal ions, and pH-

induced effects. A further useful property of DFO is its primary amine group, which facilitates

binding to mAB.[7]

The terminal amine of DFO allows for simple conjugation to antibodies or other targeting

molecules while still forming stable complexes with chelated metals, a property known as

bifunctionality.[19] A series of papers by Meijs *et al*. reported the first Zr-DFO-protein conjugates;

while *in vivo* stability was promising, accumulation of zirconium-89 in the kidneys, livers and bones

of subjects was noted.[35-36] While at first protein degradation was expected to be responsible for

this accumulation, subsequent works found the SATA-SMCC linker used by the researchers

(Figure 8, **1**) was insufficiently stable at physiological pH.[37] This led to the development of

alternative linkers, the best of which was an N-succinyl linker developed by Verel *et al* (Figure 8,

2).[13] This linker improved on complex stability and has since found wide use.[34, 38-39] However it

does have shortfalls: conjugation of DFO to an antibody first requires chelation of Fe(III), which

must then be removed by EDTA transchelation, representing challenging and redundant synthetic

steps; further, while improvements in stability were observed compared to SATA-SMCC, zirconium-89 accumulation was still seen in subjects.[14] The improvements observed did show that some association occurs between a linker and zirconium-89, prompting the search for improved linkers.
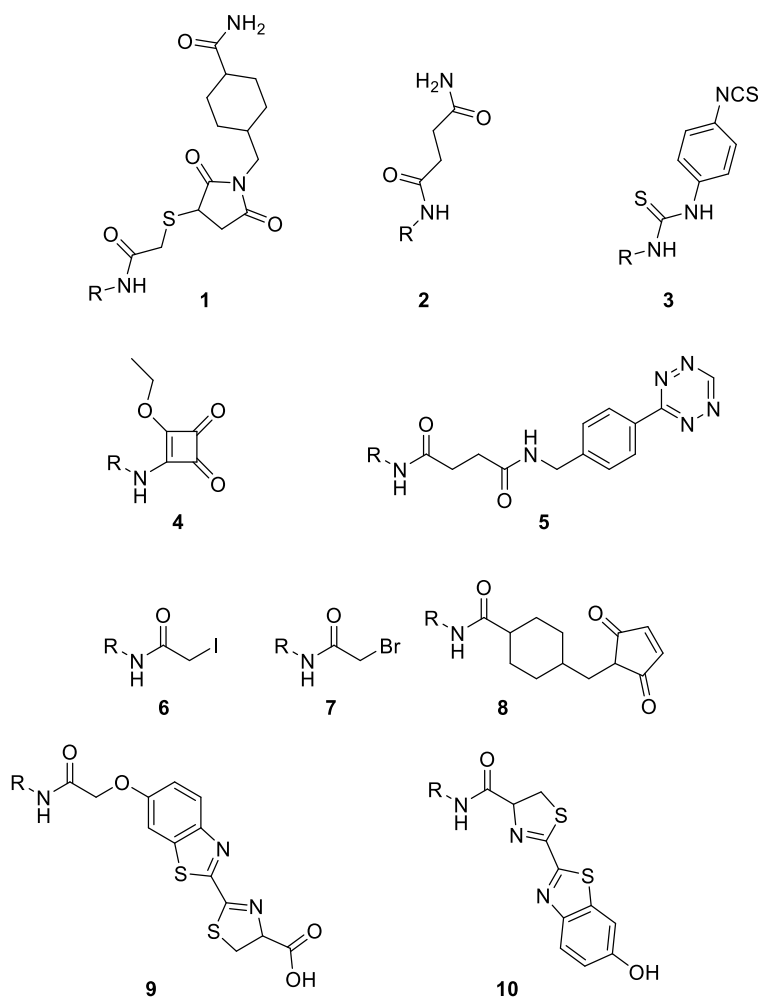

Figure 8: [89]*Zr-DFO linker moieties: SATA-SMCC (**1**); N-succinyl (**2**); p-isothiocyanatobenzyl (**3**); squaramide (**4**), tetrazine (**5**), iodoacetamido- (**6**), bromoacetamido- (**7**), (N-maleimidomethyl)-cyclohexane (**8**), 2-cyanobenzothiazole (**9**, **10**). R =* [89]*Zr-DFO.*

In the quest for a simpler radiolabelling procedure a new linker was pioneered - a *p*-isothiocyanatobenzyl group which could react with lysine residues (Figure 8, **3**). The conservation of stability between this and the N-succinyl linker, combined with the simpler synthesis of the former, led to the adoption of the *p*-isothiocyanatobenzyl linker as a standard.[40-41] There is, however, some evidence that this linker strategy leads to aggregation of the mAB during the

conjugation step.[41] *In vivo* assessments of the [89]Zr-DFO-*p*-isothiocyanatobenzyl-mAB system have shown similarity to the widely used gamma emitter ^{99m}Tc,[42] and advantages over the gamma emitter [125]I.[43] Exploration of alternative linker strategies has continued to address the persistent issue of degradation and uptake of zirconium-89 into bones.

The development of novel linker strategies for [89]Zr-DFO has focussed on a need to increase stability and also ease of synthesis. An ethyl squaramide ester linker (Figure 8, **4**) for DFO showed promising increases in tumour-to-bone uptake ratios compared to the *p*-isothiocyanatobenzyl linker.[44] It was hypothesised that greater stability was imbued by association of the dione group of the linker with the zirconium ion; the oxygen donor character of the linker binds readily with zirconium-89, increasing the coordination of the complex to an octadentate system. The N-succinyl linker was modified with the addition of a tetrazine group (Figure 8, **5**) permitting conjugation to modified antibodies via "click" chemistry.[45] This system undergoes rapid uptake in bone tissues of around 15% ID/g (injected dose per gram), suggesting that it is associated weakly with the [89]Zr[4+] ion. Tianinow *et al.* reported a set of 3 novel linkers to compare to the isothiocyanatobenzyl and N-succinyl groups: iodoacetamido-, bromoacetamido-, and maleimidocyclohexanyl moieties (Figure 8, **6** - **8**), capable of reacting with cysteine residues in mAB.[46] Of these, the maleimidocyclohexanyl linker showed the greatest uptake into tumours, lowest incubation time, and also a relatively high uptake into bone (10% ID/g). The acetamido-linkers exhibited similar biodistribution to the maleimidocyclohexanyl linker with lower tumour uptake. The 2-cyanobenzothiazole linkers (Figure 8, **9** - **10**) developed by Gao *et al* for coupling to cysteine residues showed good resistance to transchelation and reasonable stability in serum, but did not compare this novel linker to an established system to show relative stability.[47]

Only a small number of clinical trials thus far have focussed on the performance of [89]Zr-DFO-mAB systems.[18] The first reported study involved the injection of twenty late-stage cancer patients

with a zirconium-DFO-N-succinyl-antibody conjugate - in this case, the CD44v6-specific antibody U36.[48] The zirconium-conjugate system showed good sensitivity, no conjugate accumulation seen outside tumourous tissues and no adverse effects connected to the Zr-DFO system. Another pilot study in 2006 compared the biodistributions of ^{89}Zr-DFO-Zevalin and ^{90}Y-Zevalin, finding that tumour uptakes were similar for both conjugates.[49] In a separate study, seven patients with advanced lung cancer were injected with a Zr-DFO-N-succinyl-bevacizumab, a mAB which targets the vascular endothelial growth factor receptor.[50] A 4-fold increase in uptake at the tumours was observed compared to other tissues such as the lung, fat and muscles. However, high blood activity was observed during the 4-day scan, indicating that clearance of this system was low. ^{89}Zr-DFO systems have further been clinically investigated in the detection of prostate cancer (conjugated to prostate-specific membrane antigen J591)[51], rheumatoid arthritis and multiple sclerosis (conjugated to the anti-CD20 antibody rixumitab)[52-53], and HER2-positive breast cancer (with trastuzumab)[54], showing promising resolution and similar distributions to the unconjugated mABs.

Current evidence indicates that ^{89}Zr-DFO undergoes significant demetallation *in vivo*, with uptakes in bone tissues of around 10% ID/g regardless of the linker used. While ^{89}Zr-DFO is rapidly cleared if the linker is cleaved, the lengthy circulation times of mAB all but ensure that ^{89}Zr-DFO-mAB conjugates will experience demetallation to some degree. The development of new linker strategies, as discussed above, has not led to substantial improvement. The development of alternative chelators has therefore been of great interest in order to improve on the characteristics of DFO.[55]

1.3.2   Beyond DFO: novel chelator development

Based on the success and limitations of DFO, routes to novel zirconium chelators have been varied. Focus has been placed on the use of alternative functional groups for binding, the increase in denticity to octadentate, and increasing preorganisation through the use of a macrocyclic chelator, or a combination of the three factors.

1.3.2.1 Hexadentate chelators

Due to the ready availability of DFO and its known limitations, little work has focussed on producing alternative hexadentate chelators for zirconium-89. The sole published development of a non-DFO, hexadentate chelator for zirconium-89 is that of YM103 (Figure 9), which displayed inferior characteristics compared to DFO.[56]
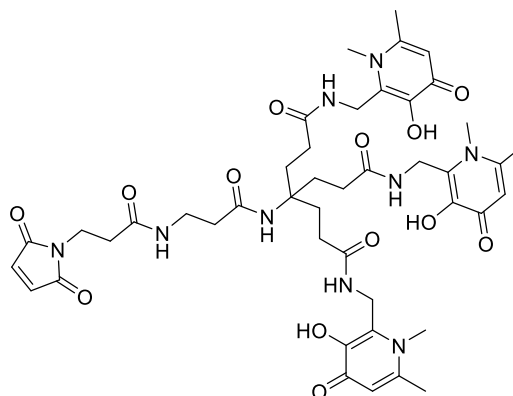

Figure 9: The hexadentate zirconium chelator YM103.[56]

1.3.2.2 Octadentate chelators

Based on the observation that Zr^{4+} coordinates with 2 H_2O molecules while bound by DFO, and the subsequent instability of the system *in vivo*, attempts have been made to improve the binding stability of the Zr-DFO complex by incorporating a fourth binding moiety to increase the coordination of the complex.
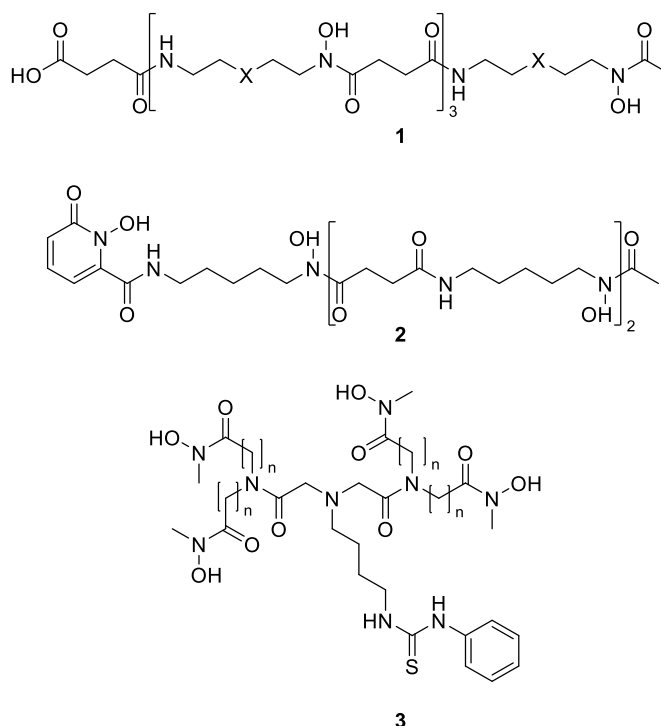
Figure 10: Linear octadentate chelators of ^{89}*Zr: DFO* (**1**, X = CH$_2$),*[57] *oxo-DFO* (**1**, X = O),*[58-59] *DFO-HOPO (**2**),*[60] *chelators developed by Rousseau* et al. *(**3**, n = 1,2).*[61]

Incorporation of a fourth hydroxamate into DFO resulted in the promising DFO* ligand (Figure 10, **1**) developed by Patra *et al.* with a carboxylic acid terminus also incorporated for conjugation.[57] This compound displayed superior stability to ^{89}Zr-DFO, resisting transchelation by DFO even at 3000-fold concentration. Comparison of the trastuzumab conjugates of DFO and DFO* found use of the DFO* conjugate caused equivalent tumour uptake but lower zirconium-89 levels in organs and bones.[62] DFO* can be prelabelled with zirconium-89 before mAB conjugation, while DFO-mAB conjugates had to be prepared before radiolabelling. This suggests the stability of ^{89}Zr-DFO-mAB conjugates depends on coordination between linker molecules and ^{89}Zr. DFO* exhibited very limited solubility in water; to allay this, modified versions containing ether groups have been synthesised.[58-59] Conjugation of this oxo-DFO* compound has not been reported, with its activity *in vivo* remaining unknown.

The affinity of zirconium-89 with DFO modified with a 1-hydroxy-2-pyridone group inserted at the *N*-terminus has been reported.[60] This molecule, known as DFO-HOPO (Figure 10, **2**), has good

affinity for zirconium-89 and the complex displays improved *in vitro* stability and rapid clearance *in vivo* even compared to Zr-DFO.[63] However, no bifunctional variant of this chelator has been reported thus far, which has prevented proper assessment of *in vivo* stability. In contrast, the tripodal tetrahydroxamates reported by Rosseau *et al.* (Figure 10, **3**) underwent significant demetallation in comparison to their DFO-conjugated counterparts, with the effect of steric hindrance marked by the greater affinity of the longer-armed variant.[61]
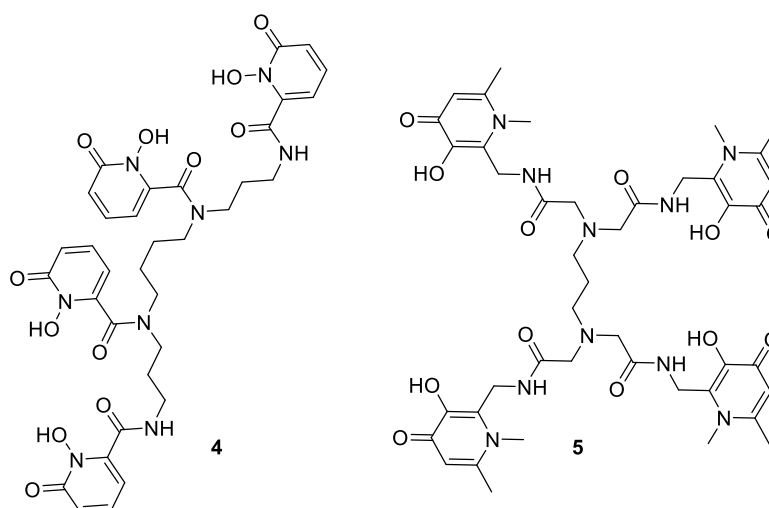

*Figure 11: Linear hydroxypyridinone chelators of ⁸⁹Zr: 3,4,3-(LI-1,2-HOPO) (**4**)[64] and THPN (**5**).[65]*

Two novel octadentate, hydroxypyridinone-based chelators of zirconium have shown extremely promising results in challenge assays. 3,4,3-(LI-1,2-HOPO) (Figure 11, **3**) shows remarkable *in vitro* stability when complexed with ⁸⁹Zr, outperforming DFO in the presence of a library of biologically relevant metal ions and at lowered pH; a low bone tissue uptake was seen in *in vivo* experiments.[64] The ⁸⁹Zr-3,4,3-(LI-1,2-HOPO) complex performs well while conjugated to trastuzumab, again displaying a much lower bone uptake than the respective DFO conjugate.[66] However the synthesis of this chelator is challenging. The hydroxypyridinone zirconium chelator THPN (Figure 11, **4**) displays rapid radiochemical complexation in excellent yield, and is resistant to transchelation and low pH. However, THPN has not yet been assessed in a conjugated system, meaning *in vivo* demetallation across a 7-day period remains yet unknown.[65]

1.3.2.3 Macrocyclic chelators

Several studies have focussed on synthesising zirconium chelators incorporating macrocyclic structures. While these are more challenging to synthesise than linear chelators, the increased organisation of the complexes can lead to more stable complexes.
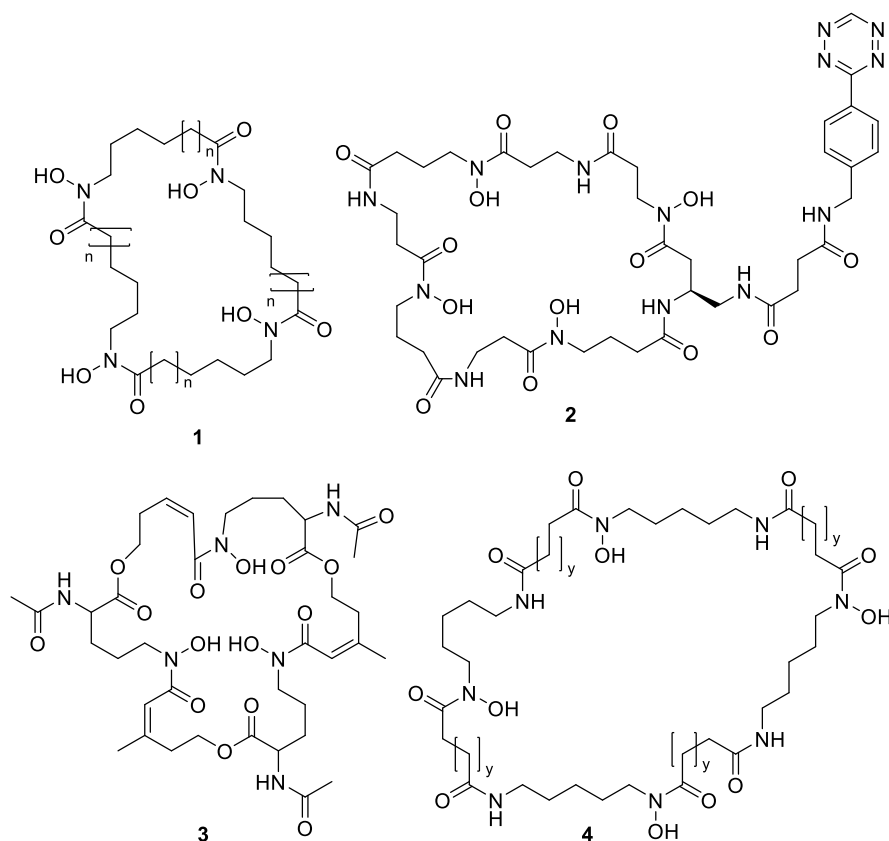

Figure 12: Macrocyclic chelators of [89]Zr: library developed by Guérard et al.[67] (1, n = 1, 2, 3), CTH36 (2),[68] triacetylfusarine-C (3), DFOT (4, y = 1) and PPDFOT (4, y = 2).[69]

A set of linear and macrocyclic peptides of 28, 32 and 36 molecules each were rationally designed by Guérard *et al.* (Figure 12, 1).[67] Both the 32 and 36-molecule systems displayed favourable properties, and the 36-member macrocycle displayed superior resistance to transchelation when compared to Zr-DFO. CTH36 (Figure 12, 2) is more resistant than DFO to transchelation *in vitro* and was conjugated efficiently; however no *in vivo* data was reported.[68] The modified siderophore triacetylfusarine-C (Figure 12, 3) forms more stable complexes with zirconium-89 than DFO and shows substantial resistance to transchelation by both EDTA and DFO.[70] No bone uptake was reported during original biodistribution studies. However, the molecule lacks a bifunctional handle

19

and must be radiolabelled at high temperatures.[71] A metal-templated synthesis has also been used to develop macrocyclic structural variants of DFO: DFOT and PPDFOT (Figure 12).[69] Both macrocycles were resistant to transchelation by EDTA; the added molecular length did not result in a reduction in efficacy.[67]

More recently, tetraazamacrocyclic chelators have been revisited as potential chelators for zirconium-89. Tetraazamacrocycles are commonly used in conjunction with other radiometals in therapy and diagnosis, such as indium-111, yttrium-90, copper-64, gallium-68 and lutetium-177; the most well-known chelator in this class is DOTA (Figure 13).[72] DOTA and its derivatives DOTP and DOTAM have shown superior *in vitro* characteristics to DFO, with DOTA displaying superior *in vivo* characteristics; however these chelators require radiolabelling in specific conditions (with $ZrCl_4$ rather than $Zr(ox)_2$, and at 80° C).[73] It is hypothesised that the carboxylate pendant arms present on DOTA bind more favourably to zirconium(IV) than the amino and phosphate groups in DOTAM and DOTP respectively. DOTA, however, is not a bifunctional chelator, a property which makes it unsuitable for use with mAB; several bifunctional variants of DOTA can be purchased (as in Figure 13),[72] but the stability of these chelators complexed with zirconium-89 has yet to be assessed. The bifunctional, tetraazomacrocyclic chelator shown in Figure 13 (**9**) contains hydroxamate groups as its pendant arms.[74] However, DFT calculations revealed that the nitrogen donors did not interact with zirconium-89 in chelation, and the resultant hexadentate chelation led to greater demetallation *in vivo* than seen with DFO, leading to 18.9% ID/g bone uptake.

Hydroxypyridinones such as BPDETLysH22-2,3-HOPO (Figure 14), have been widely used to chelate other radiometals such as gallium-68. The [89]Zr-BPDETLysH22-2,3-HOPO complex showed poor stability in serum, but *in vivo* showed similar biodistribution to [89]Zr-DFO when both chelators were conjugated to trastuzumab.[75]
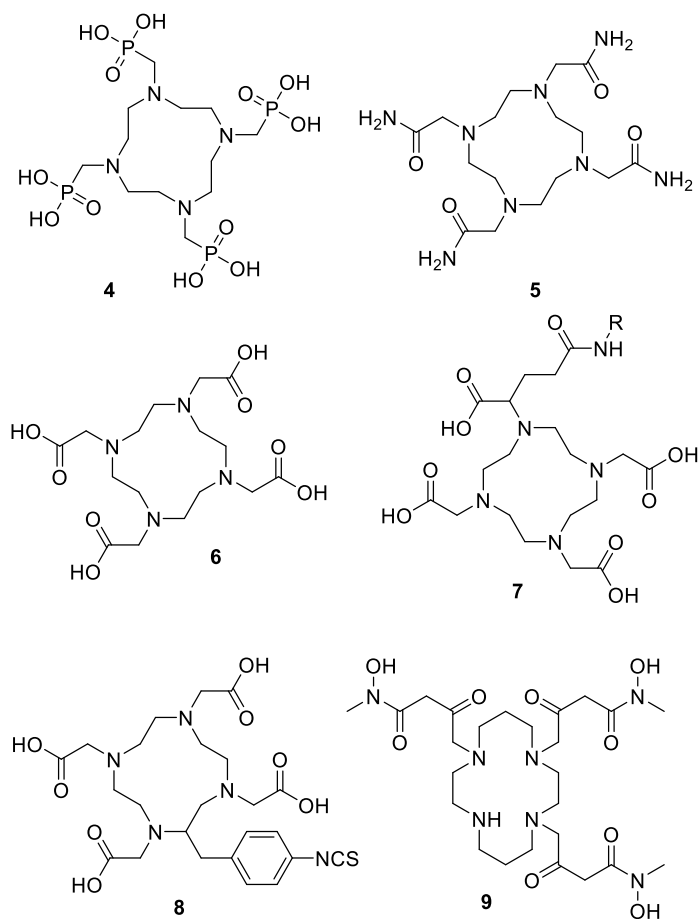
*Figure 13: Tetraazomacrocyclic chelators of zirconium-89; DOTP (**4**), DOTAM (**5**), DOTA (**6**), DOTA-GA (**7**), p-SCN-Bn-DOTA (**8**), L5 (**9**).*[74]
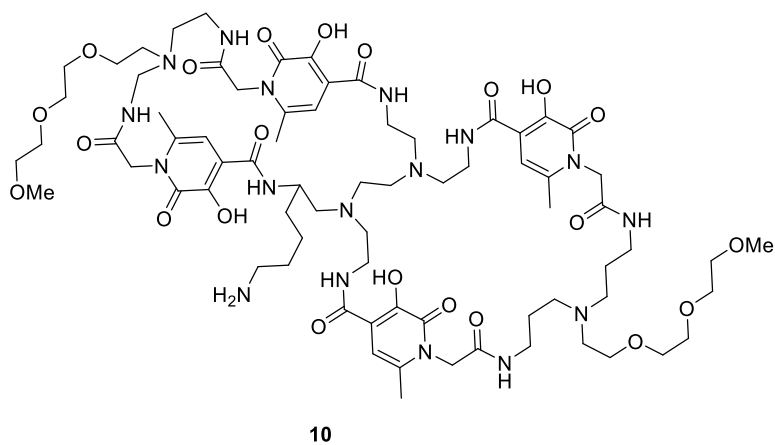

*Figure 14: BPDETLysH22-2,3-HOPO (**10**)*[75]

1.4 Gallium-68

Gallium-68 is used widely as a positron-emitter for PET imaging. It has a short half-life of around 68 minutes, is very simple to produce with a ^{68}Ge/^{68}Ga generator, and is one of few short-lived radioisotopes that can be produced in this manner.[27] Germanium-68 has a long half-life (271 d) making these generators long-lasting and relatively safe.[9] These generators can be stored in hospitals to minimise transportation time, and with no cyclotron involved they require little capital investment. Gallium-68 decays by 89% positron emission to the stable ^{67}Zn; however, the positrons have a substantially higher energy than zirconium-89, averaging 1899 keV.[76] NETSPOT, a ^{68}Ga somatostatin for diagnostic use, was approved in June 2016.[77]

Generally, gallium exists as Ga(III), and between pH 3 and pH 7 forms insoluble Ga(OH)$_3$ (Figure 15); radiolabelling can occur within this range depending on the chelator used.[9] Gallium(III) has an ionic radius of 0.62 Å, and coordinates in a similar fashion to Fe(III), with a preference for hexadentate chelation and oxygen donors.[78] Similar to Zr(IV), catechol and hydroxamate ligands form particularly stable bonds with Ga(III).
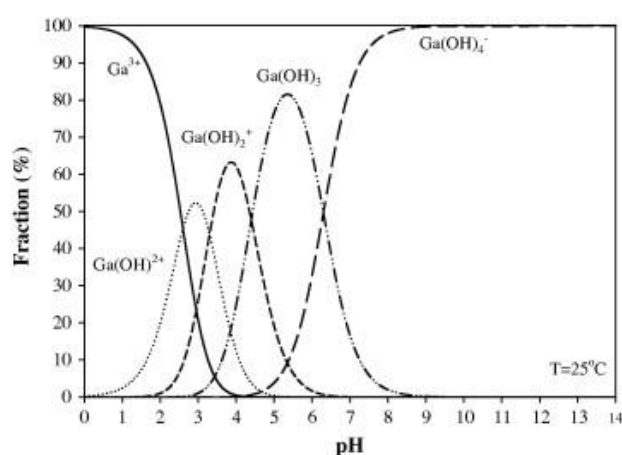

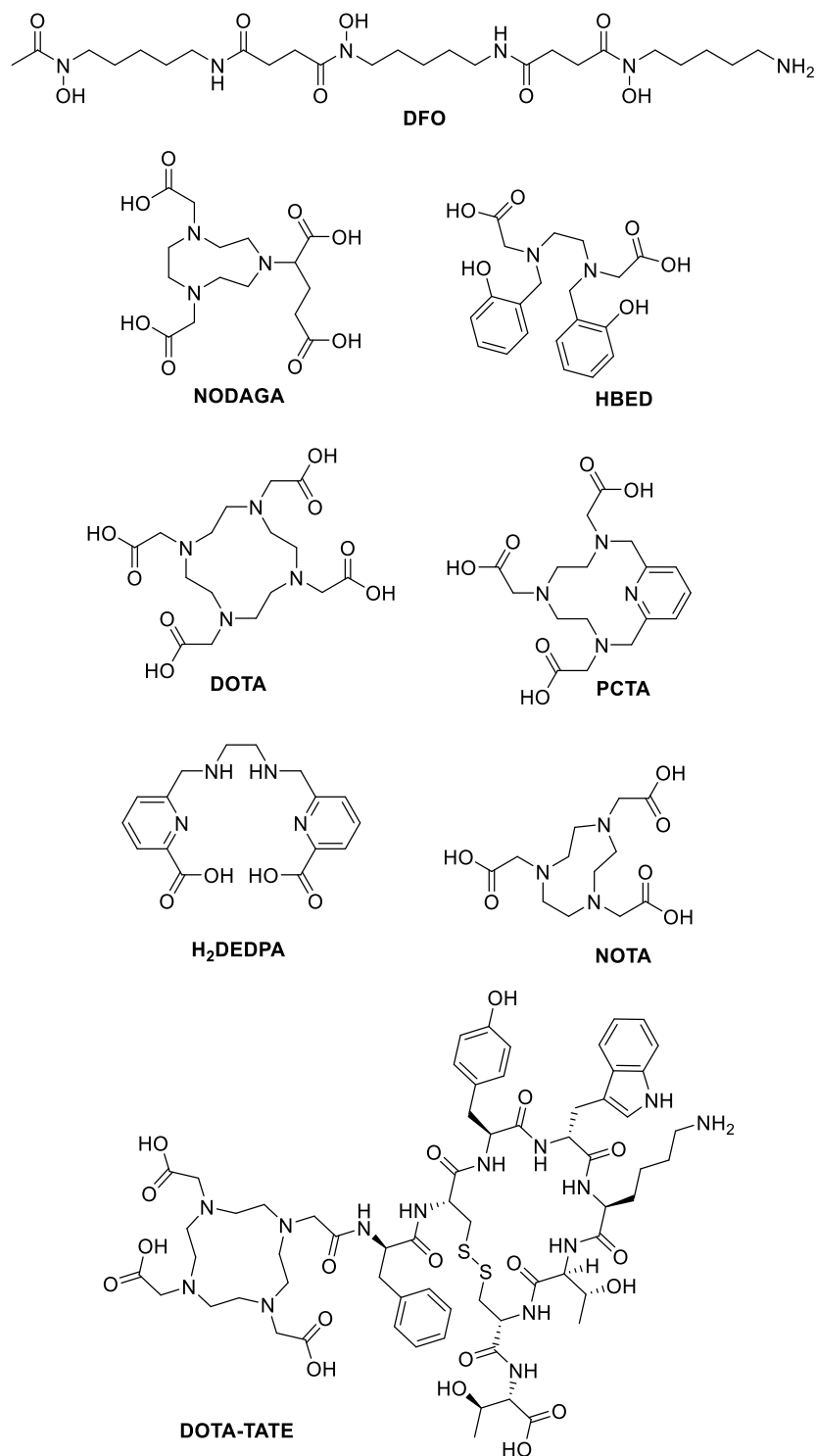Figure 15: Speciation of Ga^{3+} at 25 °C.[79]

Figure 16: Clinically used chelators of ^{68}Ga.[9, 78]

Gallium-68 has been studied with a variety of chelation strategies and in conjunction with a range of small molecules (Figure 16). DOTA and its derivatives are commonly used and can be labelled with gallium-68 at high temperatures (37 - 90° C).[72] The smaller NOTA has a stronger affinity for gallium-68, but the extra charge on the Ga-DOTA complex gives it more favourable behaviour.

Both these macrocycles bind gallium-68 due to its small atomic radius.[80] The FDA-approved ^{68}Ga-containing therapeutic NETSPOT binds gallium-68 with a DOTA-TATE group. H2DEDPA has also shown promising results *in vivo* and *in vitro* in use with gallium-68,[81-82] with good resistance to transchelation and rapid radiolabelling. HBED shows promising binding kinetics but are rarely used clinically. PCTA is a recently developed chelator which shows more promising labelling and stability attributes than DOTA.[72] As the half-life of ^{68}Ga is not suited to conjugation with mAB, it is more widely used with small peptide-based molecules for targeting receptors.[80]

As noted above, there is some crossover between chelators used for zirconium-89 and gallium-68: both are hard acids which bind preferentially to oxygen or nitrogen donors. Triacetylfusarine-C and desferrioxamine-E form the most stable gallium-68 complexes in serum and in the presence of competing chelators.[29-30] Due to the rapid decomposition of gallium-68 into the stable zinc-67, there is little risk associated with its release in the body; there is therefore potential to develop chelators with improved binding potential for both zirconium-89 and gallium-68.

1.5   Overview and project aims

DFO is a highly effective chelator of zirconium-89 that has been used with some success in clinical trials, yet further improvements in complex stability would be desirable. No zirconium-89-based therapeutic has yet been approved for medical use, and the consensus is that ^{89}Zr-DFO is kinetically unstable *in vivo.*[11] This instability is thought to be due to molecular strain caused by DFO-metal complexation, and simultaneous coordination of two H_2O molecules to ^{89}Zr^{4+} coincidentally to DFO, increasing the lability of the complex.[34] The result of this is demetallation of the complex, resulting in the accumulation of zirconium-89 in bone tissues ranging from 0.5 – 15% ID/g. The effects of this accumulation have yet to be measured in a clinical trial, but damage to bone marrow is a hypothetical risk. Therefore, measures must be taken to improve upon the stability of DFO. Modification of the linker strategy has, in some cases, led to a mild improvement in stability, but generally at the expense of synthetic simplicity. Of the alternative chelators for zirconium-89, DOTA,[73] DFO*,[57] and 3,4,3-(LI-1,2-HOPO)[64] are the best candidates thus far; each has been examined in a conjugated system and has proven stability compared to their respective DFO conjugates. This proves that a variety of approaches to the rational design of a new ^{89}Zr chelator are feasible. The goals of the synthesis of new and improved chelators for ^{89}Zr are thus:

- A chelator which demonstrates improved stability of the ^{89}Zr-complex *in vitro* and *in vivo*, achieved by the reduction of molecular strain and the addition of a fourth bidentate binding moiety;
- A chelator which can be synthesised in good yield, and which can be radiolabelled in mild conditions;
- A chelator featuring a bifunctional handle by which conjugation to mAB is possible.

The hydroxamate group remains the best candidate for novel zirconium chelators due to ease of synthesis in comparison with the hydroxypyridinones and allowing milder radiolabelling conditions

in comparison with the tetraazamacrocycles. Improving on the stability of Zr-DFO necessitates the inclusion of a fourth hydroxamate moiety. Both cyclic and acyclic hydroxamate chelators have shown promising results; macrocyclic chelators require higher temperatures for radiolabelling, and have slightly more complicated syntheses, however this is usually rewarded with increased complex stability from ligand preorganisation. Chelators with a length shorter than 32 molecules do not appear to form stable complexes with zirconium, but chelators with lengths of between 36 and 48 atoms have reported improvements in binding.[67-69] The design should seek to minimise molecular strain while introducing a fourth hydroxamate binding moiety and maintaining high solubility.

Based on the above criteria, a set of novel chelators has been designed (Figure 17). These chelators are comprised of repeating 11-molecule subunits, similar to DFO, and feature two protected bifunctional handles. While linear chelators generally show inferior binding characteristics compared to macrocycles, these chelators have the potential for macrocyclisation through these bifunctional handles. The incorporation of an α-amino acid in the structure imbues functionality, whereby amino acids with polar side chains could be substituted for the original glycine moiety in order to increase the solubility. Of interest in this synthesis is the investigation of the reported instability of α-amino acid-based hydroxamate chelators.[68] No detailed experimental work on such a structure has been published, and more thorough investigation is warranted. The focus of this project will be to move toward a synthesis of a zirconium-89 chelator incorporating α-amino acid moieties, with radiochemical assessment of the products of synthesis.
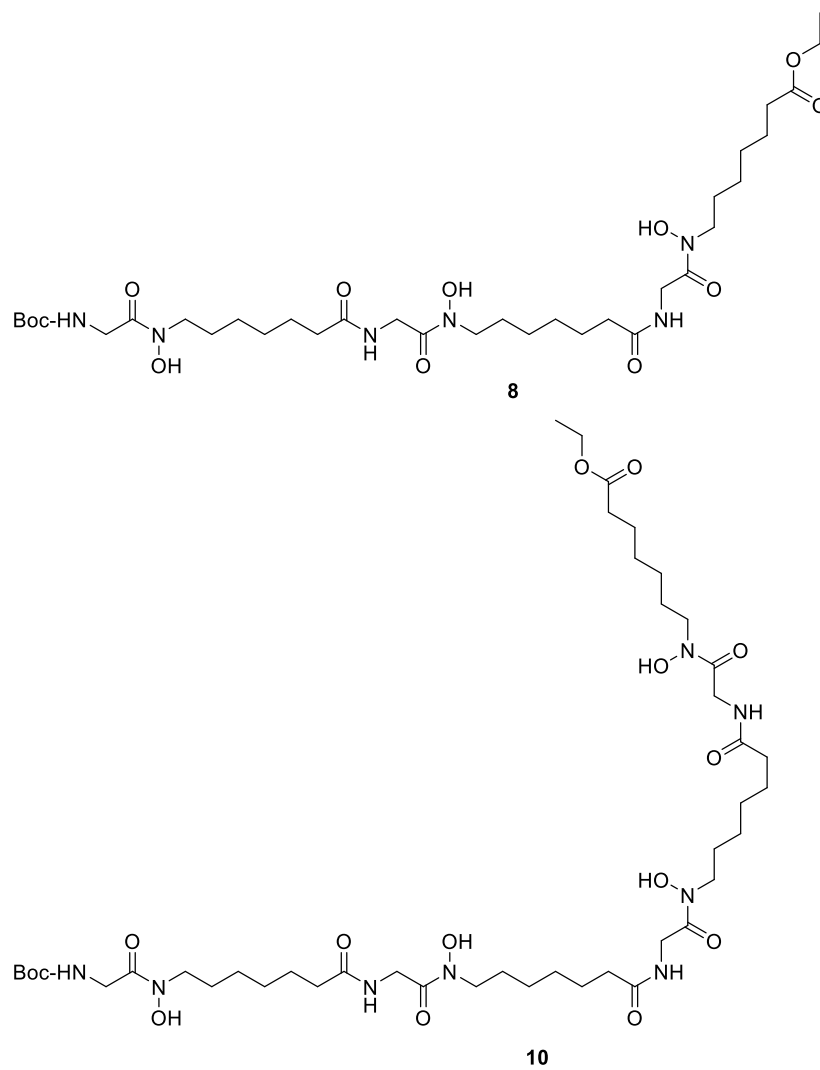
8

10

*Figure 17: The primary target molecules of this project, the tri- and tetra-hydroxamate chelators **8** and **10**.*

2 Attempted syntheses of novel zirconium-89 chelators

2.1 Chelator design

The novel chelators **8** and **10** were chosen as target molecules for this project. Both are structurally similar to DFO yet can be synthesised and functionalised by traditional peptide synthesis. Hydroxamate-based chelators are generally synthesised via solution-phase synthesis rather than solid-phase peptide synthesis. However, the peptide-based structure of **8** and **10** allow use of either method, with a retrosynthetic analysis shown in Scheme 1.

A modular synthesis was proposed given that both molecules are comprised of different numbers of repeating subunits. This then allows successive, orthogonal deprotection reactions and peptide coupling reactions. Furthermore, the required starting materials are commercially available. Orthogonal protecting groups are required to prevent undesired reactions at the amine, carboxylic acid, and hydroxylamine groups. A benzyl ether group (OBn) was chosen to protect the hydroxylamine group as it is stable in both acidic and basic conditions and is removed by hydrogenation.

Like DFO, chelators **8** and **10** are bifunctional, with amine and carboxylic acid termini to allow macrocyclisation or conjugation to mAB. Substitution of glycine for another α-amino acid would allow for further functionalisation. There remain questions around the feasibility of the use of α-amino acids in zirconium-89 chelators, and this will be assessed.[68]
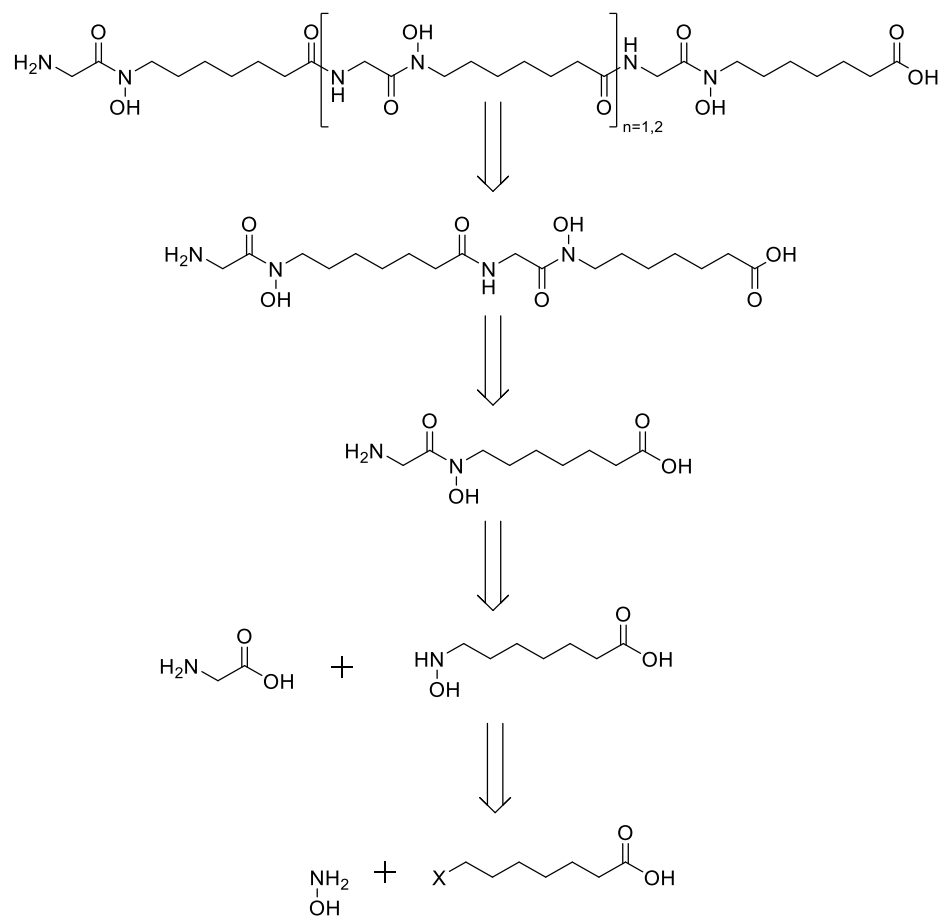
*Scheme 1: Retrosynthetic analysis of novel chelators **8** and **10**.*

2.2   Solid-phase approach to novel chelators
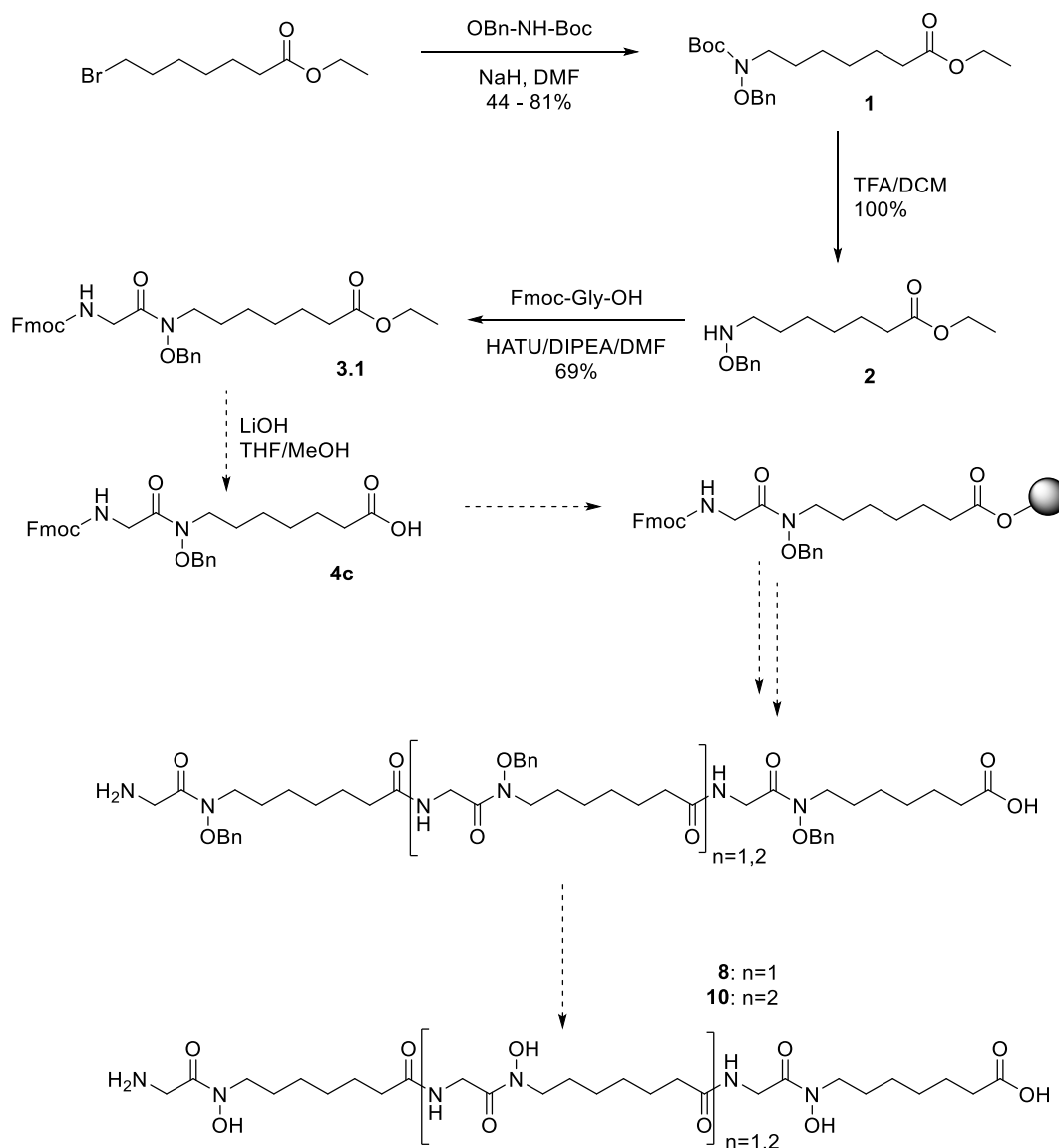
Scheme 2: Proposed synthesis of modular subunit 3.1 by solution-phase peptide synthesis

The peptide subunit **3.1** was synthesised via solution-phase peptide synthesis in preparation for the solid-phase modular synthesis of **8** and **10** (Scheme 2). *N*-Alkylation of ethyl 7-bromo heptanoate by benzyloxy(tert-butoxycarbonyl)amine was performed in the presence of NaH based on the method reported (step 1, Scheme 2).[83] Reagent ratios were modified as per Table 1 in order to improve the yield of the reaction, with some degradation of 7-bromo ethyl heptanoate observed by TLC over the course of the reaction. The optimum conditions proved to be an excess of 1.1 eq. of ethyl 7-bromo heptanoate, as shown in line 7 of Table 1, with the

course of the reaction followed by TLC. Reaction scale-up was achieved by performing the reaction at 60 °C (see line 10).[67] The crude product was separated by silica-based column chromatography in either 2:8 ethyl acetate/hexane or 1:9 acetone:hexane to give compound **1** in yields of 44 - 81%. Analysis by ^{1}HNMR revealed slight upfield translation of the triplet resonance at 3.40 ppm and singlet resonance at 4.82 ppm due to the N-alkylation of benzyloxy(tert-butoxycarbonyl)amine. Further analysis of the ^{1}HNMR spectrum is provided in section 2.5.

*Table 1: Optimisation data for the N-alkylation of ethyl 7-bromo heptanoate by benzyloxy(tert-butoxycarbonyl)amine to form **1**. Line 7 (grey) showed the maximum yield while line 10 represents a scaled-up reaction.*

| Experiment no.	Boc-NH-OBn (eq)	NaH (eq.)	$C_9H_{17}O_2Br$ (eq.)	Yield (%)
1	1.0	1.5	1.0	50
2	1.0	1.5	1.0	44
3	1.0	1.1	1.3	69
4	1.0	1.1	1.0	58
5	1.0	1.2	1.1	63
6	1.0	1.2	1.1	77
7	1.0	1.2	1.1	81
8	1.0	1.2	1.0	59
9	1.0	1.5	1.2	45
10	1.0	1.0	1.3	64

Compound **1** was then treated with 20% TFA/DCM at room temperature in order to remove the Boc group to yield the amine **2** in quantitative yield without further purification (Scheme 2). The reaction was monitored by TLC to confirm complete consumption of the starting material. An analysis of the ^{1}HNMR spectrum revealed the absence of a singlet resonance at 1.51 ppm as was observed in compound **1**, corresponding to the Boc group.

The free amine **2** was coupled with Fmoc-glycine in the presence of 1 eq. HATU, 4 eq. DIPEA, and DMF to give **3.1** in 69% yield, as per step 3 in Scheme 2. The reaction was monitored by TLC and the product separated by column chromatography in 3:7 ethyl acetate/hexane. The

product was analysed by ^{1}HNMR to reveal new resonances: a singlet at 4.11 ppm (corresponding to glycine α-protons); a triplet at 4.26 ppm; a doublet at 4.39 ppm; and a multiplet at 7.27 – 7.80 ppm (corresponding to the Fmoc group).

Deprotection of the ethyl ester of **3.1** was attempted by the addition of 3 eq. LiOH in THF/MeOH, as per step 4 of Scheme 2. However, the desired product **4c** was not isolated; analysis by ^{1}HNMR showed the absence of a key multiplet resonance between 7.50 and 7.80 ppm, indicating the simultaneous cleavage of the Fmoc group. Selective deprotection was attempted by the dissolution of **3.1** in a solution of 0.5M CaCl$_2$ in 7:3 IPA/H$_2$O and addition of 4 eq. LiOH at room temperature, but the reaction did not proceed.[84] To another sample of **3.1** was added 5 eq. MgI$_2$ in THF and the solution heated to 120 °C by microwave,[85] but again compound **4.1a** could not be isolated. The failure to complete this synthetic step prompted the use of an alternative synthetic route (Scheme 3, Scheme 4).

2.3   Solution-phase approach
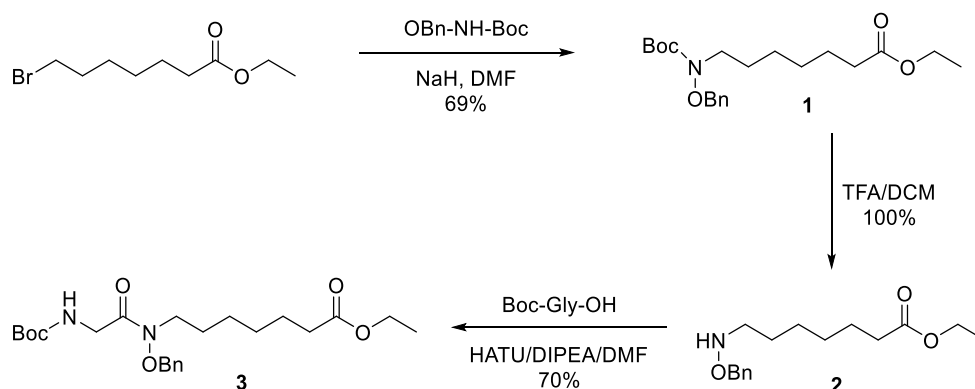
*Scheme 3: Synthesis of subunit **3** by solution-phase peptide synthesis.*

The synthetic route was altered as summarised in Scheme 3. Compounds **1** and **2** were synthesised as in the previous section. The free amine **2** was subsequently coupled with Boc-glycine in the presence of 1.2 equivalents of HATU, 4 – 5 eq. DIPEA, and DMF. The reaction was monitored by TLC and the product separated by column chromatography in 3:7 ethyl

acetate/hexane, to give compound **3** in 52 – 78% yield. Analysis by ^{1}HNMR revealed diagnostic singlet resonances at 3.97 ppm and 1.46 ppm corresponding to the glycine α-protons and Boc group respectively.
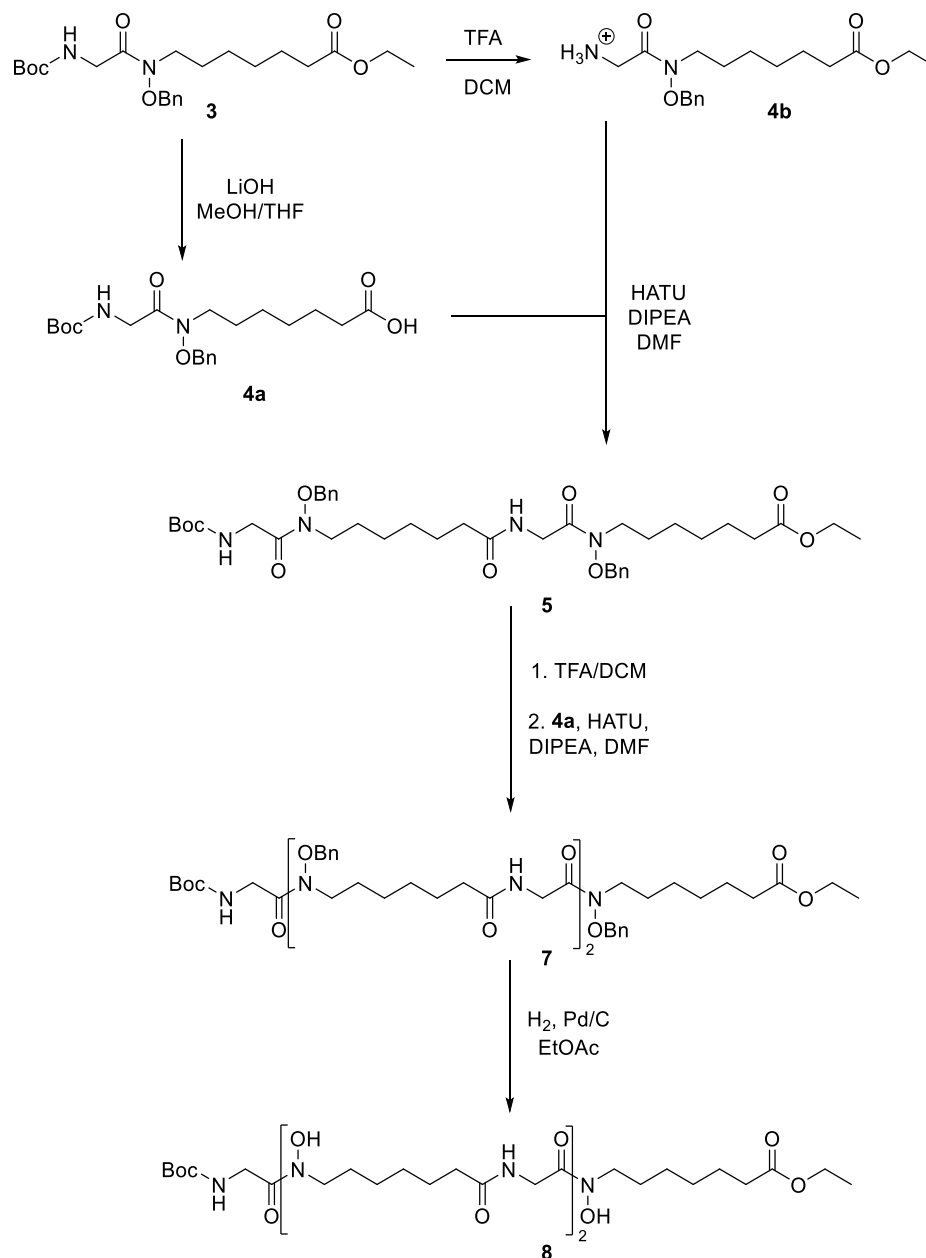
*Scheme 4: Modular synthesis of compound **8** by solution-phase peptide synthesis.*

A sample of compound **3** was treated with 20% TFA/DCM at room temperature in order to remove the Boc group as per Scheme 4, and this gave compound **4b** in quantitative yield without the need for further purification. The reaction was monitored by TLC to confirm consumption of

the starting material; further analysis of ^{1}HNMR revealed the absence of the key singlet resonance at 1.46 ppm indicating removal of the Boc group.

A separate sample of compound **3** was combined with LiOH in THF to deprotect the ethyl ester as per Scheme 4; the reaction was cooled in ice for 15 minutes and raised to room temperature for the remainder of the duration. The reaction was monitored by TLC to confirm consumption of the starting material; this analysis revealed the formation of several side-products. In contrast to similar reported reactions,[68] starting material was present in the reaction mixture up until the 12-hour mark. Different bases (LiOH and NaOH), quantities of base (between 1.1 and 6 eq.), solvent systems (THF, MeOH and H_2O) and reaction times (9 – 24 h) were trialled to optimise the reaction as per Table 2; the optimum conditions trialled are shown in line 5. Crude products of this reaction were either used without further separation or purified with column chromatography, using 1:1 ethyl acetate/hexane with 1% acetic acid or 4:96 MeOH/DCM, giving compound **4a** in yields of between 8% and 44%. Analysis by ^{1}HNMR showed the absence of key resonances: a quartet at 4.10 ppm and a triplet at 1.26 ppm, corresponding to the loss of the ethyl ester.

*Table 2: Optimisation conditions trialled for the deprotection of **3** to give **4a**. Yields marked with an asterisk (*) indicate the crude product was not purified by chromatography and yield was estimated by ^{1}HNMR (by peak intensity) and HPLC (by peak intensity).*

Base	Base (eq.)	Solvent	Reaction time (h)	Yield (%)
NaOH	1.1	MeOH/H_2O	20h	15%
LiOH	3	THF/H_2O	20h	0%
LiOH	4	THF/H_2O	20h	35%
LiOH	6	THF/H_2O	20h	8% - 40%
LiOH	6	THF/H_2O	9h	44%*
LiOH	3	THF/MeOH/H_2O	24h	27%

Analysis of the reaction mixture by HPLC revealed the production of side-products increased gradually over 10 hours (Table 3, Figure 18). Comparison between HPLC traces of this sample and another reacted for 21 hours revealed a significant decrease in the yield of **4a** after 21 hours

and an increased range of side products (Appendix, Spectrum 43 and Spectrum 44). Analysis

of crude reaction samples by ^{1}HNMR consistently revealed the appearance of a triplet

resonance at 3.2 ppm, suggesting that a competing reaction was occurring simultaneously.

*Table 3: Deesterification of compound **3** over time as measured by HPLC. Component proportions determined by integration of HPLC trace. Analysis was performed using a gradient of 10-100% MeOH over 15 minutes.*

	Peak elution time (mins)					
Reaction time (mins)	20.9	18.2	15.8	14.3	13.7	13.2
0	100	0	0	0	0	0
30	97	3	0	0	0	0
120	85.57	11.78	0	0	1.24	1.41
240	68.34	21.89	2	1.39	1.7	4.68
360	41.75	25.87	0	2.71	8.12	10.95
540	12.32	43.86	6.42	3.88	11.07	22.45
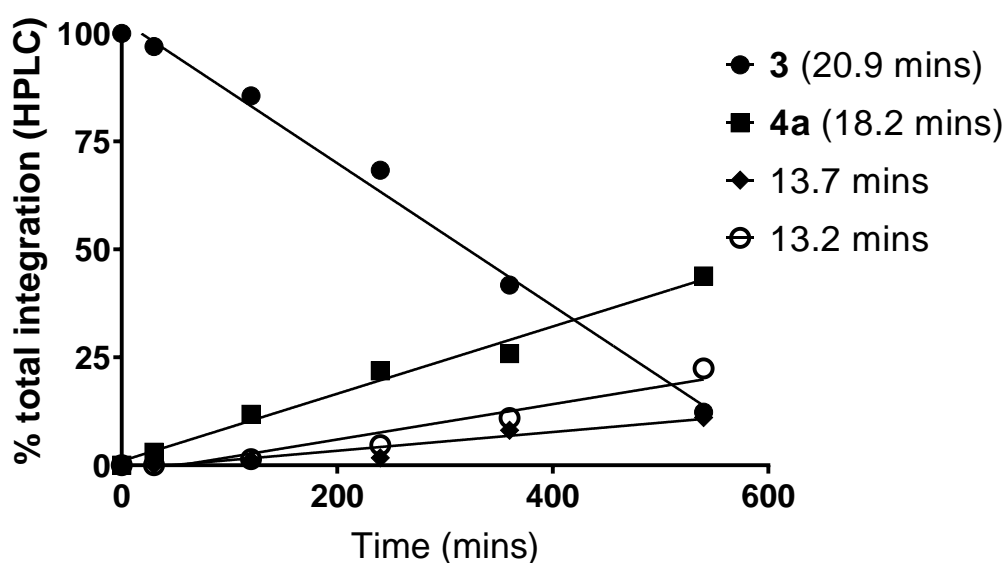
*Figure 18: Change in key components of reaction mixture over time for deesterification reaction of compound **3**. with proportions estimated by integration of HPLC traces. The starting material, compound **3**, eluted at 20.9 mins; the desired product, compound **4a**, eluted at 18.2 minutes. Peaks at 13.7 and 13.2 mins represent unknown by-products. Analysis was performed using a gradient of 10-100% MeOH over 15 minutes.*

Acid **4a** was subsequently coupled to amine **4b** in the presence of HATU (1.1 eq.), DIPEA (4 –

5 eq.) and DMF, as per Scheme 4. The reaction was monitored by TLC and the crude product

was purified by column chromatography in either 1:1 ethyl acetate/hexane or 4:96 MeOH/DCM.

Compound **5** was subsequently isolated with yields of between 11 - 21%. Analysis by ^{1}HNMR

revealed key resonances: a singlet at 1.46 ppm; a quartet at 4.10 ppm, and a triplet at 1.26 ppm,

corresponding to the Boc and ethyl ester groups respectively. Other observations made using

^{1}HNMR will be discussed further in section 2.5.

Compound **5** was then treated with 20% TFA in DCM at room temperature to cleave the Boc

protecting group, as per Scheme 4. The reaction was monitored by TLC to confirm complete

consumption of the starting material. This gave compound **6b** in quantitative yield after 2 hours.

Analysis by ^{1}HNMR revealed the absence of the key singlet resonance at 1.46 ppm,

corresponding to the Boc group.

Compound **6b** was then coupled to compound **4a** in the presence of HATU (1.1 eq.), DIPEA (4

eq.) and DMF at room temperature for 48 hours, as per Scheme 4. The reaction was monitored

by TLC and attempted separation by column chromatography in 5:95 MeOH/DCM gave a

sample containing compounds **7**, **7.1** and **7.2** (Figure 19) based on HRMS analysis. Mass peaks

corresponding to the formulae of each compound in the sample were identified by HRMS with

detected masses of 1017.6085, 784.4766 and 551.3237. Analysis by ^{1}HNMR revealed the

presence of the singlet resonance at 1.46 ppm, corresponding to the Boc group of all

compounds. The integrations of the multiplet resonances at 1.55 – 1.70 ppm and 1.31 – 1.40

ppm also suggested a mixture of several compounds; this will be discussed further in section

2.5. The product was used without further purification with the option to resolve product purity

after the following step.

The mixture containing compounds **7**, **7.1** and **7.2** was subsequently hydrogenated over Pd/C

in ethyl acetate at room temperature to cleave the benzyl ether protecting group, as per Scheme

4. The reaction was monitored by TLC and the product used without further purification. Analysis

by TLC showed a spot of lower R_f, and analysis by ^{1}HNMR revealed the absence of the multiplet

resonance between 7.3 – 7.5 and the singlet at 4.9 ppm, indicating complete cleavage of the

benzyl protecting group. However, analysis by ^{1}HNMR showed markedly low intensity for many

signals relative to the ethyl ester and Boc protecting groups, and analysis by HRMS returned a

sole peak at 483.24. Further analysis by LRMS revealed two peaks at 461.3 and 483.3.

Subsequent analyses by COSY, TOCSY and ROESY led to the proposition of an alternative

structure **8.1** (Figure 19); spectral evidence will be discussed further in section 2.5. However, it

is postulated that compound **7** underwent an aspartamide-like reaction and while details remain

unclear, there are reports of this occurring on hydroxamate-containing compounds under both

acidic and basic conditions.[86] The observed masses of 461.3 and 483.3 are consistent with the

[M+H] and [M+Na] peaks of compound **8.1** (Figure 19). It was determined that the product of

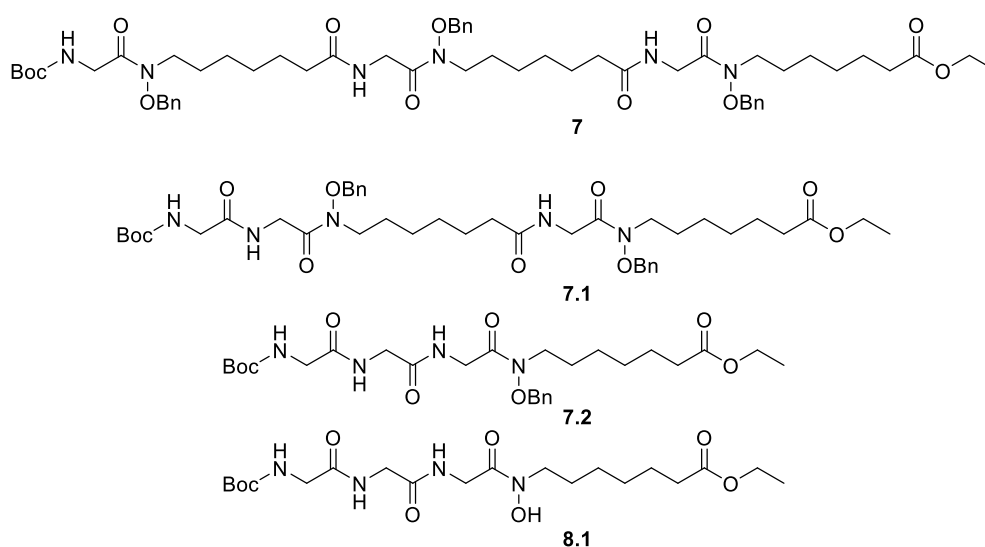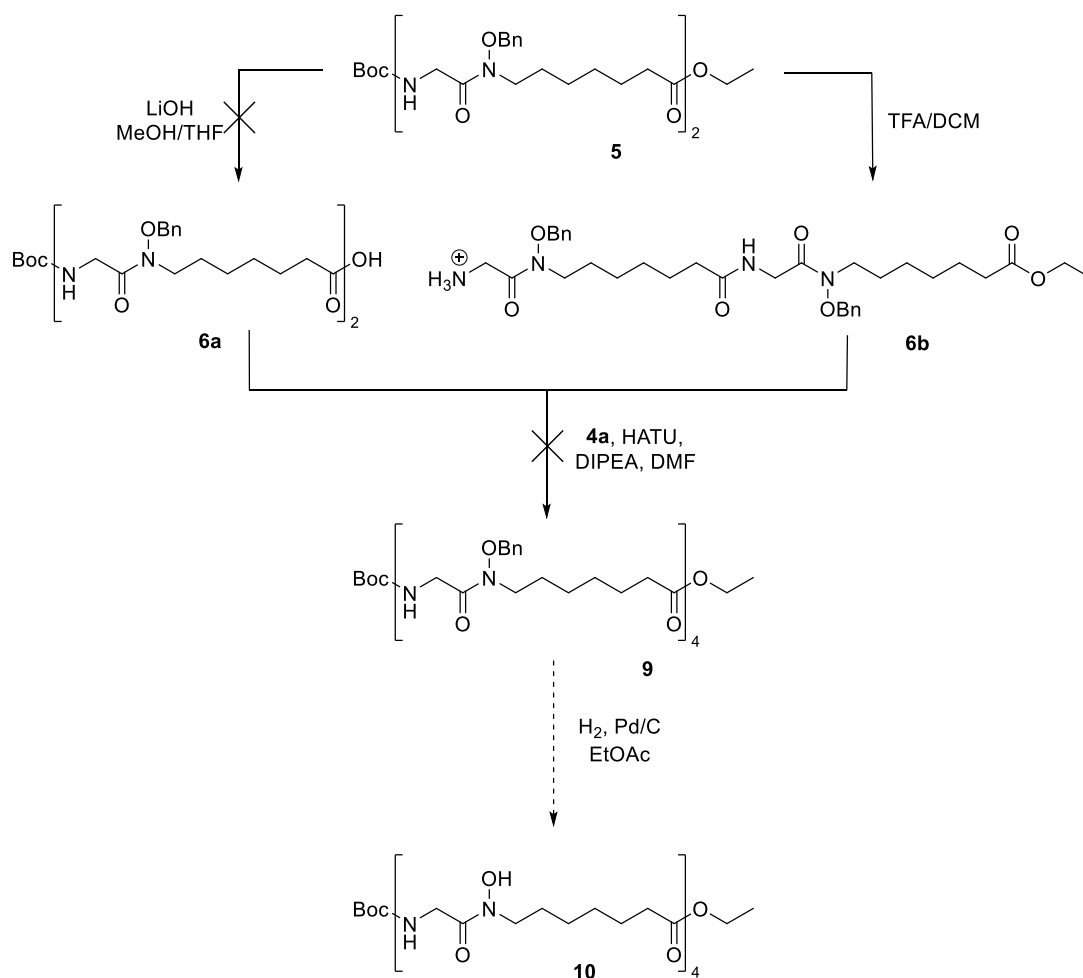this reaction was compound **8.1**.

*Figure 19: Products of decomposition; **7.1** and **7.2** observed in the mass spectrum of compound **7**, while **8.1** is the sole compound observed after the hydrogenation of compound **7**.*

*Scheme 5: Attempted scheme for synthesis of tetrameric chelator **10**.*

A sample of compound **5** was treated with 1M LiOH solution in THF/MeOH as per Scheme 5 in order to hydrolyse the ethyl ester. The reaction was monitored by TLC which revealed the formation of multiple side-products. Separation of the crude product was attempted with column chromatography, however no isolable sample of compound **6a** was obtained. A reaction was attempted between the crude product of this reaction (used without further purification) and compound **6b** in the presence of HATU, DIPEA and DMF; however this was unsuccessful.

2.4 Alternative approach: synthesis of chelator containing β-amino acid
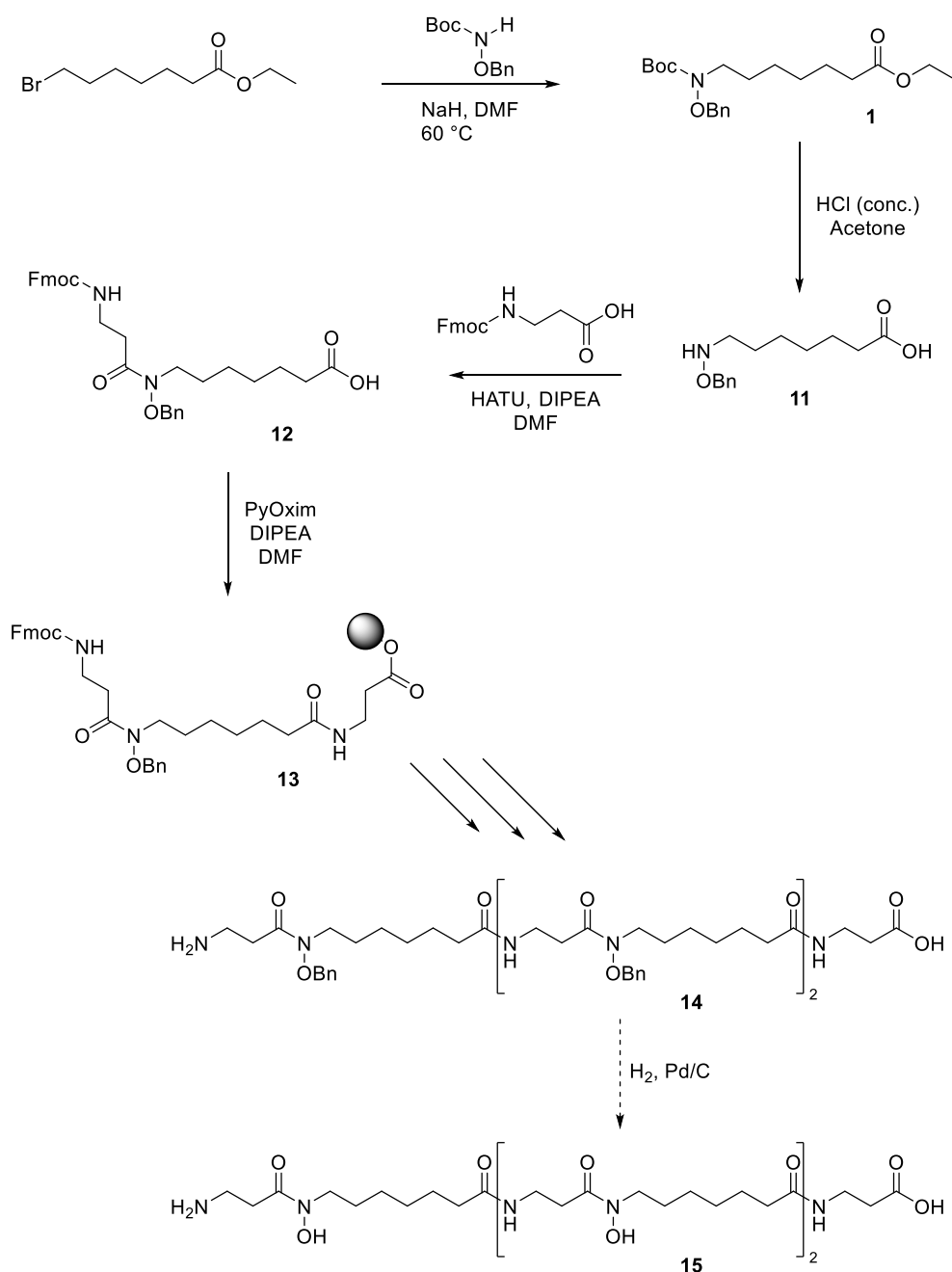
*Scheme 6: Scheme for synthesis of compound **15** by solid-phase peptide synthesis*

After the unsuccessful syntheses of compounds **8** and **10**, a synthesis of compound **14** was attempted to directly assess the validity of incorporating β-alanine rather than glycine into a hydroxamate chelator. While Seibold *et al.* have successfully synthesised 36-member macrocyclic chelators with a similar backbone (alternating β-alanine and N-hydroxyl butanoic

acid subunits), no synthesis of chelators containing α-amino acids was reported.[68] The additional terminal β-alanine group was included to allow more efficient loading onto resin.

Synthesis began with synthesis of compound **1** as reported in section 2.1 by the *N*-alkylation of ethyl 7-bromoheptanoate (Scheme 6). Following this, compound **1** was deprotected on treatment with 3M HCl in acetone by the reported method[87] to remove the ethyl ester and Boc protecting groups, as per Scheme 6. The reaction was monitored by TLC and the crude product **11** was used without further purification. Analysis by ^{1}HNMR revealed the absence of several resonances: a singlet at 1.51 ppm, a triplet at 1.26 ppm and a quartet at 4.10 ppm, corresponding to the Boc and ethyl ester groups.

The mixture containing compound **11** was then coupled to Fmoc-β-Alanine in the presence of HATU (1.0 eq.), DIPEA (4.0 eq.) and DMF, as per Scheme 6. The reaction was monitored by TLC and the crude product purified by reverse-phase column chromatography using 7:3 ACN/H_2O, to give compound **12** in 25% yield. Analysis by ^{1}HNMR revealed resonances at 2.65 and 3.48 ppm due to the β-alanine group, which were conserved from analysis of the starting material.

2-chlorotrityl resin was pre-coupled to Fmoc-β-Alanine in a solution of DCM and DIPEA (5 eq.), leading to a calculated loading of 0.44mol/g. The modified resin (0.1 mmol) was then incubated with a solution of compound **12** (0.3 mmol), PyOxim (0.3 mmol), DIPEA (1.5 mmol) and DMF (10 mL) as per Scheme 6, and agitated occasionally for 6 hours. Following this, the extent of coupling was determined with the Kaiser test.[88] Cleavage of the Fmoc-protecting group was achieved by addition of 0.1M HOBt in 20% piperidine/DMF. This process was repeated three times before final cleavage of the resin by addition of 95/2.5/2.5 TFA/TIPS/H_2O. The product was collected and purified by semi-preparative HPLC, to give compound **14** in a mass of 10 mg.

Analysis by mass spectroscopy identified a peak of mass 1002.8 m/z, corresponding to the formula of the desired product.

2.5   Spectral analyses

Due to the modular nature of the above syntheses, there was a high degree of similarity between ^{1}HNMR spectra for each novel compound. Selected spectra are contained in this section while full spectra are provided in Appendix 5.2.
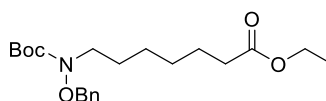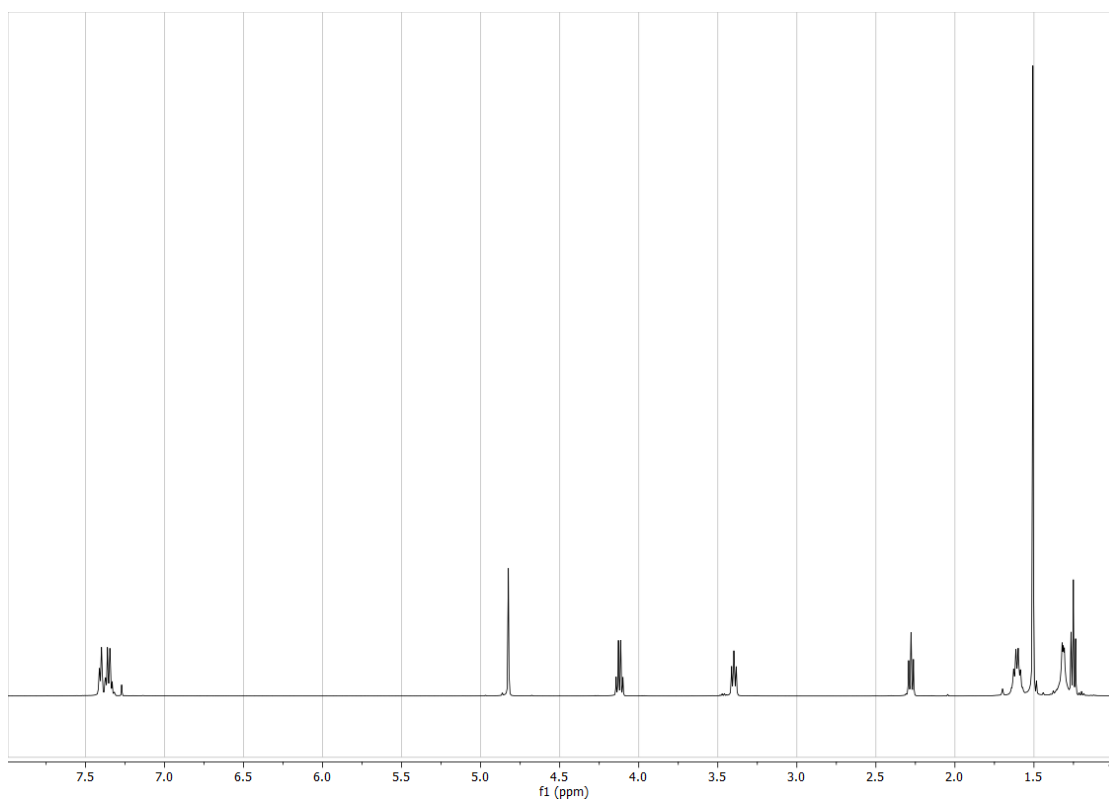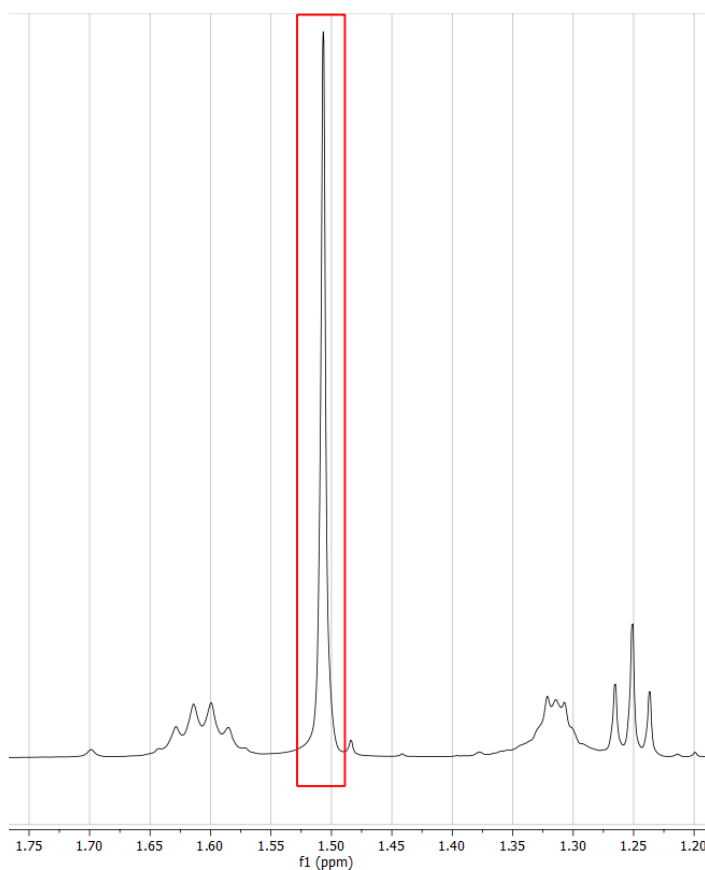

Figure 20: Compound 1

Spectrum 1: Complete ^{1}HNMR spectrum for compound 1 in CDCl3.

Analysis of a sample from the *N*-alkylation of ethyl 7-bromo heptanoate by ^{1}HNMR (Figure 20) (Spectrum 1) revealed a number of key resonances. Firstly, the singlet at 1.51 ppm, the triplet at 1.25 and the quartet at 4.10 ppm corresponded to the Boc and ethyl ester group (Spectrum 2, Spectrum 3).
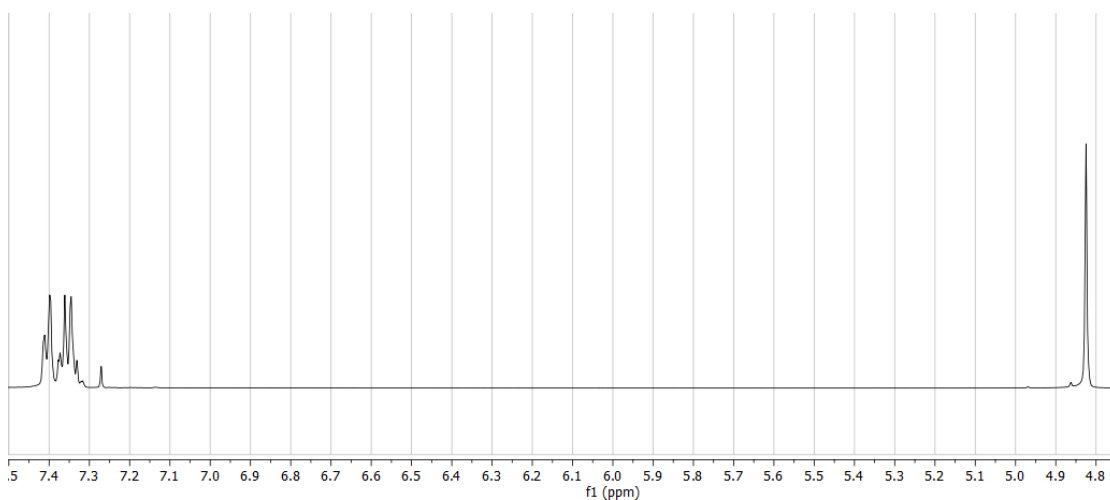
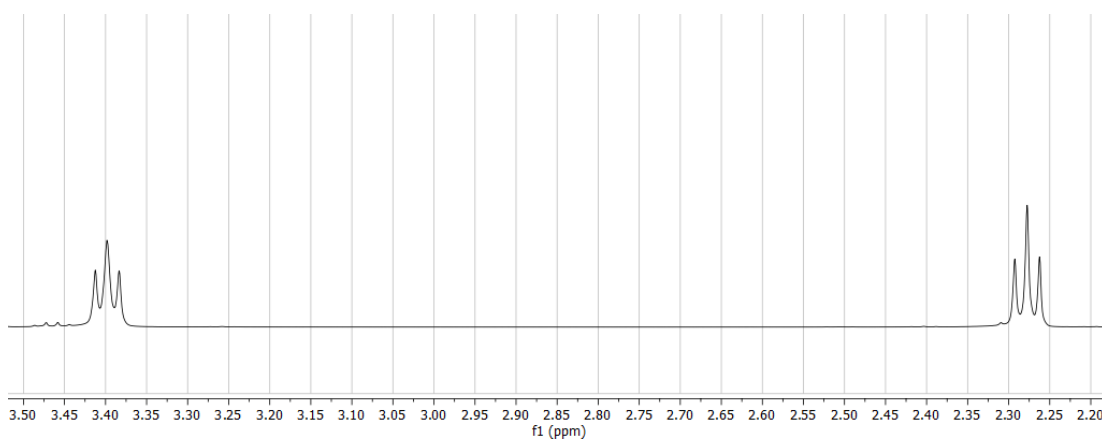*Spectrum 2: ¹HNMR resonance corresponding to the Boc protecting group.*
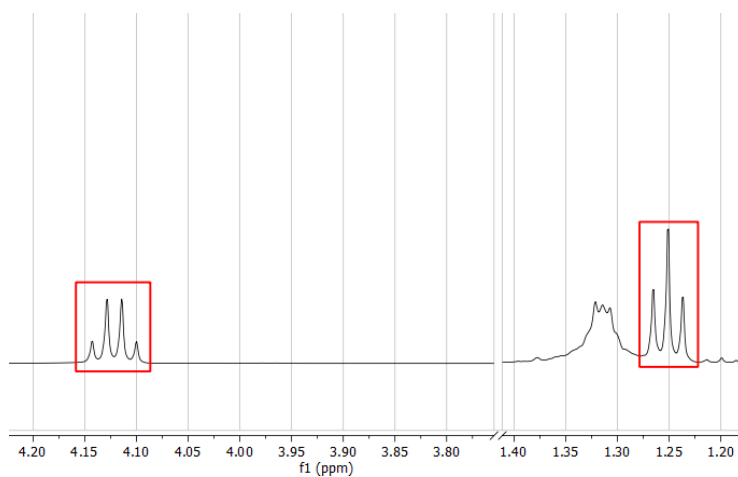
Spectrum 3 (right): ¹HNMR resonances corresponding to the ethyl ester group.

The appearance of the singlet at 4.82 ppm and the multiplet at 7.33 - 7.41 ppm, corresponding to the methyl and aromatic protons of the benzyl ether protecting group, confirmed synthesis of compound **1** (Spectrum 4). These resonances integrated at a ratio of 2:5.
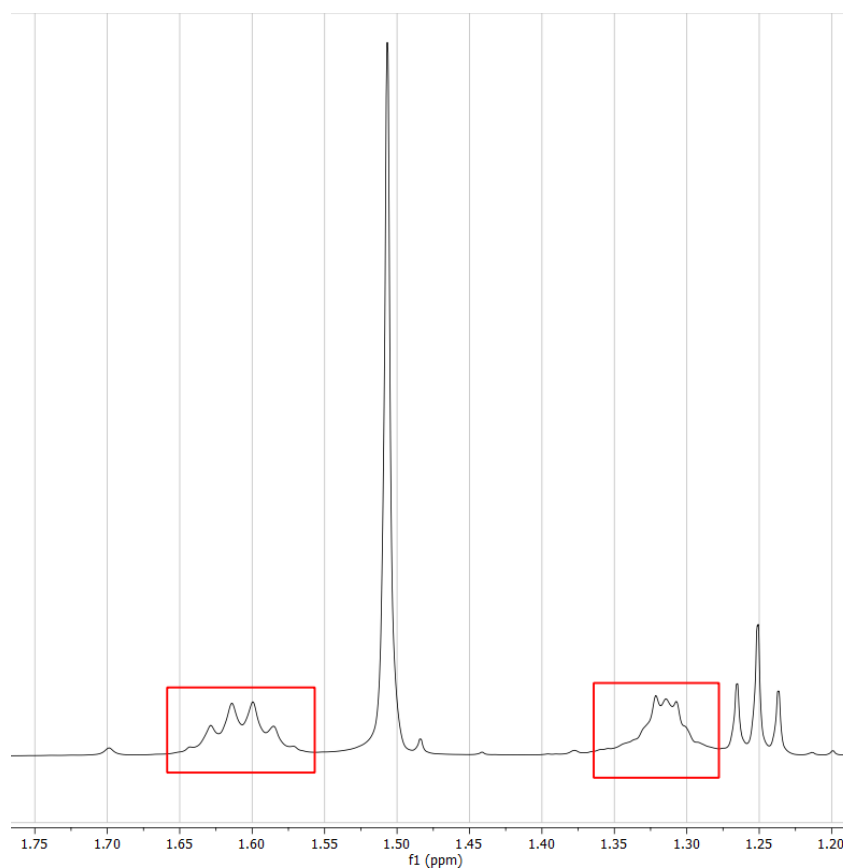
*Spectrum 4: ¹HNMR resonances corresponding to benzyl ether protecting group of compound **1**.*

The triplet resonances at 2.27 ppm and 3.39 ppm corresponded to methylene groups adjacent

to the carboxyl and amine groups respectively (Spectrum 5) and integrated with a ratio of 1:1.

*Spectrum 5: ¹HNMR resonances corresponding to methylene groups adjacent to the amine (R_2N-**CH₂**-CH₂, 3.39 ppm) and carboxyl (CH₂-**CH₂**-COO, 2.27 ppm) groups of compound **1**.*

*Spectrum 6: ¹HNMR resonances corresponding to central methylene groups in alkyl chain of compound 1; CH₂-**CH₂**-**CH₂**-CH₂ = 1.32 ppm, **CH₂**-CH₂-CH₂-**CH₂** = 1.62 ppm.*

Multiplet resonances at 1.57 – 1.64 ppm and 1.27 – 1.35 ppm corresponded to the four central

methylene groups in the alkyl chain, which formed two rough multiplets that integrated at a ratio
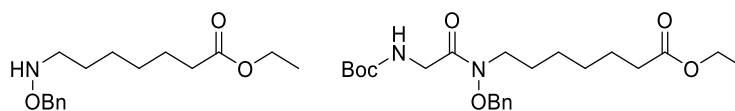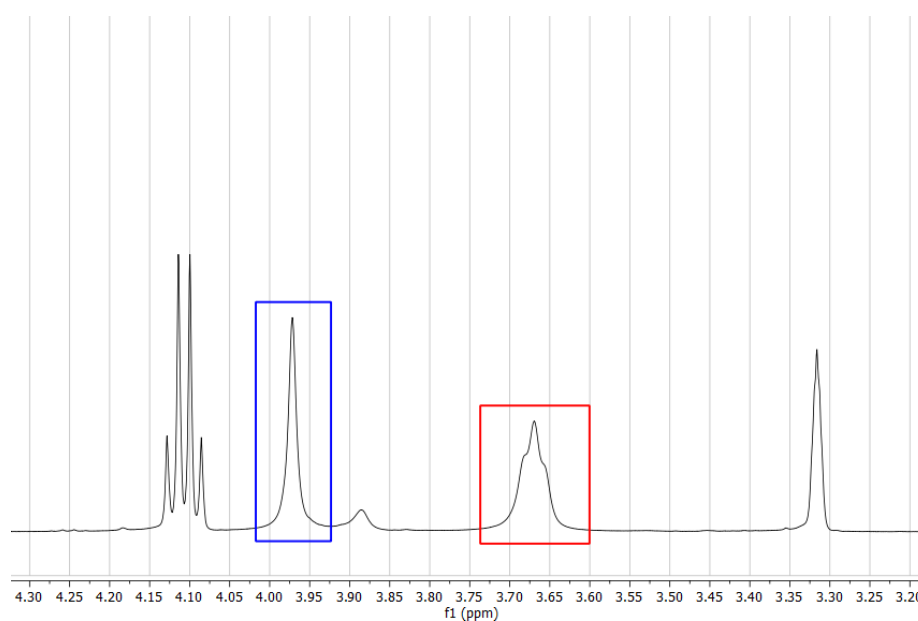
of 1:1.

*Figure 21: Structure of compounds **2** (left) and **3** (right)*

Analysis by ¹HNMR of a sample from the treatment of compound **1** with TFA/DCM (Figure 21) revealed the absence of the singlet resonance at 1.51 ppm, indicating complete cleavage of the Boc group; the triplet resonance at 3.39 ppm was replaced with a resonance at 3.31 ppm, indicating a change in character of the amine group from tertiary to secondary (Spectrum 18).

Analysis by ¹HNMR of a sample from the coupling of compound **2** to Boc-glycine (Figure 21) revealed new singlet resonances at 3.97 ppm and 1.46 ppm, corresponding to the α-protons of the glycine moiety (Spectrum 7) and the Boc group respectively. The triplet resonance at 3.31 ppm (visualised in the ¹HNMR spectrum of compound **2**) was no longer visible, with a broad triplet appearing at 3.67 ppm; as the former was assigned to the methylene group adjacent to the secondary amine, this change was attributed to the formation of an amide from this secondary amine, indicating a successful formation of compound **3**.

*Spectrum 7: ¹HNMR signals corresponding to the α-proton signal (blue) and the R_2N-**CH₂**-CH_2 group (red) of compound **3**.*
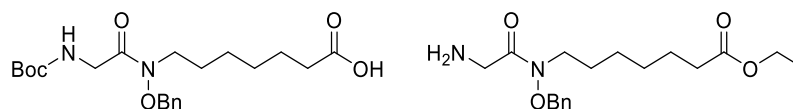
*Figure 22: Compounds **4a** (left) and **4b** (right)*

Analysis by ^{1}HNMR of a sample from the treatment of compound **3** with TFA/DCM revealed the absence of the singlet resonance at 1.46 ppm indicating complete cleavage of the Boc group (Spectrum 21).

Meanwhile, analyses of crude samples from the hydrolysis of the ethyl ester of compound **3** to form **4a** (Figure 22) by ^{1}HNMR indicated unexpected changes in resonances. In particular, the signals corresponding to the benzyl ether groups (the multiplet at 7.30 – 7.50 ppm and singlet at 4.70 ppm) were of lower intensity compared to other resonances (Spectrum 8). The triplet resonance at 3.67 ppm also displayed a decreased intensity with a new triplet resonance of equivalent intensity appearing at around 3.2 ppm. Following purification of the sample, the triplet resonance at 3.2 ppm was absent, as were the triplet at 1.24 and the quartet at 4.10 which indicated successful cleavage of the ethyl ester and successful isolation of compound **4a** (Spectrum 9). Broadening of the singlet at 4.08 ppm and poor resolution of the triplet at 3.64 ppm was observed; the former likely due to the pair of glycine α-protons.
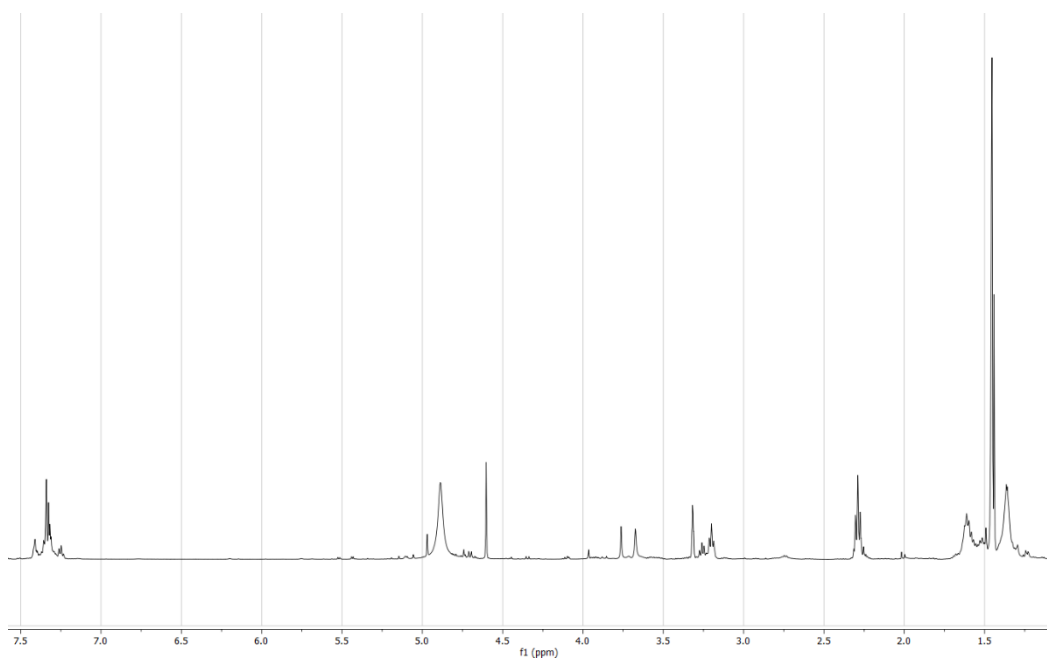
*Spectrum 8: ¹HNMR spectrum for a crude sample from the attempted deesterification of compound **3**. The decreased intensity of the resonances at 7.3 - 7.5 ppm and 4.6 ppm (corresponding to benzyl ether groups) indicate some change in these groups.*
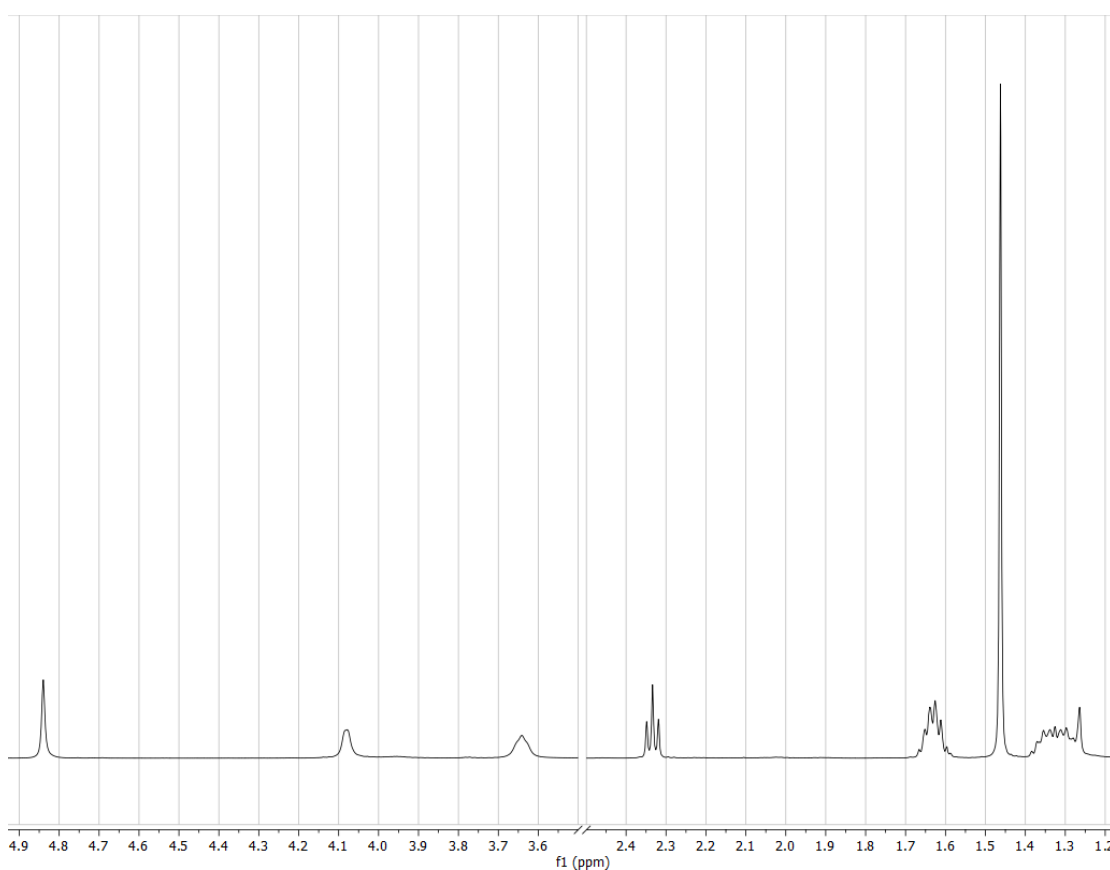
*Spectrum 9: Partial ¹HNMR spectrum for compound **4a**. The disappearance of the resonances at 1.24 ppm and 4.10 ppm indicates complete cleavage of the ethyl ester.*
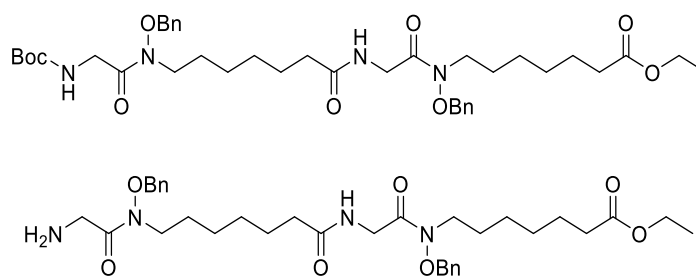
Figure 23: Compounds 5 (above) and 6b (below)

^{1}HNMR analysis of a sample from the coupling between **4a** and **4b** revealed key resonances: the triplet at 1.26 ppm, the quartet at 4.10 ppm, and the singlet at 1.46 ppm. These corresponded to the ethyl ester and Boc group respectively. Several other resonances were roughly doubled in intensity and somewhat broadened; this was noticed for the multiplets at 7.38 – 7.46 ppm, 1.51-1.69 ppm and 1.26-1.40 ppm, and the triplets at 3.67 and 2.29 ppm. The relative increase in intensity of these signals compared to those of the terminal protecting groups (as highlighted above) suggested a successful dimerisation of the molecule. An additional singlet resonance was observed at 4.09 ppm (co-incident with the quartet at 4.10 ppm), which was thought to correspond to the additional set of glycine α-protons (Spectrum 10). These factors combined with HRMS data suggested the successful formation of compound **5** (Figure 23).
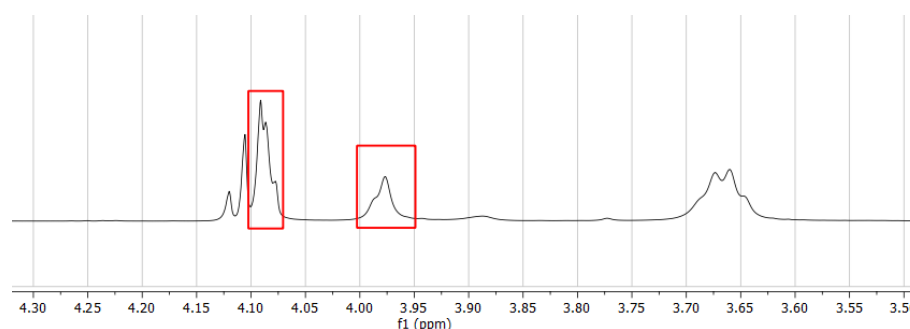
Spectrum 10: Partial ^{1}HNMR spectrum of compound 5 showing α-proton resonances (red).

Analysis by ^{1}HNMR of a sample from the treatment of compound **5** with TFA/DCM revealed the absence of the resonance at 1.46 (s) ppm, indicating cleavage of the Boc group (Spectrum 23) and the successful formation of compound **6b** (Figure 23).
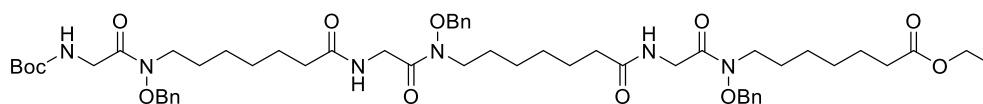
*Figure 24: Compound **7**.*

Analysis by HRMS of a sample from the attempted coupling between **4a** and **6b** revealed a mass at 1017.6085 m.u., indicating the presence of the desired product **7** (Figure 24). However, there were additional peaks present at 784.4766, 551.3237 and 280.1998 m.u. (Spectrum 50), indicating a mixture of compounds. These masses are consistent with compounds **7.1**, **7.2** (Figure 19), and **2**. Analysis by ^{1}HNMR revealed a triplet at 1.23 ppm, a multiplet at 4.05 – 4.17 ppm, singlets at 3.94 ppm, 3.75 ppm and 1.46 ppm which correspond to the ethyl ester group, α-protons, and the Boc group respectively, and displayed the expected integrations. The resonances corresponding to the hexanoate components of the molecule (i.e. multiplet resonance at 7.45 - 7.40 ppm, the singlet at 4.95 ppm, the triplets at 3.68 ppm and 2.29 ppm, and the multiplets at 1.55 – 1.70 ppm and 1.31 – 1.40 ppm) displayed lower intensity than predicted (Spectrum 24). The loss of these alkyl chains combined with the aberrant mass signals suggest a a mixture of **7**, **7.1** and **7.2** (Figure 19).

Analysis of a number of samples from the attempted preparation of compound **8** by ^{1}HNMR showed the absence of the multiplet resonance at 7.3 – 7.5 ppm and the singlet at ~4.8 ppm, indicating removal of the benzyl ether group (Spectrum 25). A number of resonances were of lower than expected intensity, particularly the triplets at 3.46 ppm and 2.26 ppm, and the multiplets at 1.43 – 1.55 ppm and 1.19 – 1.30 ppm. The presence of grease resulted in additional peaks (a triplet at 0.85 ppm and a singlet at 1.23 ppm). Analysis of the sample by mass spectroscopy detected molecules of mass 461.3 and 483.3 m.u.

*Spectrum 11: Partial COSY ¹HNMR spectrum of compound **8.1** showing coupling between amide peaks and α-proton peaks.*

Samples from the attempted preparation of compound **8** were further analysed by 2D ¹HNMR. COSY ¹HNMR (Spectrum 11) showed a crosspeak between resonances at 3.57 ppm and 6.97 ppm, 3.75 ppm and 8.01 ppm, and 3.97 ppm and 7.87 ppm. The broad doublet resonances at 3.57, 3.75 and 3.97 ppm displayed chemical shifts roughly corresponding to glycine α-protons in the preceding molecules, while the broad triplet resonances at 6.97, 7.87 and 8.01 ppm were visible only when experiments were undertaken in DMSO, but had chemical shifts in the expected range of amide protons. No other crosspeaks were revealed by the above COSY experiment for these resonances, suggesting that these resonances corresponded to the three groups of α-protons and the three amides respectively of each glycine moiety. Further analysis by ROESY ¹HNMR of the same sample showed crosspeaks between the same resonances as listed above, as well as additional crosspeaks between the doublet at 3.57 and the triplet at 8.01 ppm, and between the doublet at 3.75 and the triplet at 7.87 ppm (Spectrum 12, red). This suggests that two distinct glycine moieties are adjacent to two amide groups each. The above

data combined with the HRMS data for the same samples suggests the formation of an alternative product: compound **8.1**, which has a calculated mass of 460.25 (Figure 25). The absence of peaks representing spatial correlation between amides and the alkyl chain (Figure 25, red) supports this hypothesis.
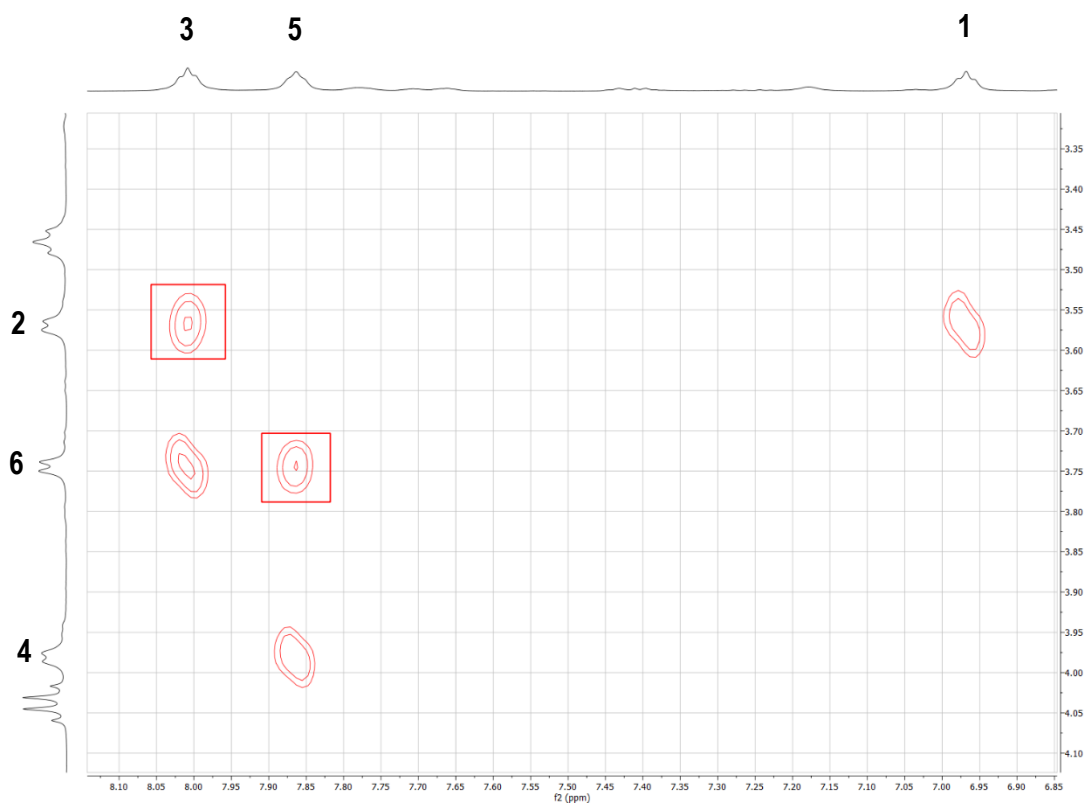
*Spectrum 12: Partial ROESY ¹HNMR spectrum of compound **8.1** showing coupling between amide peaks and α-proton peaks; peaks unique to ROESY spectrum are highlighted in red.*
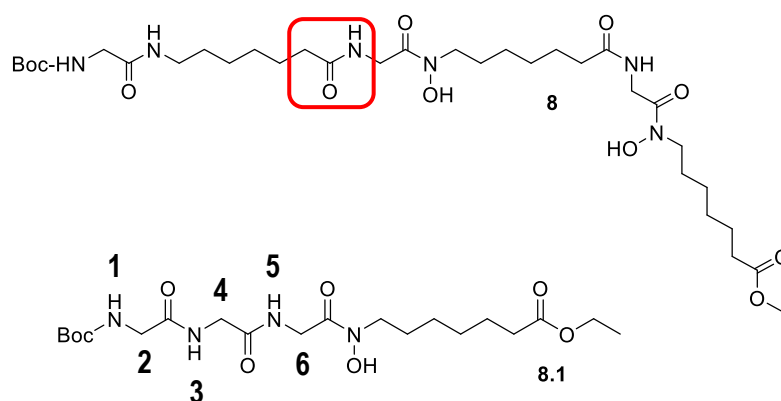

*Figure 25: Compound **8**, with diagnostic group for compound **8** shown highlighted in red, and compound **8.1**, with protons corresponding to key resonances in Spectrum 12 numbered.*
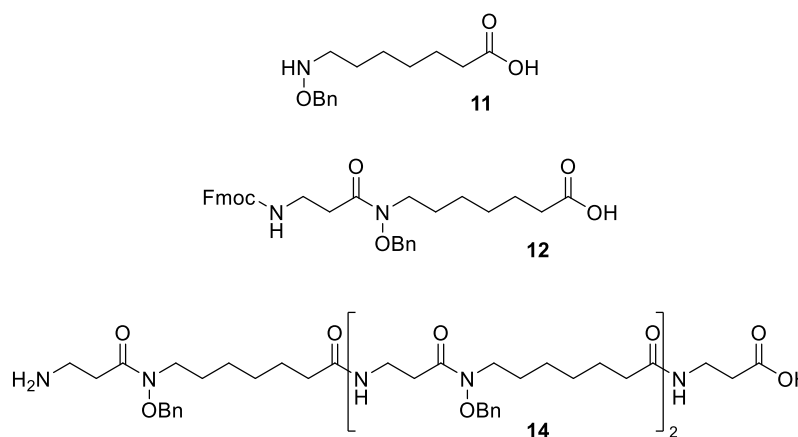
Figure 26: Compounds **11**, **12** and **14**.

¹HNMR analysis of a crude sample from hydrolysis of the ethyl ester **1** to form compound **11** (Spectrum 13) revealed the absence of a singlet resonance at 1.51 ppm, indicating complete cleavage of the Boc group. The quartet resonance at 4.11 ppm and the triplet at 1.24 ppm corresponding to the ethyl ester group were still present, but with significantly reduced intensity, indicating that approximately 80% of the sample had undergone hydrolysis. The triplet resonance at 3.40 ppm was replaced by another at 3.35 ppm, indicating the change in character of the tertiary amine to a secondary amine. Two coincident triplet resonances were present between 2.28 – 2.35 ppm due to partial hydrolysis of the ethyl ester in the sample.
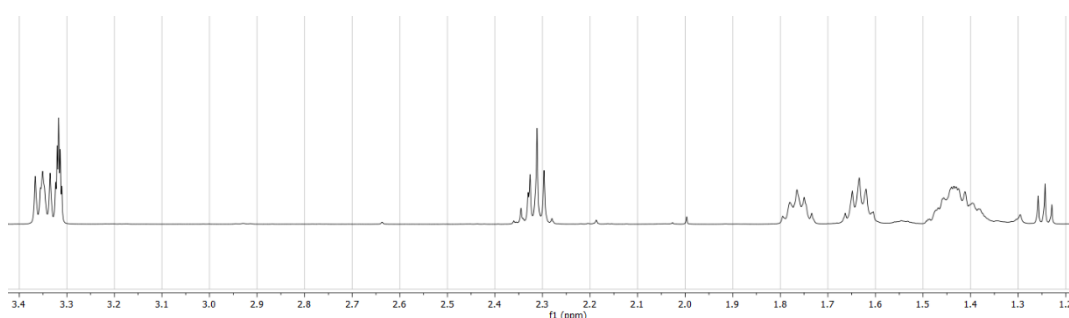
Spectrum 13: Partial ¹HNMR spectrum of compound **11**.

Analysis of a sample from the coupling between **11** and Fmoc-β-Alanine to form the intermediate **12** (Figure 26) revealed several resonances – a multiplet at 7.29 – 7.79 ppm, a doublet at 4.36 ppm and a triplet at 4.21 ppm, corresponding to the Fmoc group, as well as multiplets at 3.48 ppm and 2.65 ppm, corresponding to the α- and β-protons of β-alanine; these additional signals suggest successful coupling of the Fmoc-β-alanine moiety (Spectrum 14). The triplet resonance at 3.35 ppm was replaced by another at 3.66 ppm, suggesting a change in character of the secondary amine.
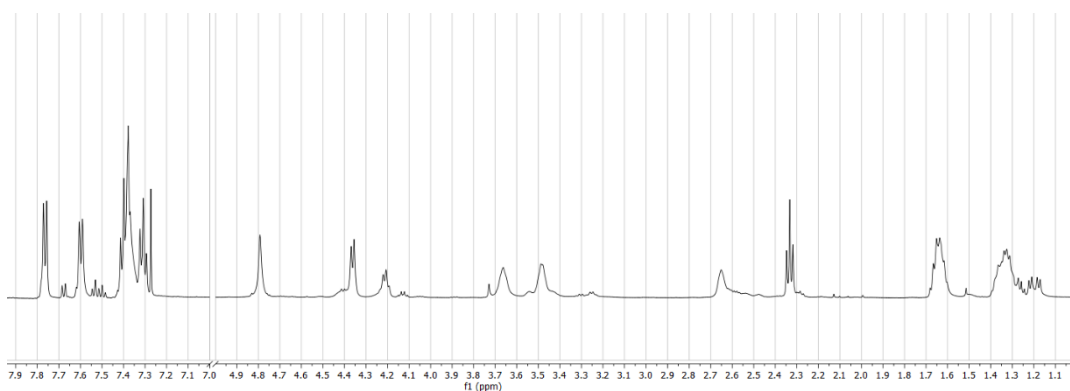
Spectrum 14: Partial ^{1}HNMR spectrum of compound **12**.

Analysis of a sample from the attempted synthesis of compound **14** by ^{1}HNMR revealed a range of key resonances (Spectrum 16). Three new resonances – two triplets at 7.83 and 7.79 ppm and a multiplet at 7.76 ppm - were apparent, with a total multiplicity suggesting these were amide protons. Several resonances were conspicuously absent including doublets at 7.77 ppm, 7.60 ppm, and 4.36 ppm and a triplet at 4.21 ppm, indicating cleavage of the Fmoc group. Resonances including the multiplet at 7.33 – 7.46 ppm, and singlets at 4.86 ppm and 4.81 ppm corresponded to the benzyl ether groups. Multiplets at 3.17 – 3.26 ppm and 2.95 – 3.04 ppm corresponded to the eight β-protons of β-alanine, and multiplets at 2.76 – 2.84 ppm and 2.51 – 2.58 ppm, and a triplet at 2.35 ppm corresponded to the eight α-protons. Analysis by TOCSY ^{1}HNMR allowed assignment of amide and β-alanine protons, as this identified which signals were located within the same spin systems. Further analysis by ROESY ^{1}HNMR (Spectrum 15)

identified a crosspeak between the suspected amide protons at 7.79 ppm and alkyl protons at 2.01 ppm. The visualisation of this crosspeak through ROESY but not TOCSY suggested that these resonances were located in different spin systems, confirming that the molecule featured β-alanine and N-hexanoic acid residues in an alternating fashion; this crosspeak was not visualised in analyses of compound **8.1**. Resonances at 0.84 ppm and 1.22 ppm are attributable to grease.[89]
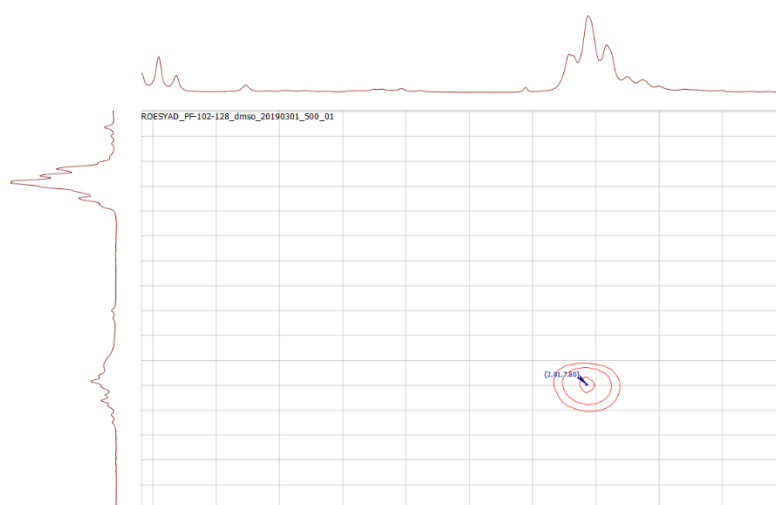
*Spectrum 15: Partial ROESY ¹HNMR spectrum of compound **14** indicating coupling between amide and methylene protons at (2.01, 7.79) ppm.*
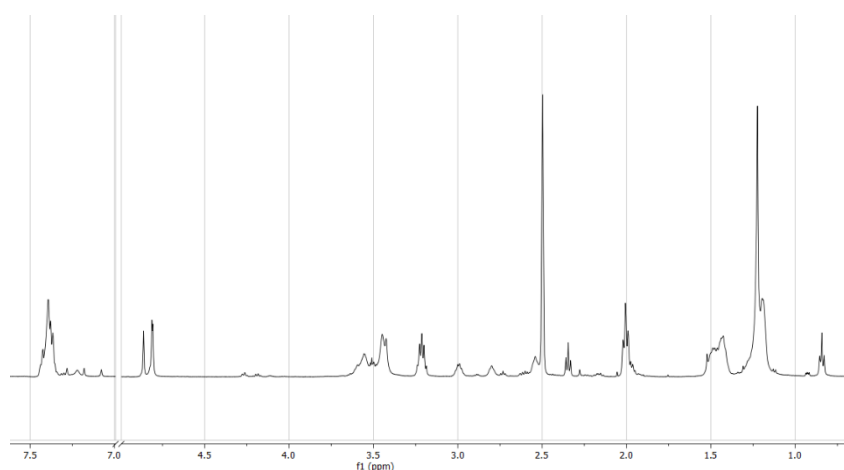
*Spectrum 16: Partial 1HNMR spectrum of compound **14**. Resonances at 0.84 and 1.22 ppm are due to grease impurities.*

The target molecules **8** and **10** were unable to be synthesised, with some evidence of intramolecular degradation. Compound **14** was successfully synthesised and characterised, suggesting the inclusion of α-amino acids in the structure of hydroxamate-based chelators leads to instability. Compound **8.1** was isolated as a pure compound and could be examined radiochemically.

3   Radiolabelling and stability assessment of novel chelator

3.1   Zirconium-89: Radiolabelling and challenge assays

The original target molecules, compounds **8** and **10**, were not successfully synthesised. Instead, compound **8.1** was isolated in sufficient purity to examine its radiochemical properties. Previous studies by Guérard *et al.* optimised the structure of zirconium bound to the simplest hydroxamate subunits - acetohydroxamic acids – using computational and experimental methods.[23,90] ^{89}Zr(ox)$_2$ was incubated with acetohydroxamic acid (AHA), N-methyl acetohydroxamic acid (Me-AHA) and DFO to assess the potential of each chelator to displace oxalic acid. The authors found that, after 30 minutes, AHA and Me-AHA had only chelated 3.5% and 20% of the ^{89}Zr in solution, compared to 99% for DFO.[23] This validated their hypothesis that the effect of the N-methyl substituent was pronounced, yet low overall binding was observed for the monohydroxamate species.
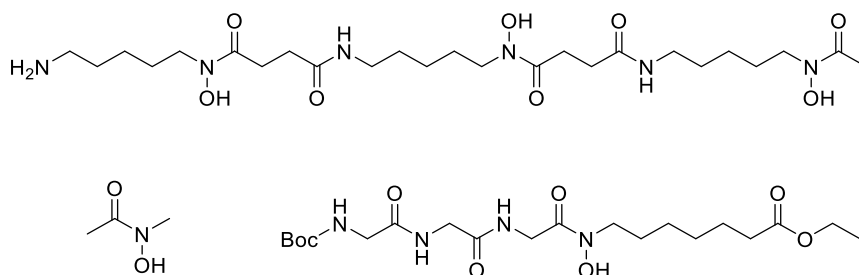
*Figure 27: DFO, N-methyl acetohydroxamic acid, and compound **8.1**.*

Compound **8.1** features several additional donor atoms compared to Me-AHA, which could feasibly facilitate binding of a greater denticity. While molecule **8.1** lacks the organisation of DFO, and will be less resistant to transchelation, it is of interest to assess the radiochemical stability of this complex.

Radiochemical assessment of chelators is performed by incubation of a chelator with a radiometal over a short period, after which the radiolabelled chelators are then subject to challenge by biologically relevant conditions. These conditions generally focus on biologically relevant criteria: incubation in serum, to measure the effect on non-specific protein binding; transchelation, to

simulate the low concentration of radiolabelled complexes *in vivo*; and transmetallation, to observe the effect of biologically relevant metals at higher concentrations. In some studies, transmetallation has focussed on a wide array of biologically relevant metal ions.[64] However, evidence from these studies has suggested that only Fe(III) causes significant demetallation of ^{89}Zr-DFO. While Al(III) displays a high affinity for DFO, it is less concentration in biological systems compared to Fe(III). As discussed earlier, the high binding constant between DFO and Fe^{3+} suggests that trivalent cations would provide the greatest competition for zirconium-89[26], and thus Fe(III) was the sole focus of our transmetallation experiments. Bovine serum albumin (BSA) is used to assess the effects of non-specific protein binding, while incubation with high concentrations of EDTA at biologically relevant pH can be used to assess transchelation.

Radio-TLC provides a simple and robust method by which to deduce the radiochemical stability of complexes.[64] This process involves the use of a trans-chelating agent at a high concentration in the mobile phase to separate unbound radioisotopes in solution from those already chelated; the TLC plates are then halved and examined to determine the ratio between the stationary (chelated) and mobile (unbound) components. Preliminary experiments were performed to confirm the TLC elution solvent; 0.1 M sodium citrate, 0.1 M ammonium acetate, and 0.1 M EDTA were used to compare radiolabelled ^{89}Zr-DFO and free ^{89}Zr^{4+}. 0.1 M EDTA was selected as the elution solvent as it resulted in consistent movement of free ^{89}Zr^{4+}, while ^{89}Zr-DFO was retained at the baseline.

3.1.1   Radiolabelling

*Table 4: Initial radiochemical yield for compound **8.1**, DFO, DOTA and DOTA-TATE labelled with [89]Zr over 2 h at 37° C (compound **8.1**, DFO) or 90° C (DOTA, DOTA-TATE), including total gamma counts for each sample.*

Time (mins)		30	60	120
8.1	*Yield*	84%	88%	86%
	Counts	152471	163132	147255
DFO	*Yield*	99%		91%
	Counts	232764		174141
DOTA	*Yield*	8.2%	7.8%	7.1%
	Counts	148412	172495	164025
DOTA-TATE	*Yield*	71%	70%	72%
	Counts	110159	101610	81458

A total of 9.79 MBq of $^{89}Zr(ox)_2$ was diluted to a volume of 400 µL with water; even aliquots of 100 µL of this solution were added to prepared solutions of 200 µL DMSO, 10 µg of the respective chelator (compound **8.1**, DFO, DOTA and DOTA-TATE), and 690 µL water. The solutions containing DOTA and DOTA-TATE were incubated at 90 °C for 45 minutes as per Pandya *et al.*,[73] then incubated at 37 °C for 75 minutes. while those containing DFO and compound **8.1** were incubated at 37 °C for 120 minutes. Radiochemical yields (the proportion of chelated to free radiometals) were assessed by radio-TLC and a gamma counter at 30, 60 and 120 minutes. The radiochemical yield can be assessed by comparing the quantity of radioactive emissions from the solvent front of each TLC plate to those on the baseline, as chelated ^{89}Zr does not migrate with the solvent front.

Analysis by radio-TLC at 30 minutes indicated that the solution containing DFO exhibited markedly higher gamma counts than the other solutions. As free $^{89}Zr^{4+}$ would migrate with the solvent front, it is possible that precipitation of $^{89}Zr^{4+}$ or ^{89}Zr-chelator complexes in the other solutions caused this effect. 100 µL aliquots of methanol were added to each solution at 30 minutes, with radiochemical yields also measured at 60 and 120 minutes. The results of radiolabelling are shown in Table 4. This led to increased radioactivity counts in the solutions containing compound **8.1** and DOTA, but not for that containing DOTA-TATE. Both DOTA and

DOTA-TATE were excluded from the following challenge assay due to the low radiolabelling yield of the former, and apparent low solubility of the latter. The results of these initial radiolabelling experiments indicated that both DFO and **8.1** formed complexes with ^{89}Zr, while DOTA did not. Challenge assays were performed on compound **8.1** and DFO as outlined below.[64] The results are summarised in Table 5, while more detailed discussions of each experiment are addressed below. Stability is presented as average total gamma counts and the proportion of complexed/uncomplexed ^{89}Zr, with calculated standard errors. Total gamma counts are only of limited use in interpreting these experiments; while they highlight some consistent differences between the solutions containing **8.1** and DFO, total counts can fluctuate significantly between TLC experiments, as they depend on the volume of radiolabelling solution applied to the TLC plate.

*Table 5: Summary of radiochemical stability experiments **3.1.2-3.1.4**. Radiochemical stability of ^{89}Zr-**8.1** and ^{89}Zr-DFO during incubation in challenge assays over 7 days at 37° C. Experiments were performed in triplicate for each group. Initial (t=0) measurements taken from radiolabelling experiment **3.1.1**.*

	% stability after incubation time											
Time (h)	**0**		**24**		**72**		**96**		**120**		**168**	
	8.1	**DFO**	**8.1**	**DFO**	**8.1**	**DFO**	**8.1**	**DFO**	**8.1**	**DFO**	**8.1**	**DFO**
Fe(III)	86	91	68 ± 2.2	99 ± 0.0	42 ± 5.3	99 ± 0.2	37 ± 3.9	96 ± 0.7	26 ± 4.2	97 ± 1.0	38 ± 6.9	96 ± 1.0
BSA	86	91	71 ± 0.6	92 ± 0.7	46 ± 1.9	91 ± 0.7	57 ± 1.6	86 ± 0.2	47 ± 3.0	85 ± 2.1	60 ± 2.2	89 ± 1.6
pH 7.4	86	91	97 ± 1.0	99 ± 0.0	87 ± 3.4	97 ± 0.4	82 ± 1.7	91 ± 2.5	83 ± 0.4	87 ± 5.7	84 ± 2.9	95 ± 0.4
pH 5	86	91	95 ± 2.0	98 ± 0.9	91 ± 2.3	96 ± 0.6	17 ± 3.3	73 ± 11	9.0 ± 2.6	66 ± 17	24 ± 8.0	65 ± 15

3.1.2   Fe(III) Challenge assay

*Table 6: Radiochemical stability and average total gamma counts for ^{89}Zr-**8.1** and ^{89}Zr-DFO, incubated for 7 days at 37 °C in 10-fold Fe(III). Initial (t=0) measurements taken from radiolabelling experiment **3.1.1**.*

Time (h)	**0**		**24**		**72**		**96**		**120**		**168**	
	8.1	**DFO**	**8.1**	**DFO**	**8.1**	**DFO**	**8.1**	**DFO**	**8.1**	**DFO**	**8.1**	**DFO**
% stability	86	91	68 ± 2.2	99 ± 0.0	42 ± 5.3	99 ± 0.2	37 ± 3.9	96 ± 0.7	26 ± 4.2	97 ± 1.0	38 ± 6.9	96 ± 1.0
Avg. total counts	7363	8707	1937	6609	2272	5807	2252	5697	1098	3545	1165	2901

Aliquots of 50 µL of the prelabelled ^{89}Zr-chelator solutions were added to solutions of 50 µL FeCl$_3$

solution (1 µM) and 300 µL PBS. The resultant solutions were incubated for 7 days at 37 °C, with

stability assessed by radio-TLC at regular intervals, as seen in Table 6.

The ^{89}Zr-**8.1** complex underwent significant demetallation over 7 days in the presence of Fe(III),

while the ^{89}Zr-DFO complex maintained stability of over 95%. The stability of the ^{89}Zr-DFO

complex is higher than reported,[64] with close clustering of results. Meanwhile, the reduced

stability of the ^{89}Zr-**8.1** complex is somewhat expected due to the decreased denticity of

compound **8.1** compared to DFO. Of note is the marked reduction in total average gamma counts

observed in samples containing the ^{89}Zr-**8.1** complex compared to those containing ^{89}Zr-DFO; as

in the radiolabelling experiment, it is postulated that insolubility contributed to this difference, as

the challenge assays contained a reduced percentage of organic solvents. It is unknown whether

the insoluble components remained chelated or as precipitated metal salts, such as the insoluble

^{89}Zr(OH)$_4$.

3.1.3   BSA challenge assay

*Table 7: Radiochemical stability and average total gamma counts for ^{89}Zr-**8.1** and ^{89}Zr-DFO, incubated for 7 days at 37 °C in 1% BSA solution. Initial (t=0) measurements taken from radiolabelling experiment **3.1.1**.*

Time (h)	0		24		72		96		120		168	
	8.1	DFO	8.1	DFO	8.1	DFO	8.1	DFO	8.1	DFO	8.1	DFO
% stability	86	91	71 ± 0.6	92 ± 0.7	46 ± 1.9	91 ± 0.7	57 ± 1.6	86 ± 0.2	47 ± 3.0	85 ± 2.1	60 ± 2.2	89 ± 1.6
Avg. total counts	7363	8707	3981	4350	4223	5789	4210	4138	2241	2235	1914	2086

Aliquots of 50 µL of the prelabelled ^{89}Zr-chelator solutions were added to solutions of 450 µL of

1% bovine serum albumin and incubated at 37° C for 7 days, in order to test the effects of non-

specific protein binding of the ^{89}Zr-chelator complexes. The resultant radiochemical stability was

assessed by radio-TLC at regular intervals; these data are shown above in Table 7.

The ^{89}Zr-**8.1** complex underwent demetallation over 7 days, with a marked reduction in metal binding observed even after 24 hours. Conversely, the ^{89}Zr-DFO complex underwent slow demetallation, remaining above 85% stable after 1 week, representing a substantially lower stability than previously reported.[64] The difference in total average gamma counts between solutions containing **8.1** and DFO was much less significant in this assay.

3.1.4 EDTA challenge assays

*Table 8: Radiochemical stability and average total gamma counts for Zr-**8.1** and Zr-DFO, incubated for 7 days at 37 °C in 100-fold EDTA at pH 7.4 or pH 5. . Initial (t=0) measurements taken from radiolabelling experiment **3.1.1**.*

	Time (h)	0		24		72		96		120		168	
		8.1	DFO	8.1	DFO	8.1	DFO	8.1	DFO	8.1	DFO	8.1	DFO
pH 7.4	% stability	86	91	97 ± 1.0	99 ± 0.0	87 ± 3.4	97 ± 0.4	82 ± 1.7	91 ± 2.5	83 ± 0.4	87 ± 5.7	84 ± 2.9	95 ± 0.4
	Avg. tot. counts	14726	17414	9199	17945	11203	23609	12454	23957	6169	16499	3936	8437
pH 5.0	% stability	86	91	95 ± 2.0	98 ± 0.9	91 ± 2.3	96 ± 0.6	17 ± 3.3	73 ± 11	9.0 ± 2.6	66 ± 17	24 ± 8.0	65 ± 15
	Avg. tot. counts	14726	17414	9714	17377	12317	28665	17432	18396	10190	13227	7044	8708

Aliquots of 100 µL of the prelabelled ^{89}Zr-chelator solutions were added to solutions containing 100 µL of 10 µM EDTA solution (approximately 100-fold) and 50 µL of PBS to assess the effects of transchelation at biologically relevant pH. One solution was maintained at pH 7.4 while the other was reduced to pH 5 by the addition of 0.05 mM HCl. These solutions were incubated at 37° C for 7 days and radiochemical stability was assessed at regular intervals by radio-TLC; these data are shown in Table 7. After 72 hours the pH of each solution was tested and corrected accordingly by the addition of 0.05 mM HCl.

At pH 7.4, both the ^{89}Zr-**8.1** complex and the ^{89}Zr-DFO complex exhibited good stability, with 84% and 95% of the complexes remaining intact after 7 days respectively. The result for the ^{89}Zr-DFO complex was comparable to the reported data.[64] The stability exhibited by the ^{89}Zr-**8.1** complex was remarkably comparable in these conditions.

Meanwhile, at ph 5, the ^{89}Zr-**8.1** complex was significantly demetallated after 7 days, while ^{89}Zr-DFO complex displayed some demetallation, reporting 24% and 65% stability respectively. Statistical error was significant particularly in the ^{89}Zr-DFO group, due in part to one sample containing ^{89}Zr-DFO which remained 93% stable after 7 days. Under both sets of conditions, the observed total counts for the ^{89}Zr-DFO group was significantly greater than for the ^{89}Zr-**8.1** group, indicating possible solubility issues. Interestingly, with the majority of the ^{89}Zr-**8.1** demetallated in pH 5 after 7 days, the differences in total counts between groups were less marked.

3.2   Gallium-68 stability studies

As previously mentioned, DFO shows affinity for Ga^{3+} ions and radiolabelling occurs quickly; however, ^{68}Ga-DFO complexes are unstable, vulnerable to transchelation and competitive metal ions (particularly Fe(III)).[28-30] The ease of production of ^{68}Ga made the radiochemical assessment of the ^{68}Ga-**8.1** complex of interest.

^{68}Ga was eluted from a ^{68}Ge/^{68}Ga generator with 0.1 M hydrochloric acid as per the reported method.[30] An aliquot of 50 µL of this solution was combined with 10 µL of selected chelators (DFO-B and compound **8.1**) and 40 µL of sodium acetate solution (0.5 M) to form standard solutions. The solutions were incubated at 37 °C for 30 minutes and binding assessed by radio-TLC; 100 µL of sodium acetate solution (0.5 M) was then added to increase the pH, and 20 µL of methanol and 10 µL of DMSO were added to both solutions.

Of these solutions, 10 µL aliquots were taken and combined with 90 µL of either 3% BSA solution or 0.1M FeCl$_3$ solution. All solutions were incubated at 37 °C for a total of 120 minutes. Binding proportion was assessed at regular intervals by radio-TLC and a gamma counter. Due to the low half-life of ^{68}Ga and the low radioactivity of each sample, radioactivity levels in some later samples

were too insignificant to be detected above background levels. The stability values are presented

below in Table 9.

Table 9: Radiochemical stability of ^{68}Ga-chelator complexes over 2 hours as percentage bound ^{68}Ga.

Time (mins)	30		60		120	
	DFO	8.1	DFO	8.1	DFO	8.1
Standard	74 ± 17	53 ± 21	97 ± 0.4	35 ± 12	97 ± 0.5	15 ± 6.3
Fe³⁺	17 ± 9	10 ± 4.1	9.1 ± 1.4	5.5 ± 2.2	7.6 ± 6.3	-
BSA	78 ± 20	62 ± 18	7.3 ± 1.4	36 ± 29	28 ± 13	40

As apparent in Table 9, in the standard solutions the ^{68}Ga-DFO complex was particularly stable,

recording 97% stability after 2 hours; meanwhile the ^{68}Ga-**8.1** complex was only partly formed

and its stability deteriorated to 15% after 2 hours. The poor performance of compound **8.1** in this

assay demonstrated its unsuitability for use with ^{68}Ga.

In the presence of Fe^{3+} ions, both the ^{68}Ga-DFO complex and ^{68}Ga-**8.1** complex were shown to

be highly unstable, undergoing rapid demetallation after the first 30 minutes. The data observed

for the ^{68}Ga-DFO complex showed decreased stability compared to reported data.[29] There was

insufficient radiation after 2 hours in samples of the ^{68}Ga-**8.1** complex; however extensive

demetallation of this complex had already occurred after 1 hour.

Both complexes displayed poor stability in solutions containing 3% BSA; an average of only 28%

of the ^{68}Ga-DFO complex remained intact, while the sole sample of the ^{68}Ga-**8.1** complex

containing measurable quantities of radiation remained 40% intact. As this sample was an outlier

during the 30- and 60-minute measurements, this data is unlikely to be accurate. The results

observed for ^{68}Ga-DFO were again markedly lower than previously reported.[29]

The above data does not suggest either chelator is suitable for therapeutic use with ^{68}Ga.

4   Conclusions and future directions

The above work has uncovered some new information with regards to the syntheses of hydroxamate-based chelators. Through the attempted syntheses of compounds **8** and **10**, it was demonstrated that chelators containing α-amino acids are susceptible to intramolecular degradation. Previous works on similar molecules had hinted at such an effect without further examination.[68] This degradation ultimately led to the synthesis of the tripeptide, monohydroxamate compound **8.1**. It is likely that the basicity of the peptide coupling reactions combined with lengthy reaction times amplified this degradation. Other previously unreported instabilities were observed under basic conditions, particularly during attempted deesterification, further hindering synthesis.

Meanwhile, compound **14** was successfully synthesised by solid-phase peptide synthesis with no signs of intramolecular degradation. While only 10 mg of the chelator was synthesised, only low quantities are required for use as radiotherapeutics. This synthesis verified the potential of SPPS in forming these compounds, while also giving credence to the hypothesis that α-amino acids are the origin of instability in compounds such as **8**.

Radiochemical assessment was undertaken on compound **8.1** to determine its binding affinities for zirconium-89 and gallium-68 compared to DFO. While **8.1** was outperformed by DFO in both functions as expected, it showed surprising radiochemical stability as a zirconium-89 chelator, with good resistance to EDTA observed at neutral pH. Given the low stability of monohydroxamate units in conjunction with zirconium-89,[23] this suggests that complexation is occurring between other groups of **8.1** and zirconium-89.

Ultimately, these observations affirm the superior stability of zirconium-89 chelators containing β-amino acids. However, it also gives basis for the future syntheses of chelators **8** and **10**: the addition of HOBt has been shown to reduce the formation of aspartimide-like side products during SPPS,[91] and the reduced reaction time required for SPPS could help reduce the formation of side-products. While the use of SPPS results in low yields, it could be useful to synthesise linear chelators such as **8** and **10**. Further work would naturally also include the substitution of other α-amino acids into these chelators to create a more diverse library of compounds.

5 Appendices

5.1 Experimental

5.1.1 Materials

All reagents were obtained from Chem-Impex international unless specified below. Ethyl acetate, methanol, dichloromethane, lithium hydroxide, and N-N-dimethylformamide were obtained from Merck. Isopropanol, acetone, acetic acid, hydrochloric acid, sodium sulfate and toluene from Chemsupply; chloroform and tetrahydrofuran from RCI Labscan, and HPLC-grade methanol and acetone from Ajax Finechem. Benzyloxy(tert-butoxycarbonyl)amine, ethyl 7-bromo heptanoate, N-N-diisopropylamine, DFO-B, sodium hydride, EDTA, BSA and trifluoroacetic acid were obtained from Sigma Aldrich. HEPES, PBS and sodium acetate were obtained from Gibco. TraceSelect™ water was obtained from Honeywell.

All commercially purchased reagents were used without further purification.

5.1.2 Analysis

5.1.2.1 Analytical Methods

Analysis by TLC was performed on TLC Silica gel 60 F_{254} obtained from Merck, eluting with ethyl acetate/hexane or methanol/DCM as specified. TLC plates were observed under UV radiation at 254nm and staining was performed with 6% w/v vanillin in EtOH, CAM solution or $KMnO_4$ solution. Purity of products was assessed by reverse-phase HPLC using a Phenomenex Luna C18(2) column over a gradient of 50-95% aq. ACN over 15 minutes unless otherwise stated. Product formulae were confirmed by HRMS on an Agilent 6230 ESI-TOF LCMS, and low-resolution mass spectrometry was performed with an Agilent 1260 Infinity LCMS.

5.1.2.2 NMR Spectroscopy

All NMR spectra were acquired using an Agilent spectrometer (Agilent DD2 Console) in 100% $CDCl_3$, 100% DMSO-D6, or 100% CD_3OD at 298° K. ^{1}HNMR were obtained at 500 MHz and ^{13}CNMR were obtained at 125 MHz. Chemical shifts are reported in ppm based on tetramethylsilane.

5.1.2.3 Purification

Normal phase column chromatography was performed with silica gel 60 obtained from Carl Roth Gmbh, while reverse phase column chromatography was performed on 60A C_{18} gel obtained from Silicycle; flash chromatography was performed under positive pressure from nitrogen gas. Purification by HPLC was undertaken with Gilson Semi-preparatory RP-HPLC using a Supelco Discovery BIO Wide Pore C18 column over 45-60% aq. ACN over 20 minutes.

5.1.2.4 Radio-TLC experiments

Radioligand stability was determined by elution on iTLC-SG chromatography paper (obtained from Agilent) in 0.1M EDTA solution; measurement of emissions occurred by HIDEX Multi-Channel Analyser and Scanram TLC/HPLC Analyser. [68]Ga was produced by an Eckert & Ziegler Model IGG100 [68]Ge/^{68}Ga generator.

Zirconium-89 was produced as per Holland *et al.* A 99.9% pure [89]Y foil target (0.15 x 0.25 mm, 99.9% pure), purchased from American Elements, was bombarded with a proton beam of 16.9 MeV and 30 µA for 300 minutes on a GE PETtrace 880 cyclotron with a Comecer Taddeo purification system.[16] The target was dissolved in 6 M hydrochloric acid; the solution was diluted with water to reach a concentration of 2M. The zirconium-89-containing solution was then purified by an automatic cassette. The zirconium-89-containing solution was placed into a column containing hydroxamate resin and washed with 2 M hydrochloric acid (x4, 2.5 mL) to remove excess Y^{3+}. Zirconium-89 was removed from the column by addition of 1.0 M oxalic acid.

5.1.3   Syntheses
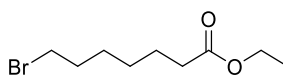
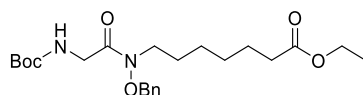### 1.   Ethyl 7-((benzyloxy)(tert-butoxycarbonyl)amino)heptanoate

To a solution of *tert*-butyl N-(benzyloxy)carbamate (0.447 g, 2.0 mmol) in DMF (5 mL) was added 60% NaH in mineral oil (0.088 g, 2.2 mmol) and the mixture was stirred for 15 minutes on ice. To the mixture was added ethyl 7-bromo heptanoate (0.593 g, 0.49 mL, 2.5 mmol) dropwise, and the resulting solution was stirred for 20 hours at RT. H_2O (20 mL) was added and the solution was extracted with ethyl acetate (3 x 10 mL). The organic eluents were combined and washed with saturated sodium chloride solution (3 x 20 mL). The organic solvent was removed under reduced pressure yielding a crude product of mass of 0.650 g. The crude product was purified by column chromatography using 1:4 ethyl acetate:hexane to yield a clear gum (0.524 g, 69%).

To a solution of *tert*-butyl N-(benzyloxy)carbamate (3.350 g, 15 mmol) in DMF (75 mL) was added 60% NaH in mineral oil (0.600 g, 15 mmol) and the mixture was stirred for 30 minutes on ice. To the mixture was added ethyl 7-bromo heptanoate (4.450 g, 3.70 mL, 19 mmol) dropwise, and the resulting solution was stirred for 20 hours at 60°C. The solvent was removed under reduced pressure and the products dissolved in ethyl acetate (50 mL) and washed with water (3 x 50 mL) and saturated sodium chloride solution (2 x 50 mL). The organic layer was dried with Na_2SO_4 and removed under reduced pressure to yield a crude oil of mass 5.513 g. The crude product was purified by column chromatography using 1:9 acetone:hexane to yield **(1)** as a clear oil (3.672 g, 64%).

^{1}HNMR (CDCl$_3$ 500 MHz) δ 7.33 – 7.41 (5H, m); 4.82 (2H, s); 4.12 (2H, q); 3.40 (2H, t); 2.28 (2H, t); 1.57 – 1.64 (4H, m); 1.51 (9H, s); 1.28 - 1.35 (4H, m); 1.25 (3H, t).

^{13}CNMR (CDCl$_3$ 125 MHz) δ 176.38, 159.25, 138.37, 131.05, 83.77, 62.81, 52.21, 36.93, 31.47, 31.00, 29.55, 29.08, 27.52, 16.90.

HRMS: *m/z* = 379.24 [M + H] 380.2429, [M + Na$^+$] 402.2260.

HPLC: 21.89 mins.

3. Ethyl 7-(N-(benzyloxy)-2-((tert-butoxycarbonyl)amino)acetamido)heptanoate

Ethyl 7-((benzyloxy)(tert-butoxycarbonyl)amino)heptanoate **(1)** (1.840 g, 4.8 mmol) was dissolved in dichloromethane (4 mL) and to this was added TFA (1 mL). The resultant solution was stirred for 2 h at RT. The solvent was removed under nitrogen gas and then under reduced pressure to give ethyl 7-((benzyloxy)amino)heptanoate **(2)** as a brown gum (1.345 g, 100%).

^{1}HNMR (CDCl$_3$ 500 MHz) δ 10.54 (4H, ws), 7.35 – 7.45 (5H, m), 5.10 (2H, s), 4.15 (2H, q) 3.31 (2H, t), 2.31 (2H, t), 1.76 (2H, quint.), 1.61 (2H, quint.), 1.35 (4H, m), 1.26 (3H, t).

LRMS: *m/z* = 279.18, [M + H] 280.2.

HPLC: 5.88 mins

To a sample of Ethyl 7-((benzyloxy)amino)heptanoate **(2)** (1.345 g, 4.8 mmol) was added a solution of Boc-glycine (1.019 g, 5.8 mmol), HATU (2.212 g, 5.8 mmol) and DIPEA (3.80 mL, 22 mmol) in DMF (15 mL). The resultant solution was stirred for 16 hours at room temperature and monitored by TLC. The solution was neutralised with NaHCO$_3$ (20 mL) and extracted with ethyl acetate (3 x 20 mL). The organic extracts were combined and washed with H$_2$O (3 x 20 mL) and brine (5 x 20mL), dried with Na$_2$SO$_4$ and the solvent removed under reduced pressure to yield a brown oil (2.409 g, crude). This oil was purified by column chromatography using 0:1 → 3:7 EtOAc:hexane to yield Ethyl 7-(N-(benzyloxy)-2-((tert-butoxycarbonyl)amino)acetamido)heptanoate **(3)** as a yellow oil (1.790 g, 70%).

^{1}HNMR (CD$_3$OD 500 MHz) δ 7.42 (5H, m), 4.93 (2H, s), 4.11 (2H, q), 3.97 (2H, s), 3.67 (2H, t), 2.29 (2H, t), 1.55 – 1.70 (4H, m), 1.46 (9H, s), 1.33 (4H, m), 1.24 (3H, t).

^{13}CNMR (CD$_3$OD 125 MHz) δ 176.76, 159.80, 137.27, 131.84, 131.30, 131.00, 78.68, 62.62, 43.97, 36.22, 30.91, 29.97, 28.53, 27.11, 15.80.

HRMS: *m/z* = 436.26 [M+H]; 475.22 [M+K]. [M+H] = 437.2633, [M+K$^+$] = 475.2192.

HPLC: 17.41 mins.
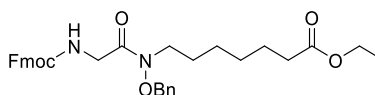
3.1. Ethyl 7-(N-(benzyloxy)-2-((fluorenylmethyloxycarbonyl)amino)acetamido)heptanoate

To a sample of Ethyl 7-((benzyloxy)amino)heptanoate **(2)** (0.139 g, 0.5 mmol) was added a solution of Fmoc-glycine (0.156 g, 0.5 mmol), HATU (0.224 g, 0.6 mmol) and DIPEA (0.340 mL, 2.0 mmol) in DMF (4 mL). The resultant solution was stirred for 16 hours at room temperature and monitored by TLC. The solution was neutralised with $NaHCO_3$ (20 mL) and extracted with ethyl acetate (3 x 20 mL). The organic extracts were combined and washed with H_2O (3 x 20 mL) and brine (5 x 20mL), dried with Na_2SO_4 and the solvent removed under reduced pressure to yield a brown oil (0.252 g, crude). This oil was purified by column chromatography using 0:1 $\rightarrow$ 3:7 ethyl acetate/hexane to yield the intermediate ethyl 7-(N-(benzyloxy)-2-((fluorenylmethyloxycarbonyl)amino)acetamido)heptanoate **(3.1)** as a yellow oil (0.194 g, 69%).

^{1}HNMR ($CDCl_3$ 500 MHz) δ 7.77 (2H, d), 7.62 (2H, d), 7.29 – 7.46 (9H, m), 4.87 (2H, s), 4.39 (2H, d), 4.26 (1H, t), 4.10 – 4.18 (4H, m), 3.67 (2H, t), 2.29 (2H, t), 1.58 – 1.71 (4H, m), 1.29 – 1.40 (4H, m), 1.26 (3H, t).
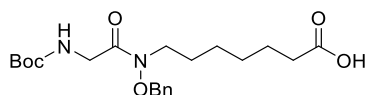
4a. Ethyl 7-(N-(benzyloxy)-2-((tert-butoxycarbonyl)amino)acetamido)heptanoic acid

A sample of Ethyl 7-(N-(benzyloxy)-2-((tert-butoxycarbonyl)amino)acetamido)-heptanoate **(3)** (0.370 g, 0.8 mmol) was dissolved in THF (5 mL) and cooled on ice. To this was added 1M LiOH solution (5.10 mL). The reaction was stirred on ice for 15 minutes, then stirred at room temperature for a further 20 h. The solution was neutralised by the addition of 2M HCl (3 mL) and was extracted with ethyl acetate (3 x 20 mL); the organic eluents were dried with Na_2SO_4 and removed under reduced pressure to yield a clear oil (0.234 g, crude). The crude product was purified by column chromatography using 1:1 EtOAc/hexane with 1% AcOH to yield **4a** as a yellow oil (0.079 g, 23%).

^{1}HNMR (CDCl$_3$ 500 MHz) δ 7.39 (5H, s), 4.84 (2H, s), 4.08 (2H, s), 3.64 (2H, s), 2.33 (2H, t), 1.63 (4H, m), 1.46 (9H, s), 1.33 (4H, m).

^{13}CNMR (CD$_3$OD 125 MHz) δ 131.84, 131.30, 131.00, 81.82, 78.69, 43.97, 36.07, 30.98, 29.97, 28.78, 28.59, 27.15.

HPLC: 18.236 min (10-100% MeOH over 15 minutes).
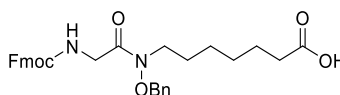
4c.   Ethyl 7-(N-(benzyloxy)-2-((fluorenylmethyloxycarbonyl)amino)acetamido)

heptanoic acid

Attempted

Fmoc-Gly-ethyl heptanoate (0.046 g, 0.083 mmol) was dissolved in anhydrous THF (2 mL) and

combined with MgI_2 (0.115 g, 0.41 mmol). The resultant mixture was heated to 120°C by

microwave radiation for 2 hours. The solution was neutralised by addition of 0.1M sodium

thiosulfate solution (2 mL); analysis by ^{1}HNMR found that compound **4c** was not successfully

produced.

Fmoc-Gly-ethyl heptanoate (0.030 g, 0.054 mmol) was dissolved in IPA (3.5 mL); to this was

added a solution of LiOH (0.005 g, 0.22 mmol) in H_2O (1.5 mL). To this overall solution was added

$CaCl_2$ (0.278 g, 2.5 mmol) to bring the solution to a concentration of 0.5M. This reaction was

stirred for 21 h and monitored by TLC, then neutralised by addition of 1M HCl (1 mL). The solution

was extracted with EtOAc (3 x 20 mL) and the organic eluents were washed with brine (3 x 20

mL) and dried with Na_2SO_4. Analysis of the crude organic extracts by ^{1}HNMR showed the reaction

had not progressed.
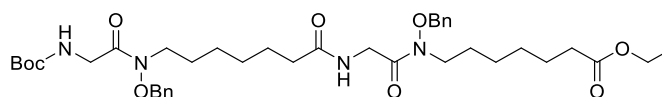
5. Ethyl 7-(N-(benzyloxy)-2-((tert-butoxycarbonyl)amino)acetamido)heptanoate

To compound **3** (0.280 g, 0.6 mmol) was added a solution of 20% TFA in DCM (10 mL) and the resultant solution was stirred for 2 hours. The progress of the reaction was monitored by TLC. The TFA/DCM solution was subsequently removed by nitrogen gas and under reduced pressure, yielding compound **4b** as a brown oil (0.216 g, 100%).

^{1}HNMR (CDCl$_3$ 500 MHz) δ 7.37 (5H, d), 4.82 (2H, s), 4.10 (2H, q), 3.88 (2H, s), 3.63 (2H, s), 2.27 (2H, t), 1.57 (4H, m), 1.26 (7H, m).

HPLC: 5.59 mins.

To a sample of **4b** (0.216 g, 0.6 mmol) was added a solution of compound **4a** (0.270 g, 0.7 mmol), HATU (0.302 g, 0.8 mmol) and DIPEA (0.6 mL, 3.4 mmol) in DMF (4 mL); further DIPEA (0.5 mL, 2.9 mmol) was added to quench residual TFA and increase the solution pH. The solution was stirred for 48 hours and the progress monitored by TLC; at the 24-hour mark, more HATU (0.1 g, 0.2 mmol) and DMF (2.0 mL) was added. The reaction was quenched with sodium hydrogen carbonate (30 mL) and extracted with ethyl acetate (3 x 20 mL). The organic eluents were combined and washed with water (20 mL) and saturated sodium chloride solution (5 x 20 mL); following this they were dried with sodium sulfate and the solvent was removed under reduced pressure to yield a yellow oil (0.320 g, crude). This was purified by flash chromatography (1:1 ethyl acetate/hexane) to yield compound **5** as a clear oil (m = 0.028 g). The remaining crude solution was purified again by flash chromatography (7:3 ethyl acetate/hexane) yielding compound **5** as a clear oil (0.072 g), and both eluents were combined (0.100 g, 21%).

¹HNMR (CD₃OD 500 MHz) δ 7.38 – 7.46 (10H, m), 4.82 (4H, s), 4.10 (2H, q), 4.09 (2H, S), 3.98 (2H, s), 3.67 (4H, d), 2.29 (2H, t), 1.51 – 1.69 (8H, m), 1.46 (9H, s), 1.26 – 1.40 (8H, m), 1.24 (3H, t).

¹³CNMR (CD₃OD 125 MHz) δ 177.85, 176.70, 171.41, 159.76, 137.28, 131.90, 131.86, 131.33, 131.02, 130.71, 130.40, 130.17, 81.79, 78.67, 62.63, 47.78, 44.02, 42.87, 41.58, 37.99, 37.95, 36.24, 31.35, 31.04, 30.96, 30.93, 30.02, 29.92, 28.78, 28.60, 28.56, 27.96, 27.88, 27.12, 15.86.

HRMS: *m/z* = 726.42 [M+H], 749.41 [M+Na]; [M+H] = 727.4280, [M+Na] = 749.4098.

HPLC: 18.15 mins
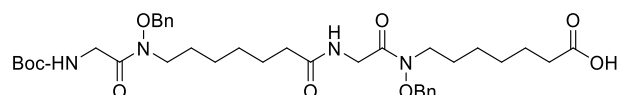
6a. Attempted

Compound **5** (0.080 g, 0.1 mmol) was dissolved in THF (0.7 mL) and cooled on ice. To this solution was added 1M LiOH solution (0.66 mL) and the resultant solution was stirred for 12 hours. The excess LiOH was neutralised and the solution acidified by addition of HCl (1 mL) and H_2O (10 mL), before extraction with ethyl acetate (3 x 20 mL). The organic eluents were dried with Na_2SO_4 and the solvent removed under reduced pressure to yield a clear oil (0.065 g, crude). The crude product was unable to be purified by column chromatography using 1:24 MeOH/DCM, with the reaction yielding a mixture of by-products.
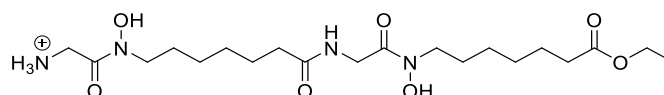
6b. To a solution of compound **5** (0.075 g, 0.1 mmol) in DCM (6 mL) was added TFA (1.5 mL) and the solution was stirred for 2 hours. The TFA was removed by nitrogen gas and under reduced pressure yielding **6b** as a brown oil (0.076 g, 100%).

^{1}H NMR (CD$_3$OD 500 MHz) δ 7.42 (10H, m), 4.94 (4H, s), 4.13 (6H, m), 3.75 (3H, s), 3.69 (3H, m), 2.29 (4H, t), 1.62 (8H, m), 1.32 (8H, m), 1.23 (3H, t).

^{13}CNMR (CD$_3$OD 125 MHz) δ 176.82, 169.16, 162.13, 161.82, 161.51, 161.20, 137.17, 132.53, 132.07, 131.91, 131.88, 131.40, 131.34, 131.16, 131.05, 131.03, 119.25, 116.96, 78.67, 62.66, 50.79, 50.62, 50.56, 50.45, 50.28, 50.11, 49.94, 49.77, 43.00, 42.87, 42.78, 40.16, 37.92, 36.23, 34.30, 33.08, 32.17, 32.05, 31.98, 31.70, 31.35, 31.00, 30.91, 30.90, 28.71, 28.54, 28.51, 27.93, 27.84, 27.09, 24.97, 15.79, 15.69.

HPLC: 5.39 mins.
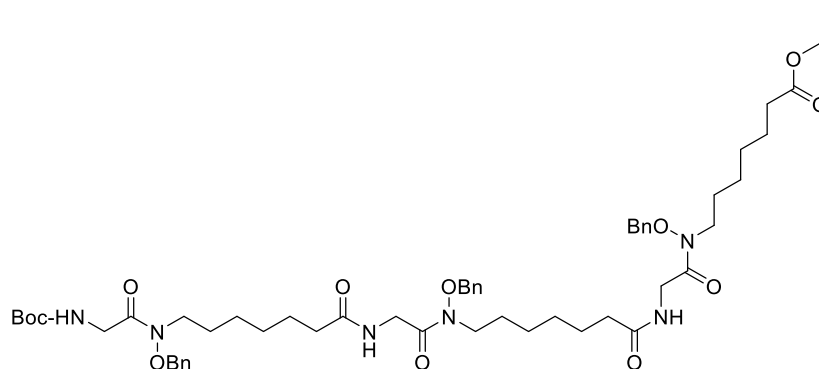
7.   Compound **4a** (0.079 g, 0.2 mmol) was combined with HATU (0.110 g, 0.3 mmol), DIPEA (0.17 mL, 1.0 mmol) and DMF (2 mL) and mixed vigorously for 2 minutes. To this solution was then added compound **6b** (0.076 g) in DMF (2 mL) and the resultant solution was stirred at room temperature for 40 hours. At the 24-hour mark, HATU (0.040 g, 0.1 mmol) and DIPEA (0.04 mL, 0.2 mmol) were added to the reaction mixture based on analysis by TLC. The solution was neutralised by addition of $NaHCO_3$ (5 mL) and H_2O (10 mL) and extracted with ethyl acetate (3 x 20 mL); the organic extracts were combined, washed with brine (5 x 20 mL) and dried with Na_2SO_4. The solvent was removed *in vacuo* to yield a clear oil (0.114 g, crude). Flash chromatography was performed using 1:24 MeOH/DCM to give a mixture of **7**, **7.1** and **7.2** based on HRMS (0.066 g).

HRMS: m/z: 1016.58; [M+H] 1017.6085, 784.4766, 551.3237.

^{1}HNMR (CD_3OD 500 MHz) of mixture δ 7.45 - 7.40 (m), 4.95 (s), 4.05 – 4.17 (m), 3.94 (s), 3.75 (s), 3.68 (t), 2.29 (t), 1.55 – 1.70 (m), 1.46 (s), 1.31 – 1.40 (m), 1.23 (t).

^{13}CNMR (CD_3OD 125 MHz) of mixture δ 176.73, 174.34, 131.89, 131.35, 131.02, 78.70, 62.63, 46.16, 44.62, 42.85, 36.23, 30.91, 29.98, 28.74, 28.53, 27.09, 15.81.

HPLC: 11.16 mins.
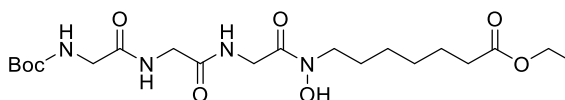
8.1.   The mixture containing compounds **7**, **7.1** and **7.2** (0.032 g) was dissolved in ethyl acetate (1 mL) and was stirred under a nitrogenous atmosphere. To this was added Pd/C (60% w/w, 0.020 g) in ethyl acetate (2 mL) and air was again evacuated from the reaction vessel by nitrogen gas. The atmosphere was saturated with H_2 at 1atm and the solution was stirred overnight. To this solution was added TraceSelect™ water (1 mL) and the solution was filtered. The solvent was removed under reduced pressure to yield **8.1** as a clear gum (m = 0.025 g, 100%).

^{1}HNMR (DMSO 500 MHz) δ 8.01 (1H, t), 7.86 (1H, t), 6.97 (1H, t), 4.04 (2H, q), 3.98 (2H, d), 3.74 (2H, d), 3.57 (2H, d), 3.45 (2H, t), 2.26 (2H, t), 2.07 (s, acetonitrile), 1.42 – 1.55 (5H, m), 1.38 (9H, s), 1.19 – 1.31 (10H, m), 1.17 (3H, t), 0.85 (1H, t).

^{13}C NMR (DMSO 125 MHz) δ 175.98, 172.73, 172.14, 171.65, 121.16, 81.23, 62.76, 50.57, 46.42, 45.03, 36.58, 31.32, 31.23, 29.14, 28.84, 27.49, 17.25, 17.05, 4.26.

MS: *m/z* = 460.25, 483.24; [M+H] = 461.3 [M+Na] = 483.2442.

HPLC: 5.66 min.
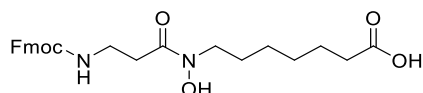
12.   Compound **1** (1.00 g, 2.6 mmol) was dissolved in acetone (10 mL) to which was added 32% hydrochloric acid solution (2.9 mL, 30 mmol) and stirred for 16 hours. The solution was diluted by the addition of acetone (40 mL) and the solvent removed under reduced pressure to yield the deprotected compound **12** as a crude mixture (0.486 g, 68%,).

^{1}HNMR (CD$_3$OD 500 MHz) δ 7.42 – 7.49 (5H, m), 5.13 (2H, s), 4.12 (0.3 H, q), 3.34 (2H, t), 2.31 (2H, t), 1.76 (2H, p), 1.63 (2H, p), 1.35 – 1.49 (4H, m), 1.24 (0.6H, t).

LRMS: *m/z* = 251.15, [M+H] = 252.1

The crude compound **12** was subsequently dissolved in DMF (5 mL) to which was added a precombined mixture of Fmoc-β-Alanine (1.115 g, 3.5 mmol), HATU (1.362 g, 3.6 mmol), and DIPEA (3.12 mL, 18 mmol) in DMF (24 mL); the resultant solution was stirred for 16h under inert atmosphere and monitored by TLC. The reaction was ended by the removal of solvent under reduced pressure and the resultant oil dissolved in ethyl acetate (50 mL); this organic extract was washed with saturated ammonium chloride solution (3 x 20 mL) and brine (5 x 20 mL). The organic solvent was removed under reduced pressure and the crude orange oil was purified by reverse-phase column chromatography (60% ACN/H$_2$O) to yield **13** as an orange oil (0.440 g, 23%).

^{1}HNMR (DMSO 500 MHz) δ 7.77 (2H, d), 7.60 (2H, d), 7.28 – 7.42 (9H, m), 4.79 (2H, s), 4.36 (2H, d), 4.21 (1H, t), 3.67 (2H, t), 3.48 (2H, m), 2.65 (2H, m), 2.33 (2H, t), 1.59 – 1.69 (4H, m), 1.28 – 1.40 (4H, m).

^{13}CNMR (CDCl$_3$ 125 MHz) δ 146.61, 143.95, 131.88, 131.78, 131.45, 130.34, 129.70, 127.79, 122.62, 79.93, 79.68, 79.42, 79.02, 69.52, 49.86, 36.21, 35.29, 31.17, 29.20, 28.90, 27.11.

HRMS: m/z = 544.26, 567.25; [M+H] = 545.2641, [M+Na] = 567.2461.
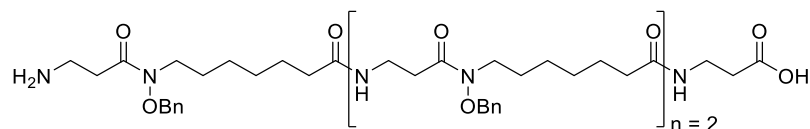
14.   2-chlorotrityl resin (2.000 g, 1.15 mmol/g) was weighed and swelled in anhydrous DCM (15 mL) for 15 minutes. Fmoc-protected-β-alanine (2.3 mmol, 1 eq.) was dissolved in anhydrous DCM (15 mL) and DIPEA (2 mL, 11.5 mmol, 5 eq.) The amino acid solution was added to the resin and the solution shaken. The mixture was agitated to 2 hours and MeOH (5 mL) was added; the resultant solution was further rocked for 30 minutes. The solvent was removed and the resin washed with DMF (5 x 10 mL), DCM (2 x 10 mL), DMF (2 x 10 mL) and DCM (5 x 10 mL), with the resin then dried by washing with diethyl ether (5 x 10 mL). The remaining solvent was left to dry overnight and the loading calculated, yielding a final loading of 0.44 mmol/g. The resin was deprotected by addition of a 0.1M solution of HOBt in 20% piperidine/DMF (2 x 5 mL).

Compound **12** (0.163 g, 0.3 mmol) was combined with DMF (10 mL), PyOxim (0.158 g, 0.3 mmol) and DIPEA (0.193 mL, 1.5 mmol, 5 eq) and agitated for 10 minutes. This solution was added to the resin and incubated for 6 hours with occasional stirring. The solvent was removed, and the resin washed with DMF (3 x 10 mL), DCM (3 x 10 mL) and DMF (3 x 10 mL). Coupling completion was assessed by the Kaiser test.[88] The Fmoc-protecting group was cleaved by by addition of a 0.1M solution of HOBt in 20% piperidine/DMF (2 x 5 mL); deprotection was again assessed by the Kaiser test. This coupling and deprotection procedure was repeated a total of 3 times.

The resin was cleaved by addition of a solution of 95/2.5/2.5 TFA/TIPS/H_2O for 10 minutes and the solvent collected and extracted by addition of diethyl ether. The solvent was removed by rotary evaporation. The crude compound was purified by semi-preparative HPLC (45:55 → 60:40 ACN/H_2O) and lyophilised to yield compound **14** as a white crystalline solid (0.010 g).

^{1}HNMR (DMSO 500 MHz) δ 7.83 (1H, t), 7.79 (2H, t), 7.76 (2H, bs), 7.33 – 7.46 (15H, m), 4.86 (2H, s), 4.81 (4H, m), 3.53 – 3.66 (6H, m), 3.17 – 3.26 (6H, m), 2.95 – 3.04 (2H, m), 2.76 – 2.84

(2H, t), 2.51 – 2.58 (4H, m), 2.35 (2H, t), 2.01 (6H, t), 1.38 – 1.54 (12H, m), 1.22 (16H, s), 1.15 – 1.22 (12H, m), 0.84 (3H, t).

^{13}CNMR (DMSO 125 MHz) 176.03, 175.41, 132.78, 132.48, 132.42, 131.80, 131.66, 131.60, 43.07, 42.90, 42.74, 42.57, 42.40, 42.23, 42.07, 38.33, 38.22, 37.85, 37.68, 37.04, 34.39, 32.12, 31.90, 31.81, 31.77, 31.67, 31.35, 29.02, 28.27, 28.24, 25.19.

LRMS: *m/z* = 1001.58 [M+H] = 1002.8.

HPLC = 9.6 minutes (45-60% ACN/H_2O, 15 min).

5.1.4   Experimental

5.1.4.1 Zirconium-89 Radiolabelling

Zirconium oxalate (9.79 MBq) was neutralised with 1M sodium carbonate (100 µL) and the solution diluted to 400 µL with water.

Desferrioxamine-B (1 mg, 1.8 µmol) was dissolved in water (1 mL); 10 µL of this solution was combined with DMSO (200 µL), water (690 µL) and the diluted $^{89}Zr(ox)_2$ solution (100 µL). The resultant solution was incubated at 37 °C for 120 minutes.

Compound **8.1** (1 mg, 2.1 µmol) was dissolved in water (1 mL); 10 µL of this solution was combined with DMSO (200 µL), water (690 µL) and the diluted $^{89}Zr(ox)_2$ solution (100 µL). The resultant solution was incubated at 37 °C for 120 minutes.

DOTA (1 mg, 2.5 µmol) was dissolved in water (1 mL); 10 µL of this solution was combined with DMSO (200 µL), water (690 µL) and the diluted $^{89}Zr(ox)_2$ solution (100 µL). The resultant solution was incubated at 90 °C for 45 minutes and at 37 °C for a further 75 minutes.

DOTA-TATE (1 mg, 0.7 µmol) was dissolved in water (1 mL); 10 µL of this solution was combined with DMSO (200 µL), water (690 µL) and the diluted $^{89}Zr(ox)_2$ solution (100 µL). The resultant solution was incubated at 90 °C for 45 minutes and at 37 °C for a further 75 minutes.

Radiolabelling proportions were assessed by radio-TLC and a gamma counter at 30, 60 and 120 minutes. 100 µL aliquots of methanol were added to each solution at 30 minutes.

Radio-TLC involves the spotting of radiochemical solutions onto a paper medium before elution with a predetermined solvent (0.1M EDTA solution). After elution, gamma counts are measured for the baseline and solvent front and compared to assess the proportion of chelated radiometal. The average of total gamma counts and calculated standard errors across each sample are presented for each challenge assay.

5.1.4.2 Zirconium-89 Challenge Assays

The radiolabelled chelators were incubated for 7 days in the following solutions: (i) 100-fold EDTA at pH 7.4; (ii) 100-fold EDTA at pH 5.0; (iii) in 1% BSA solution; (iv) with 10-fold Fe^{3+}. Triplicate solutions were prepared for each set of conditions, with results presented as average proportions with calculated standard errors. Radiolabelling proportions were assessed by radio-TLC at regular intervals. Elution of TLC was performed in 0.1M EDTA solution.

Fe(III): Aliquots of 50 µL of the prelabelled ^{89}Zr-chelator solutions were added to solutions of 50 µL FeCl$_3$ solution (1 µM) and 300 µL PBS. The resultant solutions were incubated for 7 days at 37 °C.

BSA: Aliquots of 50 µL of the prelabelled ^{89}Zr-chelator solutions were added to solutions of 450 µL of 1% bovine serum albumin and incubated at 37° C for 7 days.

EDTA (pH 7.4): Aliquots of 100 µL of the prelabelled ^{89}Zr-chelator solutions were added to solutions containing 100 µL of 10 µM EDTA solution (approximately 100-fold) and 50 µL of PBS. These solutions were incubated at 37° C for 7 days.

EDTA (pH 5): Aliquots of 100 µL of the prelabelled ^{89}Zr-chelator solutions were added to solutions containing 100 µL of 10 µM EDTA solution (approximately 100-fold) and 50 µL of PBS. These solutions were incubated at 37° C for 7 days. To each solution was added 0.05 mM HCl (1 µL) to reduce the pH to 5. After 72 hours further 0.05M HCl (1 µL) was added to each solution to maintain pH at 5.

5.1.4.3 ^{68}Ga radiolabelling

^{68}GaCl$_3$ (700 μL, 4.79MBq) was eluted from a ^{68}Ge/^{68}Ga generator with 0.1 M HCl. 50 μL aliquots of this solution were incubated with 10 μL solutions of the chelators DFO-B (1 μg/μL in H$_2$O) and **8.1** (1 μg/μL in MeOH) and 0.5M sodium acetate (40 μL) at 37 °C for 30 minutes. To each solution was added a further 100 μL of 0.5M sodium acetate. ^{68}Ga-complex formation was measured by radio-TLC by elution with 0.1 M citric acid. The solutions were incubated for a further 90 minutes with radio-TLC performed at 60 and 120 minutes.

5.1.4.4 ^{68}Ga challenge assay

10 μL aliquots of the above solutions were combined with 90 μL of either 0.1M FeCl$_3$ solution or 3% bovine serum albumin solution and incubated at RT for 2 hours, with TLC eluted in 0.1 M citric acid solution at 30, 60 and 120 minutes. Stability was determined by radio-TLC.

5.2   Characterisation

5.2.1   1-dimensional ^{1}HNMR Spectra
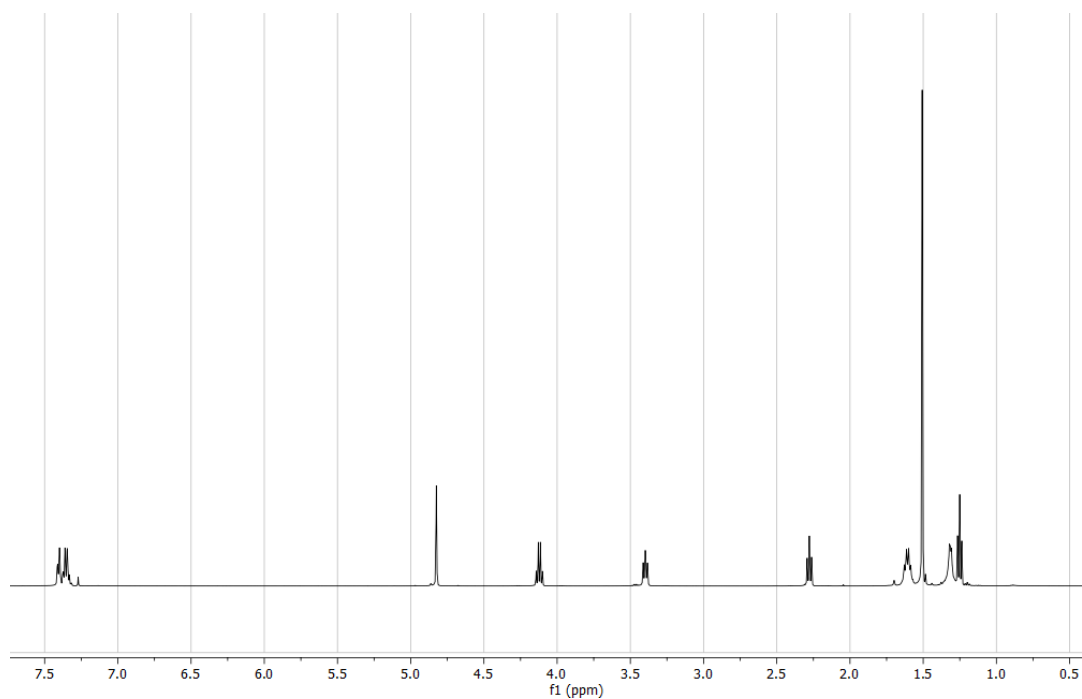
*Spectrum 17: ^{1}HNMR spectrum of compound **1** in CDCl$_3$.*
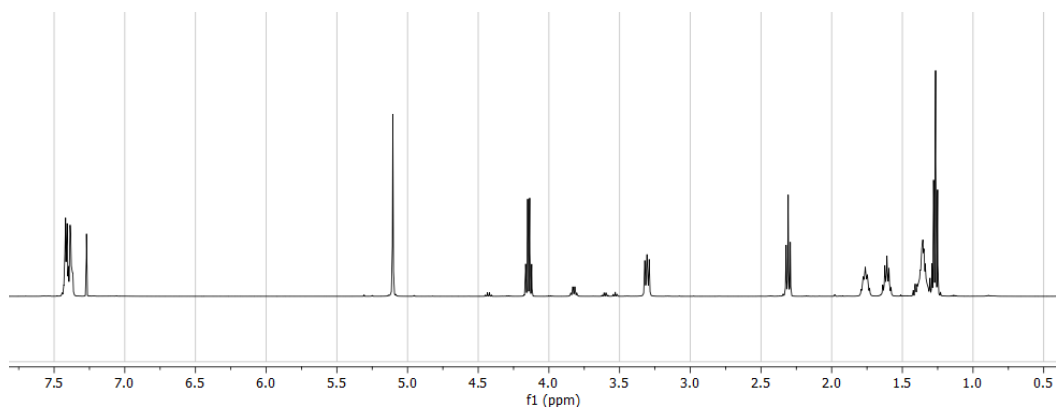
*Spectrum 18: ^{1}HNMR spectrum of compound **2** in CDCl$_3$.*
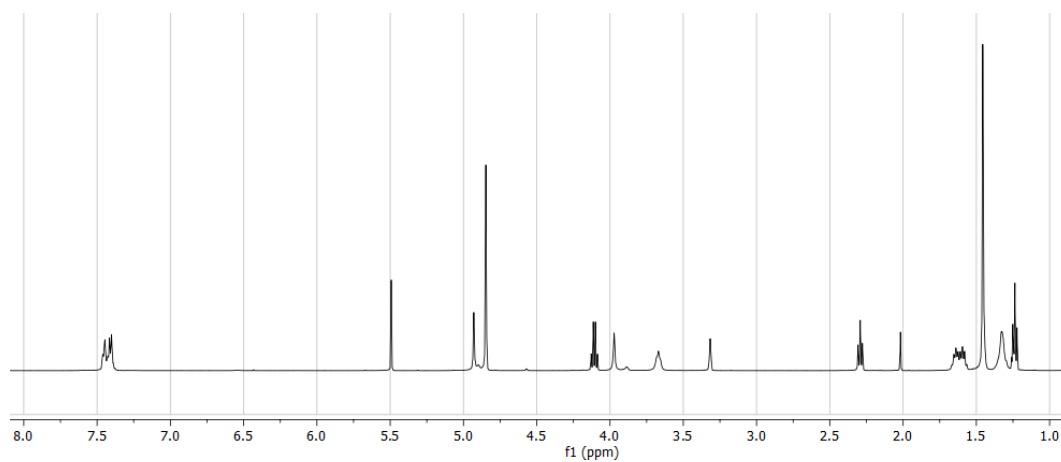
*Spectrum 19: ¹HNMR spectrum of compound **3** in CD₃OD.*
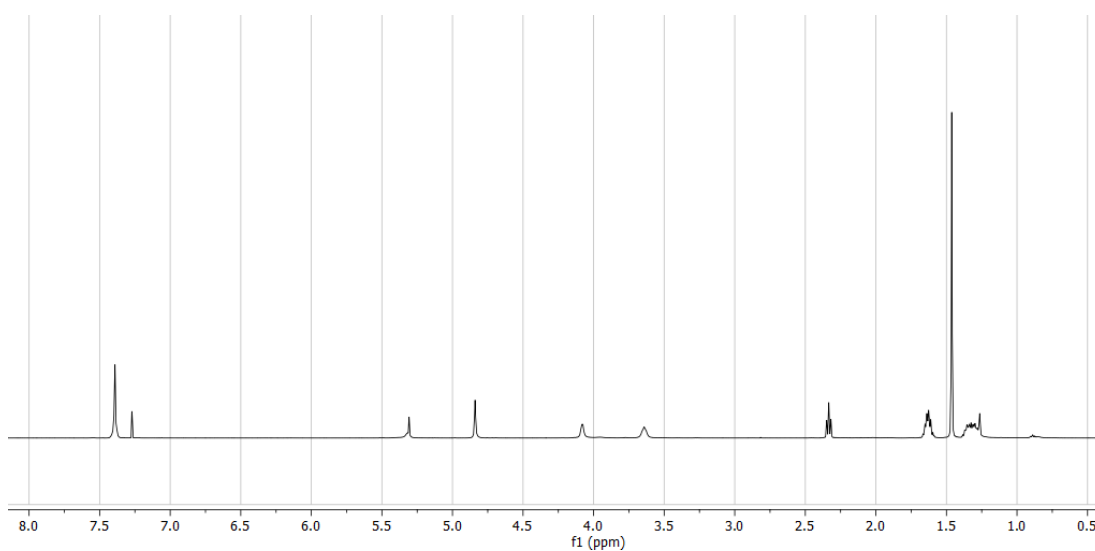
*Spectrum 20: ¹HNMR spectrum of compound **4a** in CDCl₃.*
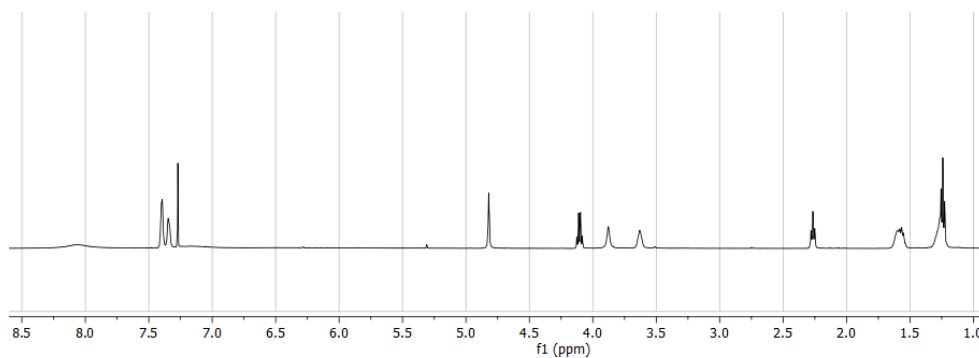
*Spectrum 21: ¹HNMR spectrum of compound **4b** in CDCl₃.*
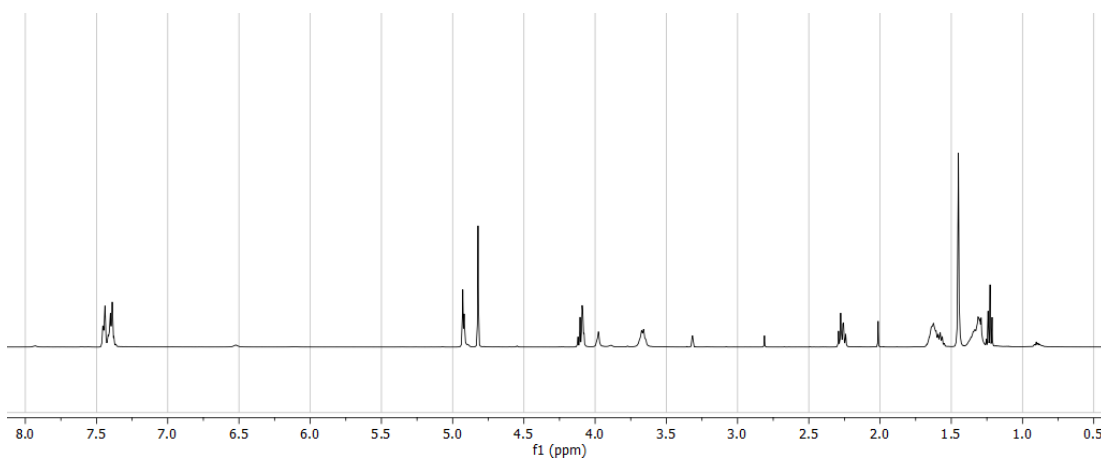
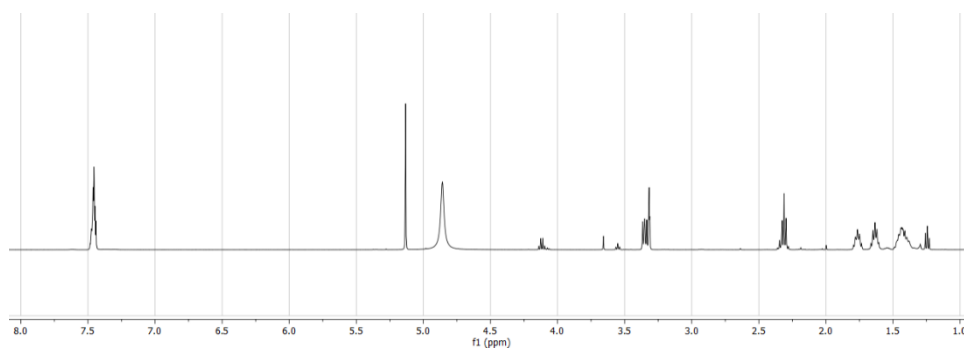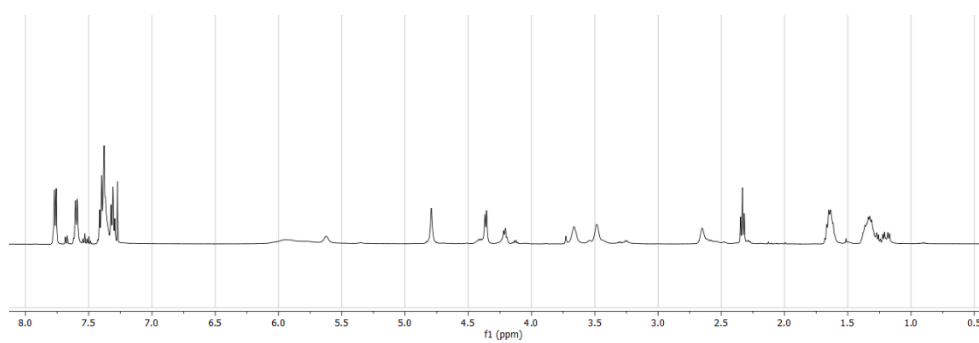*Spectrum 22: ¹HNMR spectrum of compound **5** in CD₃OD.*
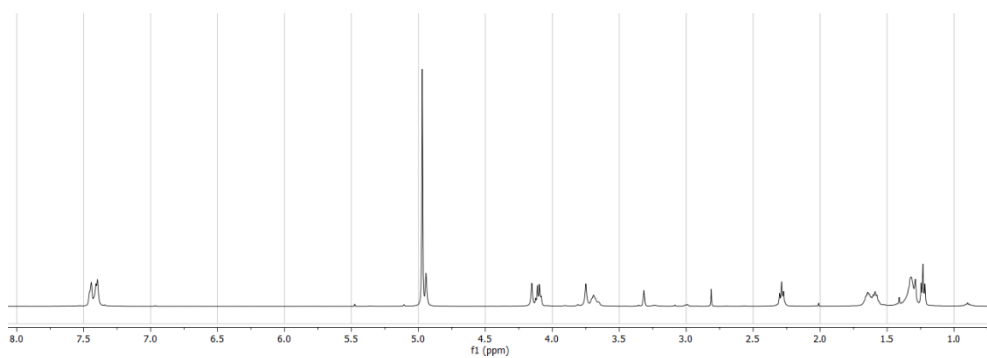
*Spectrum 23: ¹HNMR spectrum of compound **6b** in CD₃OD.*
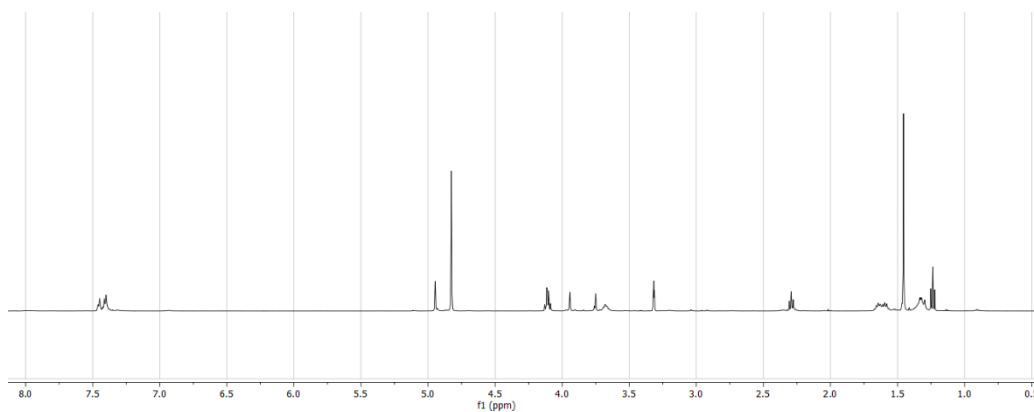
*Spectrum 24: ¹HNMR spectrum of mixture containing compounds **7**, **7.1** and **7.2** in CD₃OD.*
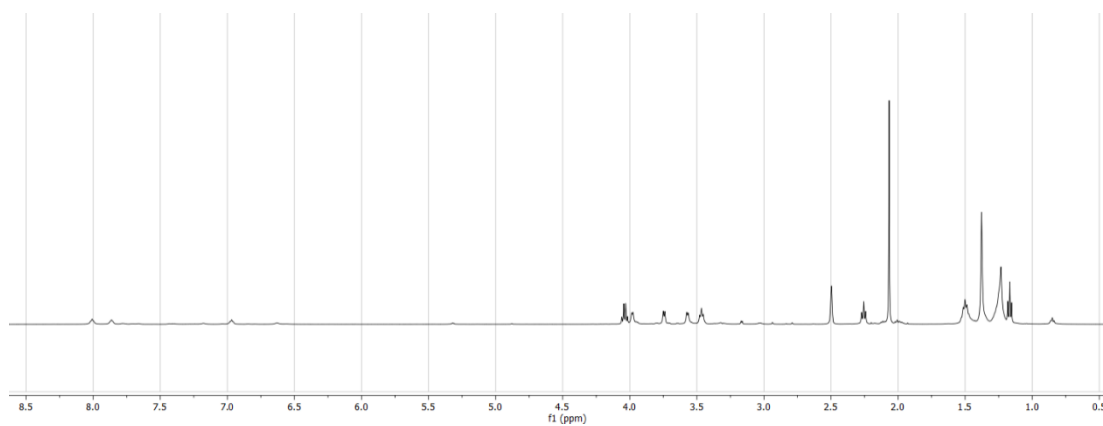
*Spectrum 25: ¹HNMR spectrum of compound **8.1** in DMSO.*

*Spectrum 26: ¹HNMR spectrum of mixture containing compound **11** in CD₃OD.*

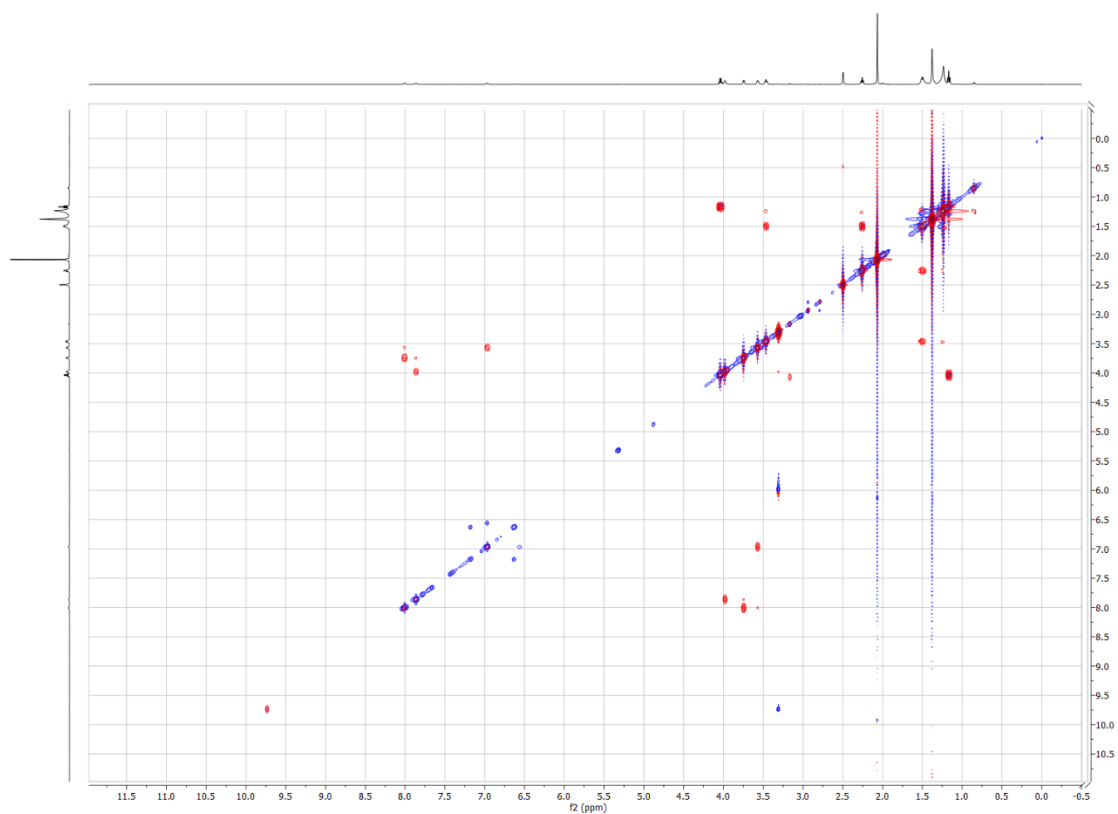*Spectrum 27: ¹HNMR spectrum of compound **12** in CDCl₃.*
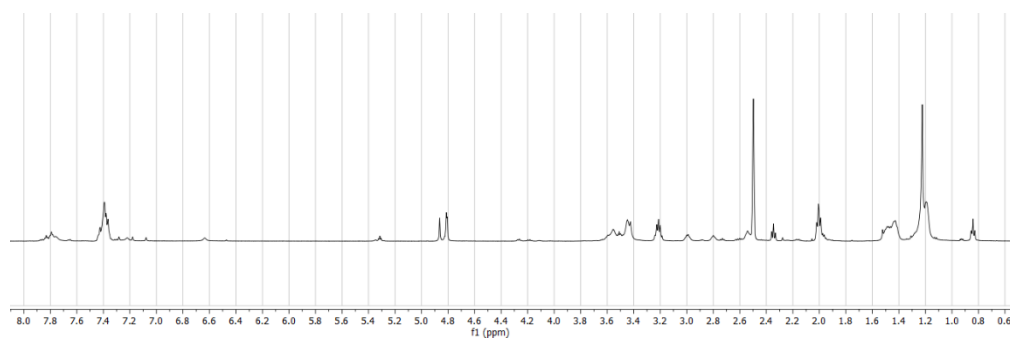
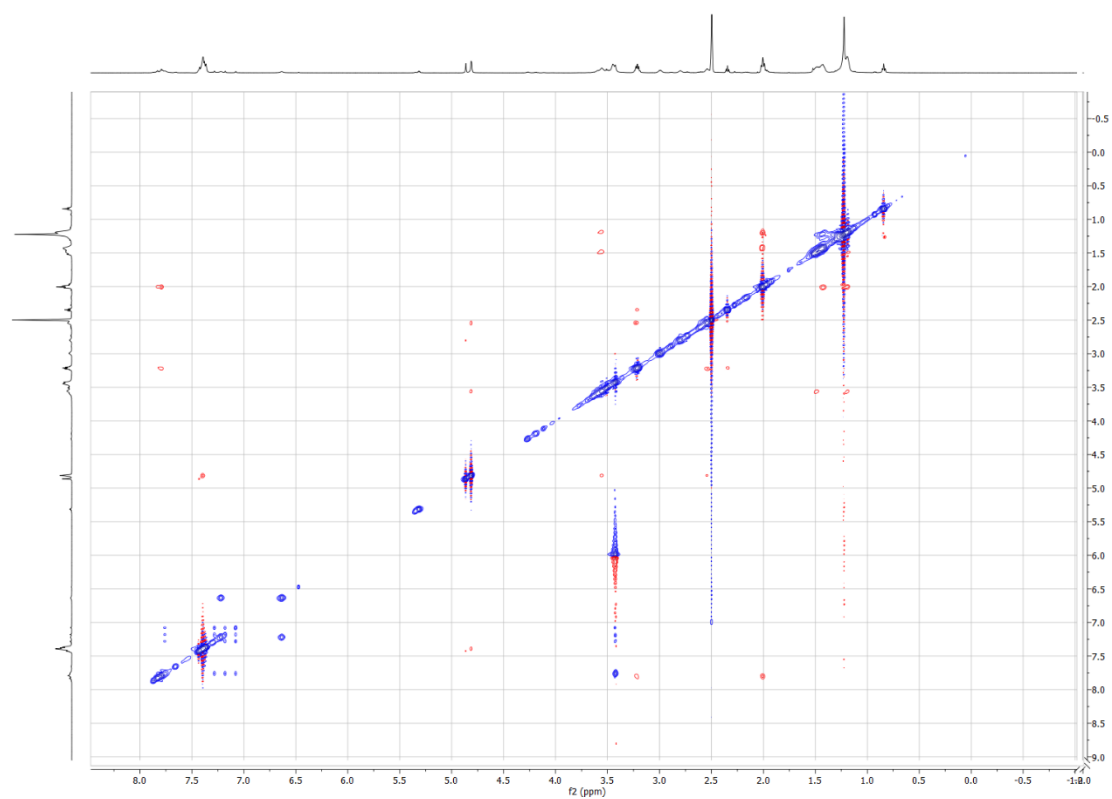*Spectrum 28: ¹HNMR spectrum of compound **14** in DMSO.*
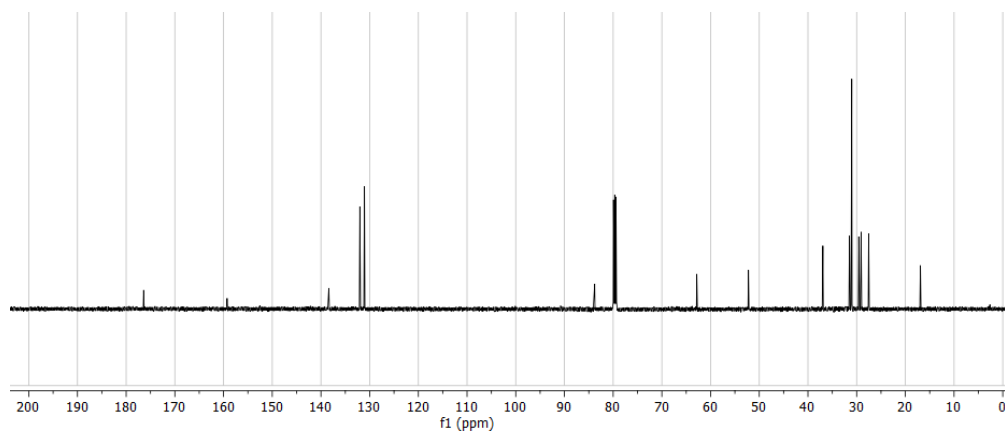
5.2.2 2-dimensional ¹HNMR
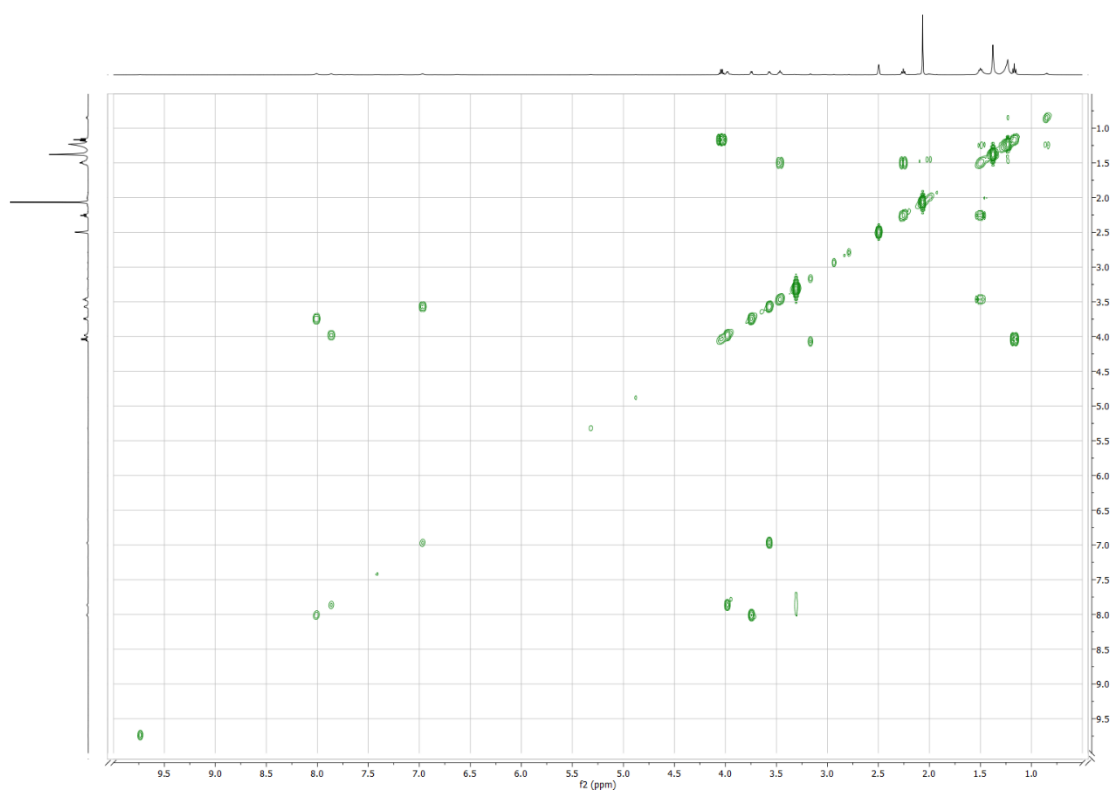
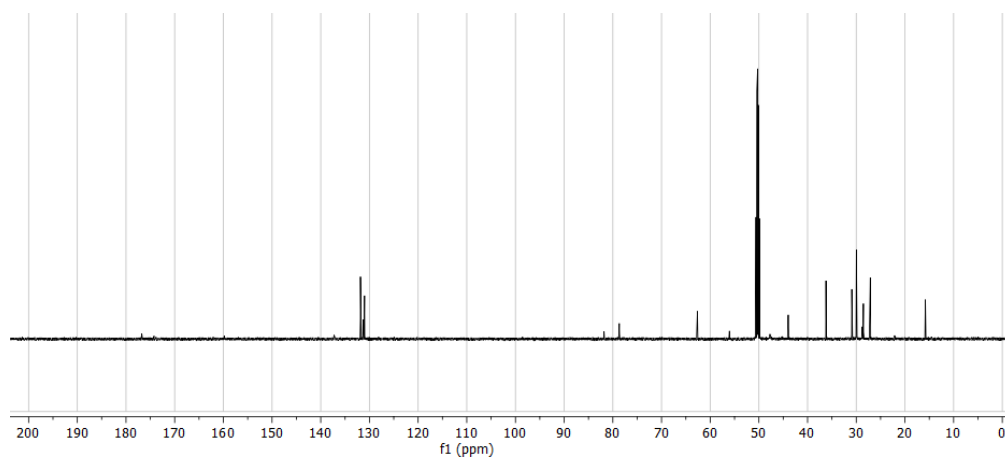*Spectrum 29: COSY ¹HNMR of compound **8.1** in DMSO.*

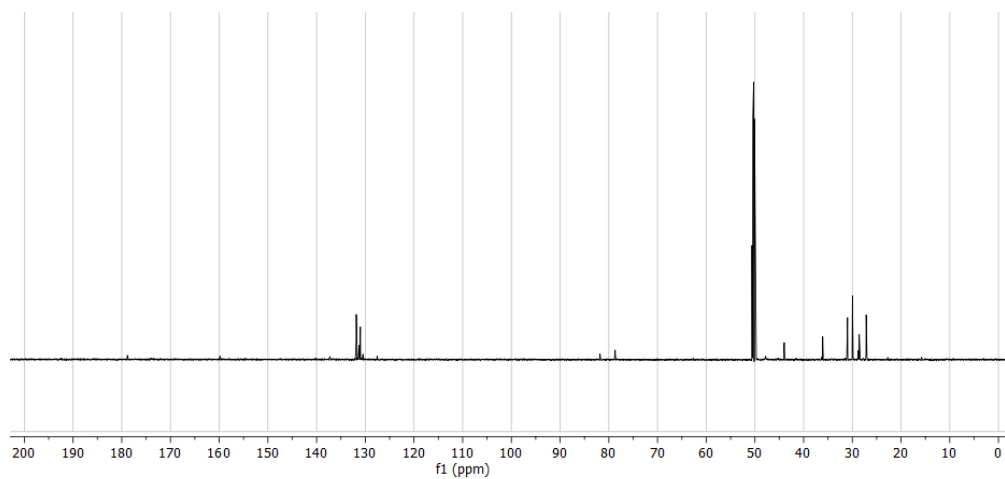*Spectrum 30: ROESY ¹HNMR spectrum of compound **8.1** in DMSO.*

*Spectrum 31: ROESY ¹HNMR spectrum of compound **14** in DMSO.*
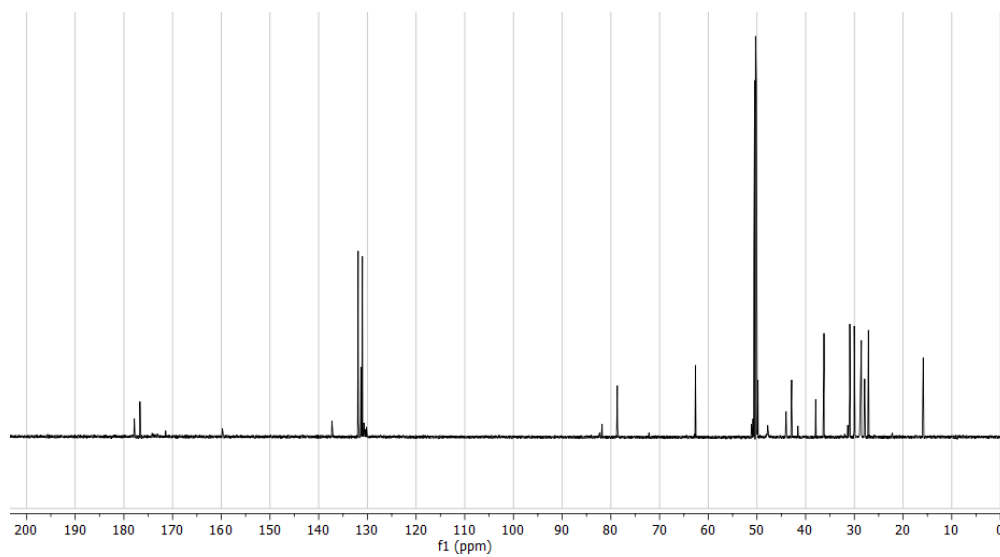
5.2.3 ^{13}CNMR Spectra

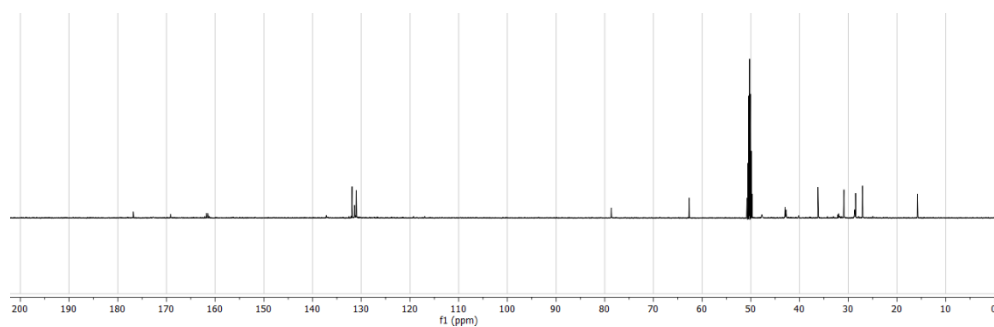*Spectrum 32: ^{13}CNMR spectrum of compound **1** in CDCl$_3$.*

*Spectrum 33: ^{13}CNMR spectrum of compound **3** in CD$_3$OD.*

*Spectrum 34: ^{13}CNMR spectrum of compound **4a** in CD$_3$OD.*
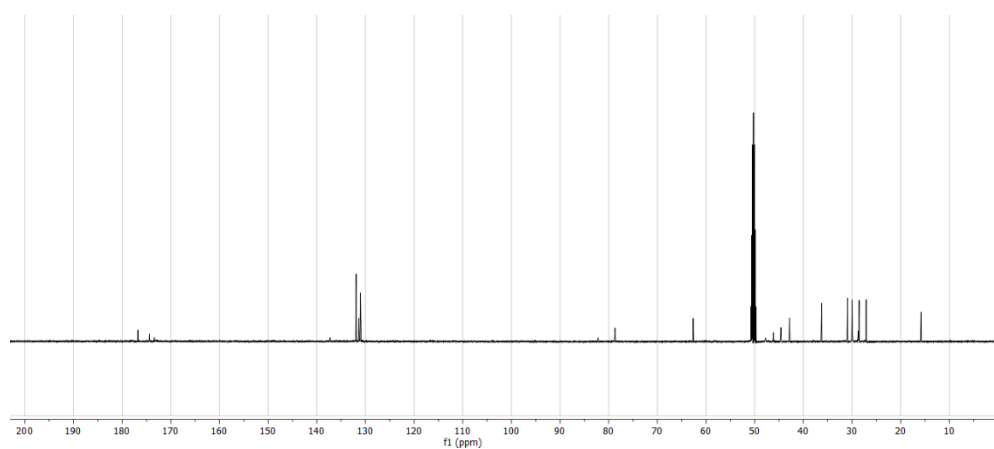
*Spectrum 35: ^{13}CNMR spectrum of compound **5** in CD$_3$OD.*

*Spectrum 36: ^{13}CNMR spectrum of compound **6b** in CD$_3$OD.*

*Spectrum 37: ^{13}CNMR spectrum of mixture containing compounds **7**, **7.1**, and **7.2** in CD$_3$OD.*
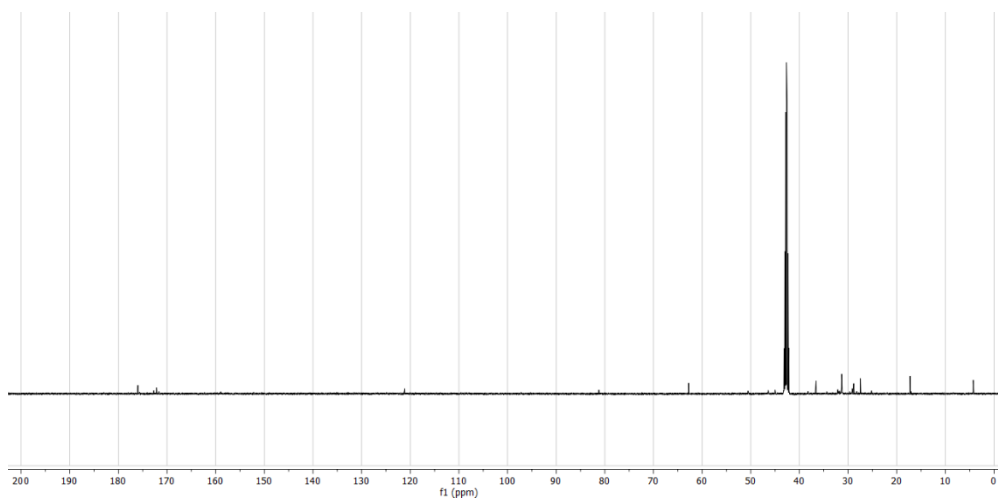
*Spectrum 38: ¹³CNMR spectrum of compound **8.1** in DMSO.*
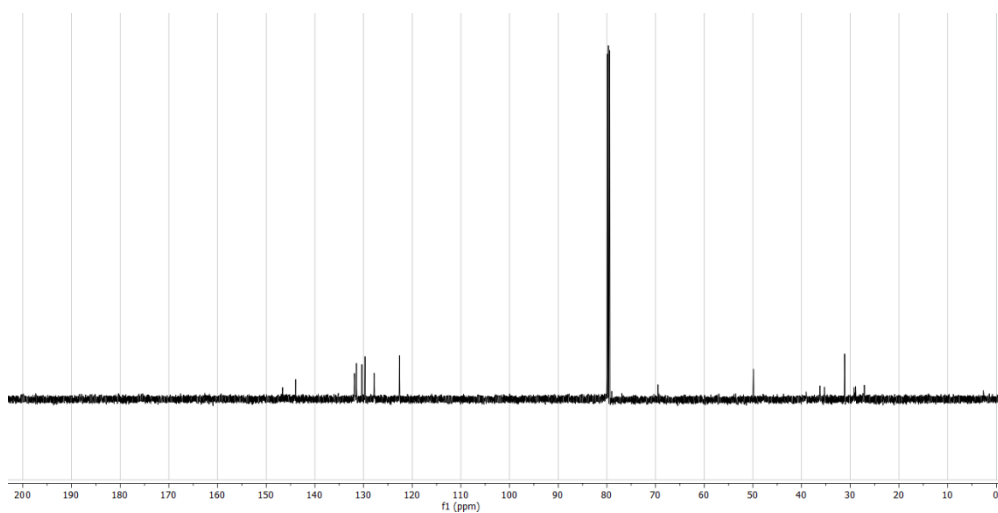
*Spectrum 39: ¹³CNMR spectrum of compound **12** in CDCl₃.*
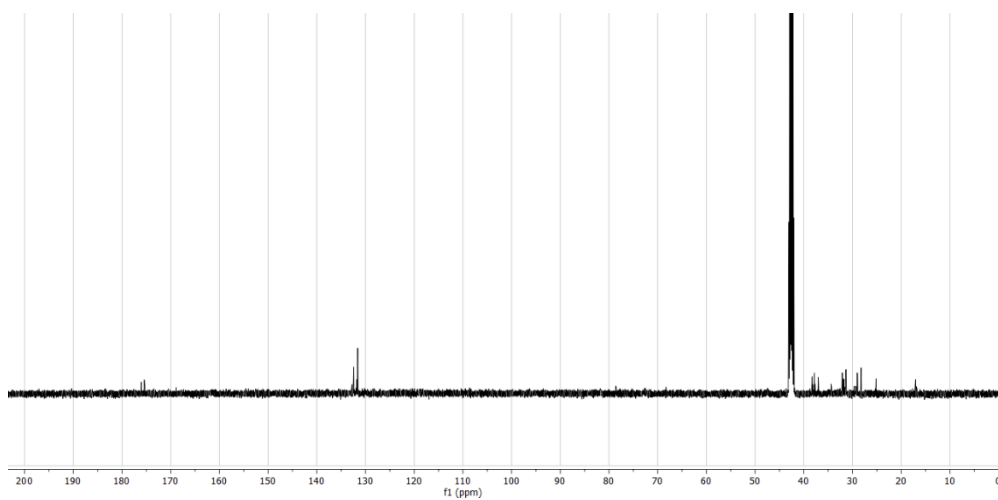
*Spectrum 40: ¹³CNMR spectrum of compound **14** in DMSO.*

5.2.4 HPLC Traces
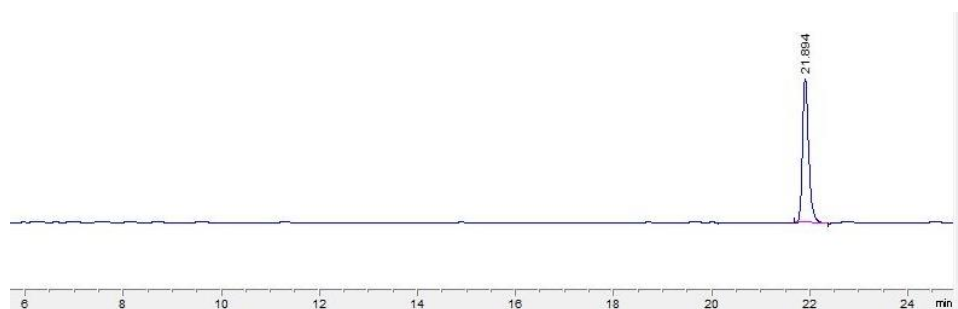
*Spectrum 41: HPLC trace for compound **1**.*
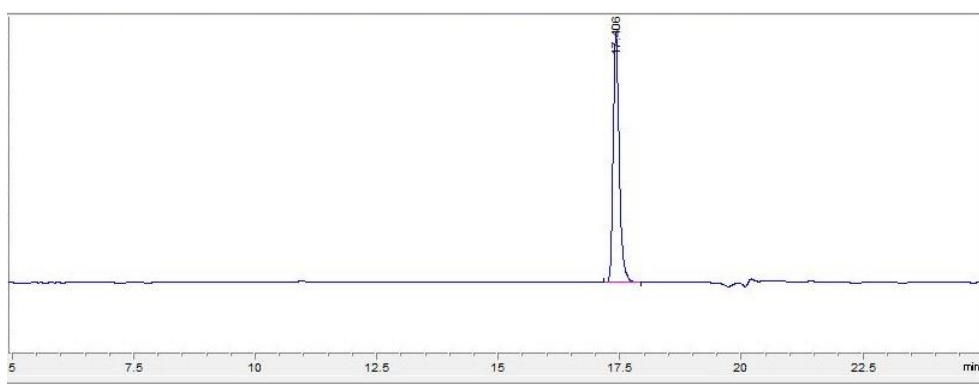
*Spectrum 42: HPLC trace for compound **3**.*
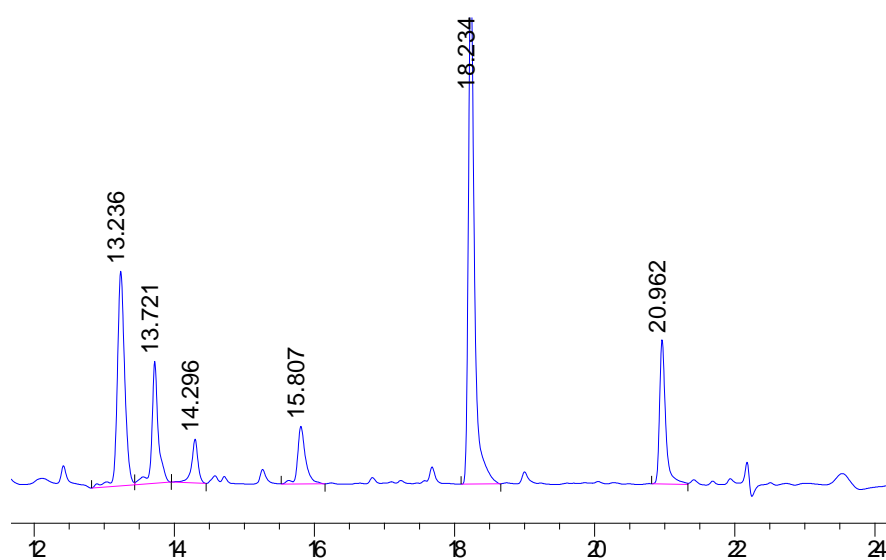
*Spectrum 43: HPLC trace of crude deesterification reaction mixture after 9h. The desired product, compound **4a**, can be seen eluting at 18.2 minutes. Analysis was performed using a gradient of 10-100% MeOH over 15 minutes.*
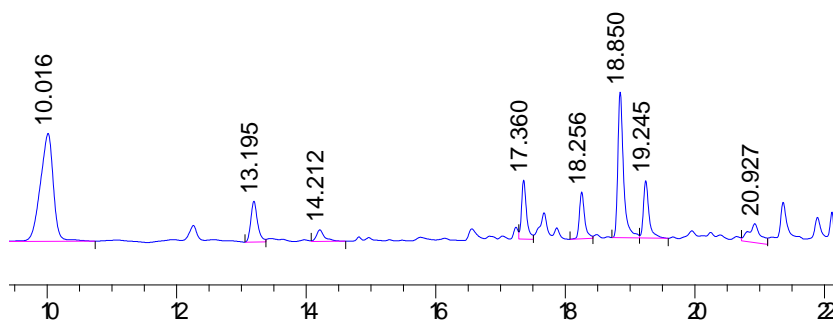
*Spectrum 44: HPLC trace of crude deesterification reaction mixture after 21h. Compound **4a** can be seen eluting at roughly 18.3 minutes. Analysis was performed using a gradient of 10-100% MeOH over 15 minutes.*
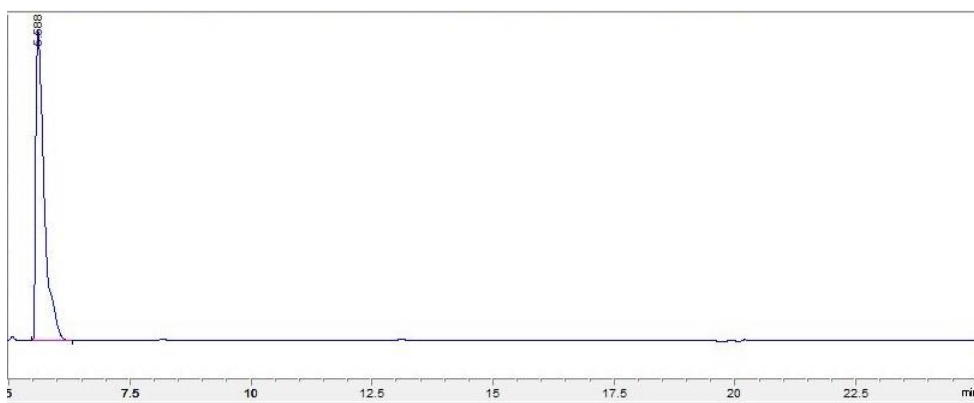
*Spectrum 45: HPLC trace for compound **4b.***
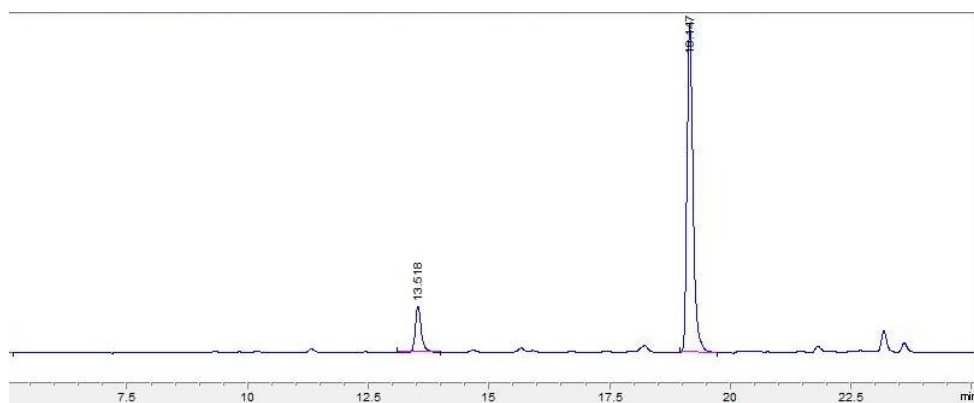
*Spectrum 46: HPLC trace for compound **5**. Analysis was performed using a gradient of 10-100% MeOH over 15 minutes.*
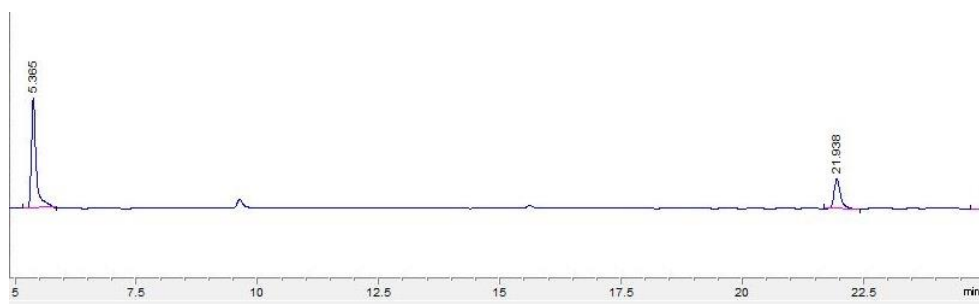
*Spectrum 47: HPLC trace of compound **6b**.*
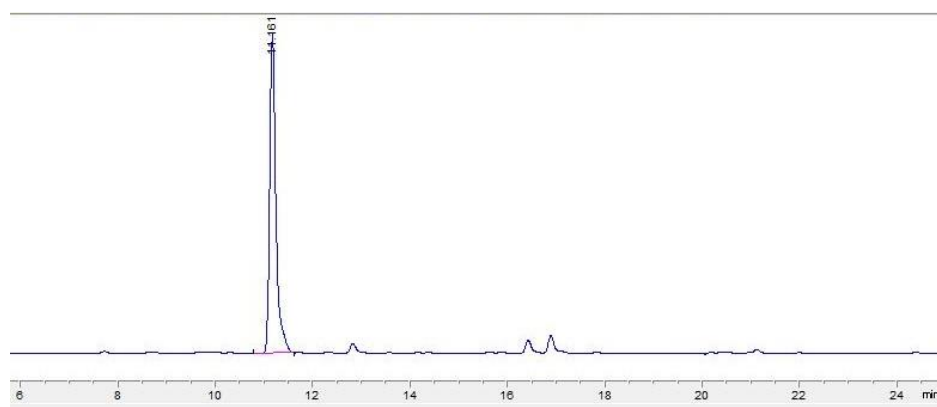
*Spectrum 48: HPLC trace of mixture containing compounds **7**, **7.1**, and **7.2**.*
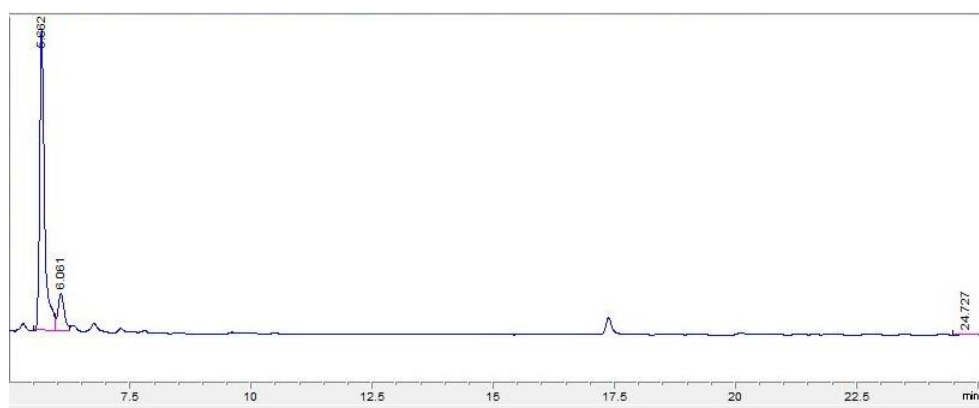
*Spectrum 49: HPLC trace of compound **8.1**.*

5.2.5   HRMS Spectra
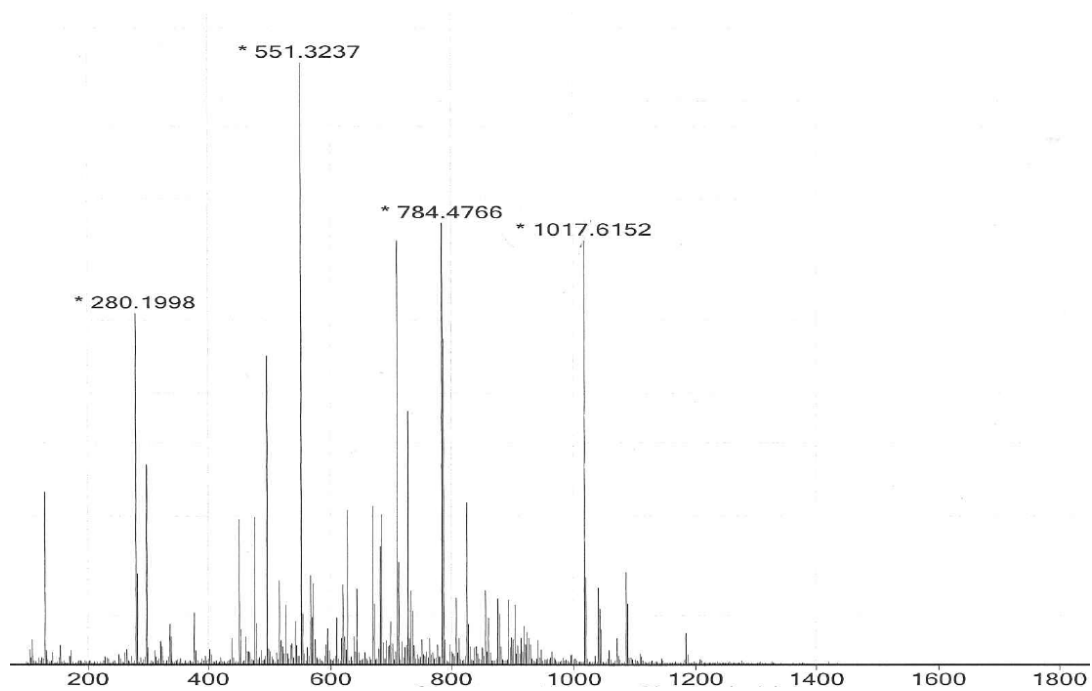
*Spectrum 50: HRMS spectrum of sample containing compounds **7**, **7.1**, and **7.2**.*

References

1.   AIHW, Cancer in Australia 2017. Australian Institute of Health and Welfare, Ed. 2017.

2.   National Cancer Control Indicators, National cancer stage at diagnosis data. Cancer Australia, Ed. Cancer Australia: Canberra, Australia, 2018.

3.   National Cancer Institute, Cancer Staging. U.S. Department of Health and Human Services, Ed. National Cancer Institute,: 2015; Vol. 2018.

4.   Dasari, S.; Tchounwou, P. B., Cisplatin in cancer therapy: molecular mechanisms of action. *Eur J Pharmacol* **2014,** *740*, 364-78.

5.   Begg, A. C.; Stewart, F. A.; Vens, C., Strategies to improve radiotherapy with targeted drugs. *Nature Reviews Cancer* **2011,** *11*, 239.

6.   Chang, S. S., Overview of prostate-specific membrane antigen. *Rev Urol* **2004,** *6 Suppl 10* (10), S13-8.

7.   van de Watering, F. C.; Rijpkema, M.; Perk, L.; Brinkmann, U.; Oyen, W. J.; Boerman, O. C., Zirconium-89 labeled antibodies: a new tool for molecular imaging in cancer patients. *Biomed Res Int* **2014,** *2014*, 203601.

8.   Gambhir, S. S., Molecular imaging of cancer with positron emission tomography. *Nat Rev Cancer* **2002,** *2* (9), 683-93.

9.   McInnes, L. E.; Rudd, S. E.; Donnelly, P. S., Copper, gallium and zirconium positron emission tomography imaging agents: The importance of metal ion speciation. *Coordination Chemistry Reviews* **2017,** *352*, 499-516.

10. National Research Council (US) and Institute of Medicine (US) Committee on the Mathematics and Physics of Emerging Dynamic Biomedical Imaging, Chapter 6: Positron Emission Tomography. In *Mathematics and Physics of Emerging Biochemical Imaging*, National Academies Press (US): 1996.

11. Dilworth, J. R.; Pascu, S. I., The chemistry of PET imaging with zirconium-89. *Chem Soc Rev* **2018,** *47* (8), 2554-71.

12. Pham, L. V.; Bryant, J. L.; Yang, D.; Ford, R. J., Theranostic Approaches for Pathway-Activated Systems in Oncology. In *Personalized Pathway-Activated Systems Imaging in Oncology: Principal and Instrumentation*, Inoue, T.; Yang, D.; Huang, G., Eds. Springer Singapore: Singapore, 2017; pp 17-42.

13. Verel, I.; Visser, G. W.; Boellaard, R.; Stigter-van Walsum, M.; Snow, G. B.; van Dongen, G. A., 89Zr immuno-PET: comprehensive procedures for the production of 89Zr-labeled monoclonal antibodies. *J Nucl Med* **2003,** *44* (8), 1271-81.

14. Perk, L. R.; Stigter-van Walsum, M.; Visser, G. W.; Kloet, R. W.; Vosjan, M. J.; Leemans, C. R.; Giaccone, G.; Albano, R.; Comoglio, P. M.; van Dongen, G. A., Quantitative PET imaging of Met-expressing human cancer xenografts with 89Zr-labelled monoclonal antibody DN30. *Eur J Nucl Med Mol Imaging* **2008,** *35* (10), 1857-67.

15. Severin, G. W.; Engle, J. W.; Barnhart, T. E.; Nickles, R. J., 89Zr radiochemistry for positron emission tomography. *Med Chem* **2011,** *7* (5), 389-94.

16. Holland, J. P.; Sheh, Y.; Lewis, J. S., Standardized methods for the production of high specific-activity zirconium-89. *Nucl Med Biol* **2009,** *36* (7), 729-39.

17. Yadav, M. P.; Ballal, S.; Tripathi, M.; Damle, N. A.; Sahoo, R. K.; Seth, A.; Bal, C., (177)Lu-DKFZ-PSMA-617 therapy in metastatic castration resistant prostate cancer: safety, efficacy, and quality of life assessment. *Eur J Nucl Med Mol Imaging* **2017,** *44* (1), 81-91.

18.   Deri, M. A.; Zeglis, B. M.; Francesconi, L. C.; Lewis, J. S., PET imaging with (8)(9)Zr: from radiochemistry to the clinic. *Nucl Med Biol* **2013,** *40* (1), 3-14.

19.   Meijs, W. E.; Herscheid, J. D. M.; Haisma, H. J.; Pinedo, H. M., Evaluation of Desferal as a Bifunctional Chelating Agent for Labeling Antibodies with Zr-89. *Applied Radiation and Isotopes* **1992,** *43* (12), 1443-7.

20.   Meijs, W. E.; Herscheid, J. D. M.; Haisma, H. J.; Wijbrandts, R.; van Langevelde, F.; van Leuffen, P. J.; Mooy, R.; Pinedo, H. M., Production of Highly Pure No-carrier Added 89Zr for the Labelling of Antibodies with a Positron Emitter. *Applied Radiation and Isotopes* **1994,** *45* (12), 1143-7.

21.   O'Hara, M. J.; Murray, N. J.; Carter, J. C.; Kellogg, C. M.; Link, J. M., Hydroxamate column-based purification of zirconium-89 ((89)Zr) using an automated fluidic platform. *Appl Radiat Isot* **2018,** *132*, 85-94.

22.   Lin, M.; Mukhopadhyay, U.; Waligorski, G. J.; Balatoni, J. A.; Gonzalez-Lepera, C., Semi-automated production of (8)(9)Zr-oxalate/(8)(9)Zr-chloride and the potential of (8)(9)Zr-chloride in radiopharmaceutical compounding. *Appl Radiat Isot* **2016,** *107*, 317-322.

23.   Guérard, F.; Lee, Y. S.; Tripier, R.; Szajek, L. P.; Deschamps, J. R.; Brechbiel, M. W., Investigation of Zr(IV) and 89Zr(IV) complexation with hydroxamates: progress towards designing a better chelator than desferrioxamine B for immuno-PET imaging. *Chem. Commun.* **2013,** *49*, 1002-4.

24.   Ghosh, S.; Sharma, A.; Talukder, G., Zirconium. An abnormal trace element in biology. *Biol Trace Elem Res* **1992,** *35* (3), 247-71.

25.   Codd, R.; Richardson-Sanchez, T.; Telfer, T. J.; Gotsbacher, M. P., Advances in the Chemical Biology of Desferrioxamine B. *ACS Chem Biol* **2018,** *13* (1), 11-25.

26. Hider, R. C.; Kong, X., Chemistry and biology of siderophores. *Nat Prod Rep* **2010,** *27* (5), 637-57.

27. Green, M. A.; Welch, M. J., Gallium Radiopharmaceutical Chemistry. *Nucl. Med. Biol.* **1989,** *16* (5), 435-48.

28. Govindan, S. V.; Michel, R. B.; Griffiths, G. L.; Goldenberg, D. M.; Mattes, M. J., Deferoxamine as a chelator for 67Ga in the preparation of antibody conjugates. *Nucl Med Biol* **2005,** *32* (5), 513-9.

29. Petrik, M.; Haas, H.; Schrettl, M.; Helbok, A.; Blatzer, M.; Decristoforo, C., In vitro and in vivo evaluation of selected 68Ga-siderophores for infection imaging. *Nucl Med Biol* **2012,** *39* (3), 361-9.

30. Petrik, M.; Zhai, C.; Novy, Z.; Urbanek, L.; Haas, H.; Decristoforo, C., In Vitro and In Vivo Comparison of Selected Ga-68 and Zr-89 Labelled Siderophores. *Mol Imaging Biol* **2016,** *18* (3), 344-52.

31. Price, T. W.; Greenman, J.; Stasiuk, G. J., Current advances in ligand design for inorganic positron emission tomography tracers (68)Ga, (64)Cu, (89)Zr and (44)Sc. *Dalton Trans* **2016,** *45* (40), 15702-24.

32. Agrawal, Y. K., Hydroxamic Acids and Their Metal Complexes. *Russian Chemical Reviews* **1979,** *48* (10), 948-63.

33. Abou, D. S.; Ku, T.; Smith-Jones, P. M., In vivo biodistribution and accumulation of 89Zr in mice. *Nucl Med Biol* **2011,** *38* (5), 675-81.

34. Holland, J. P.; Divilov, V.; Bander, N. H.; Smith-Jones, P. M.; Larson, S. M.; Lewis, J. S., 89Zr-DFO-J591 for immunoPET of prostate-specific membrane antigen expression in vivo. *J Nucl Med* **2010,** *51* (8), 1293-300.

35. Meijs, W. E.; Haisma, H. J.; Van der Schors, R.; Wijbrandts, R.; Van den Oever, K.; Klok, R. P.; Pinedo, H. M.; Herscheid, J. D., A facile method for the labeling of proteins with zirconium isotopes. *Nucl Med Biol* **1996,** *23* (4), 439-48.

36.   Meijs, W. E.; Haisma, H. J.; Klok, R. P.; van Gog, F. B.; Kievit, E.; Pinedo, H. M.; Herscheid, J. D., Zirconium-Labeled Monoclonal Antibodies and Their Distrobution in Tumour-Bearing Nude Mice. *J Nucl Med* **1997,** *38* (1), 112-118.

37.   Lewis, M. R.; Shively, J. E., Maleimidocysteineamido-DOTA Derivatives: New Reagents for Radiometal Chelate Conjugation to Antibody Sulfhydryl Groups Undergo pH-Dependent Cleavage Reactions. *Bioconjug Chem* **1998,** *9*, 72 - 86.

38.   Holland, J. P.; Evans, M. J.; Rice, S. L.; Wongvipat, J.; Sawyers, C. L.; Lewis, J. S., Annotating MYC status with 89Zr-transferrin imaging. *Nat Med* **2012,** *18* (10), 1586-91.

39.   Evans, M. J.; Holland, J. P.; Rice, S. L.; Doran, M. G.; Cheal, S. M.; Campos, C.; Carlin, S. D.; Mellinghoff, I. K.; Sawyers, C. L.; Lewis, J. S., Imaging tumor burden in the brain with 89Zr-transferrin. *J Nucl Med* **2013,** *54* (1), 90-5.

40.   Perk, L. R.; Vosjan, M. J.; Visser, G. W.; Budde, M.; Jurek, P.; Kiefer, G. E.; van Dongen, G. A., p-Isothiocyanatobenzyl-desferrioxamine: a new bifunctional chelate for facile radiolabeling of monoclonal antibodies with zirconium-89 for immuno-PET imaging. *Eur J Nucl Med Mol Imaging* **2010,** *37* (2), 250-9.

41.   Vosjan, M. J.; Perk, L. R.; Visser, G. W.; Budde, M.; Jurek, P.; Kiefer, G. E.; van Dongen, G. A., Conjugation and radiolabeling of monoclonal antibodies with zirconium-89 for PET imaging using the bifunctional chelate p-isothiocyanatobenzyl-desferrioxamine. *Nat Protoc* **2010,** *5* (4), 739-43.

42.   Sugyo, A.; Tsuji, A. B.; Sudo, H.; Nagatsu, K.; Koizumi, M.; Ukai, Y.; Kurosawa, G.; Zhang, M. R.; Kurosawa, Y.; Saga, T., Evaluation of (89)Zr-labeled human anti-CD147 monoclonal antibody as a positron emission tomography probe in a mouse model of pancreatic cancer. *PLoS One* **2013,** *8* (4), e61230.

43.   Heuveling, D. A.; Visser, G. W.; Baclayon, M.; Roos, W. H.; Wuite, G. J.; Hoekstra, O. S.; Leemans, C. R.; de Bree, R.; van Dongen, G. A., 89Zr-nanocolloidal albumin-based PET/CT lymphoscintigraphy for sentinel node detection in head and neck cancer: preclinical results. *J Nucl Med* **2011,** *52* (10), 1580-4.

44.   Rudd, S. E.; Roselt, P.; Cullinane, C.; Hicks, R. J.; Donnelly, P. S., A desferrioxamine B squaramide ester for the incorporation of zirconium-89 into antibodies. *Chem Commun (Camb)* **2016,** *52* (80), 11889-92.

45.   Zeglis, B. M.; Mohindra, P.; Weissmann, G. I.; Divilov, V.; Hilderbrand, S. A.; Weissleder, R.; Lewis, J. S., Modular strategy for the construction of radiometalated antibodies for positron emission tomography based on inverse electron demand Diels-Alder click chemistry. *Bioconjug Chem* **2011,** *22* (10), 2048-59.

46.   Tinianow, J. N.; Gill, H. S.; Ogasawara, A.; Flores, J. E.; Vanderbilt, A. N.; Luis, E.; Vandlen, R.; Darwish, M.; Junutula, J. R.; Williams, S. P.; Marik, J., Site-specifically 89Zr-labeled monoclonal antibodies for ImmunoPET. *Nucl Med Biol* **2010,** *37* (3), 289-97.

47.   Gao, F.; Ieritano, C.; Chen, K. T.; Dias, G. M.; Rousseau, J.; Benard, F.; Seimbille, Y., Two bifunctional desferrioxamine chelators for bioorthogonal labeling of biovectors with zirconium-89. *Org Biomol Chem* **2018,** *16* (28), 5102-06.

48.   Boerjesson, P. K.; Jauw, Y. W.; Boellaard, R.; de Bree, R.; Comans, E. F.; Roos, J. C.; Castelijns, J. A.; Vosjan, M. J.; Kummer, J. A.; Leemans, C. R.; Lammertsma, A. A.; van Dongen, G. A., Performance of immuno-positron emission tomography with zirconium-89-labeled chimeric monoclonal antibody U36 in the detection of lymph node metastases in head and neck cancer patients. *Clin Cancer Res* **2006,** *12* (7.1), 2133-40.

49.   Perk, L. R.; Visser, O. J.; Stigter-van Walsum, M.; Vosjan, M. J. W. D.; Visser, G. W. M.; Zijlstra, J. M.; Huijgens, P. C.; van Dongen, G. A. M. S., Preparation and evaluation of 89Zr-Zevalin for monitoring

of 90Y-Zevalin biodistribution with positron emission tomography. *European Journal of Nuclear Medicine and Molecular Imaging* **2006,** *33* (11), 1337-45.

50.   Bahce, I.; Huisman, M. C.; Verwer, E. E.; Ooijevaar, R.; Boutkourt, F.; Vugts, D. J.; van Dongen, G. A.; Boellaard, R.; Smit, E. F., Pilot study of (89)Zr-bevacizumab positron emission tomography in patients with advanced non-small cell lung cancer. *EJNMMI Res* **2014,** *4* (1), 35.

51.   Osborne, J. R.; Green, D. A.; Spratt, D. E.; Lyashchenko, S.; Fareedy, S. B.; Robinson, B. D.; Beattie, B. J.; Jain, M.; Lewis, J. S.; Christos, P.; Larson, S. M.; Bander, N. H.; Scherr, D. S., A prospective pilot study of (89)Zr-J591/prostate specific membrane antigen positron emission tomography in men with localized prostate cancer undergoing radical prostatectomy. *J Urol* **2014,** *191* (5), 1439-45.

52.   Bruijnen, S.; Tsang-A-Sjoe, M.; Raterman, H.; Ramwadhdoebe, T.; Vugts, D.; van Dongen, G.; Huisman, M.; Hoekstra, O.; Tak, P.-P.; Voskuyl, A.; van der Laken, C., B-cell imaging with zirconium-89 labelled rituximab PET-CT at baseline is associated with therapeutic response 24 weeks after initiation of rituximab treatment in rheumatoid arthritis patients. *Arthritis Research & Therapy* **2016,** *18* (1), 266.

53.   Hagens, M. H.; Killestein, J.; Yaqub, M. M.; van Dongen, G. A.; Lammertsma, A. A.; Barkhof, F.; van Berckel, B. N., Cerebral rituximab uptake in multiple sclerosis: A (89)Zr-immunoPET pilot study. *Mult Scler* **2018,** *24* (4), 543-5.

54.   Dijkers, E. C.; Oude Munnink, T. H.; Kosterink, J. G.; Brouwers, A. H.; Jager, P. L.; de Jong, J. R.; van Dongen, G. A.; Schroder, C. P.; Lub-de Hooge, M. N.; de Vries, E. G., Biodistribution of 89Zr-trastuzumab and PET imaging of HER2-positive lesions in patients with metastatic breast cancer. *Clin Pharmacol Ther* **2010,** *87* (5), 586-92.

55.   Bhatt, N. B.; Pandya, D. N.; Wadas, T. J., Recent Advances in Zirconium-89 Chelator Development. *Molecules* **2018,** *23* (3).

56.   Ma, M. T.; Meszaros, L. K.; Paterson, B. M.; Berry, D. J.; Cooper, M. S.; Ma, Y.; Hider, R. C.; Blower, P. J., Tripodal tris(hydroxypyridinone) ligands for immunoconjugate PET imaging with (89)Zr(4+): comparison with desferrioxamine-B. *Dalton Trans* **2015,** *44* (11), 4884-900.

57.   Patra, M.; Bauman, A.; Mari, C.; Fischer, C. A.; Blacque, O.; Haussinger, D.; Gasser, G.; Mindt, T. L., An octadentate bifunctional chelating agent for the development of stable zirconium-89 based molecular imaging probes. *Chem Commun (Camb)* **2014,** *50* (78), 11523-5.

58.   Briand, M.; Aulsebrook, M. L.; Mindt, T. L.; Gasser, G., A solid phase-assisted approach for the facile synthesis of a highly water-soluble zirconium-89 chelator for radiopharmaceutical development. *Dalton Trans* **2017,** *46* (47), 16387-9.

59.   Richardson-Sanchez, T.; Tieu, W.; Gotsbacher, M. P.; Telfer, T. J.; Codd, R., Exploiting the biosynthetic machinery of Streptomyces pilosus to engineer a water-soluble zirconium(iv) chelator. *Org Biomol Chem* **2017,** *15* (27), 5719-30.

60.   Allott, L.; Da Pieve, C.; Meyers, J.; Spinks, T.; Ciobota, D. M.; Kramer-Marek, G.; Smith, G., Evaluation of DFO-HOPO as an octadentate chelator for zirconium-89. *Chem Commun (Camb)* **2017,** *53* (61), 8529-32.

61.   Rousseau, J.; Zhang, Z.; Dias, G. M.; Zhang, C.; Colpo, N.; Benard, F.; Lin, K. S., Design, synthesis and evaluation of novel bifunctional tetrahydroxamate chelators for PET imaging of (89)Zr-labeled antibodies. *Bioorg Med Chem Lett* **2017,** *27* (4), 708-12.

62.   Vugts, D. J.; Klaver, C.; Sewing, C.; Poot, A. J.; Adamzek, K.; Huegli, S.; Mari, C.; Visser, G. W.; Valverde, I. E.; Gasser, G.; Mindt, T. L.; van Dongen, G. A., Comparison of the octadentate bifunctional chelator DFO*-pPhe-NCS and the clinically used hexadentate bifunctional chelator DFO-pPhe-NCS for (89)Zr-immuno-PET. *Eur J Nucl Med Mol Imaging* **2017,** *44* (2), 286-95.

63.   White, D. L.; Durbin, P. W.; Jeung, N.; Raymond, K. N., Specific sequestering agents for the actinides. 16. Synthesis and initial biological testing of polydentate oxohydroxypyridinecarboxylate ligands. *Journal of Medicinal Chemistry* **1988,** *31* (1), 11-18.

64.   Deri, M. A.; Ponnala, S.; Zeglis, B. M.; Pohl, G.; Dannenberg, J. J.; Lewis, J. S.; Francesconi, L. C., Alternative chelator for (8)(9)Zr radiopharmaceuticals: radiolabeling and evaluation of 3,4,3-(LI-1,2-HOPO). *J Med Chem* **2014,** *57* (11), 4849-60.

65.   Buchwalder, C.; Rodriguez-Rodriguez, C.; Schaffer, P.; Karagiozov, S. K.; Saatchi, K.; Hafeli, U. O., A new tetrapodal 3-hydroxy-4-pyridinone ligand for complexation of (89)zirconium for positron emission tomography (PET) imaging. *Dalton Trans* **2017,** *46* (29), 9654-63.

66.   Deri, M. A.; Ponnala, S.; Kozlowski, P.; Burton-Pye, B. P.; Cicek, H. T.; Hu, C.; Lewis, J. S.; Francesconi, L. C., p-SCN-Bn-HOPO: A Superior Bifunctional Chelator for (89)Zr ImmunoPET. *Bioconjug Chem* **2015,** *26* (12), 2579-91.

67.   Guerard, F.; Lee, Y. S.; Brechbiel, M. W., Rational design, synthesis, and evaluation of tetrahydroxamic acid chelators for stable complexation of zirconium(IV). *Chemistry* **2014,** *20* (19), 5584-91.

68.   Seibold, U.; Wangler, B.; Wangler, C., Rational Design, Development, and Stability Assessment of a Macrocyclic Four-Hydroxamate-Bearing Bifunctional Chelating Agent for (89) Zr. *ChemMedChem* **2017,** *12* (18), 1555-71.

69.   Tieu, W.; Lifa, T.; Katsifis, A.; Codd, R., Octadentate Zirconium(IV)-Loaded Macrocycles with Varied Stoichiometry Assembled From Hydroxamic Acid Monomers using Metal-Templated Synthesis. *Inorg Chem* **2017,** *56* (6), 3719-28.

70. Zhai, C.; Summer, D.; Rangger, C.; Franssen, G. M.; Laverman, P.; Haas, H.; Petrik, M.; Haubner, R.; Decristoforo, C., Novel Bifunctional Cyclic Chelator for (89)Zr Labeling-Radiolabeling and Targeting Properties of RGD Conjugates. *Mol Pharm* **2015,** *12* (6), 2142-50.

71. Summer, D.; Garousi, J.; Oroujeni, M.; Mitran, B.; Andersson, K. G.; Vorobyeva, A.; Lofblom, J.; Orlova, A.; Tolmachev, V.; Decristoforo, C., Cyclic versus Noncyclic Chelating Scaffold for (89)Zr-Labeled ZEGFR:2377 Affibody Bioconjugates Targeting Epidermal Growth Factor Receptor Overexpression. *Mol Pharm* **2018,** *15* (1), 175-85.

72. Price, E. W.; Orvig, C., Matching chelators to radiometals for radiopharmaceuticals. *Chem Soc Rev* **2014,** *43* (1), 260-90.

73. Pandya, D. N.; Bhatt, N.; Yuan, H.; Day, C. S.; Ehrmann, B. M.; Wright, M.; Bierbach, U.; Wadas, T. J., Zirconium tetraazamacrocycle complexes display extraordinary stability and provide a new strategy for zirconium-89-based radiopharmaceutical development. *Chem Sci* **2017,** *8* (3), 2309-14.

74. Boros, E.; Holland, J. P.; Kenton, N.; Rotile, N.; Caravan, P., Macrocycle-Based Hydroxamate Ligands for Complexation and Immunoconjugation of (89)Zirconium for Positron Emission Tomography (PET) Imaging. *Chempluschem* **2016,** *81* (3), 274-81.

75. Tinianow, J. N.; Pandya, D. N.; Pailloux, S. L.; Ogasawara, A.; Vanderbilt, A. N.; Gill, H. S.; Williams, S. P.; Wadas, T. J.; Magda, D.; Marik, J., Evaluation of a 3-hydroxypyridin-2-one (2,3-HOPO) Based Macrocyclic Chelator for (89)Zr(4+) and Its Use for ImmunoPET Imaging of HER2 Positive Model of Ovarian Carcinoma in Mice. *Theranostics* **2016,** *6* (4), 511-21.

76. Bartholomä, M. D.; Louie, A. S.; Valliant, J. F.; Zubieta, J., Technetium and Gallium Derived Radiopharmaceuticals: Comparing and Contrasting the Chemistry of Two Important Radiometals for the Molecular Imaging Era. *Chemical Reviews* **2010,** *110* (5), 2903-20.

77.   Food and Drug Administration, FDA approves new diagnostic imaging agent to detect rare neuroendocrine tumors. Administration, U. S. F. a. D., Ed. Silver Spring, MD, 2016.

78.   Hider, R. C.; Hall, A. D., Clinically Useful Chelators of Tripositive Elements. In *Progress in Medicinal Chemistry*, Ellis, G. P.; West, G. B., Eds. Elsevier: 1991; Vol. 28, pp 41-173.

79.   Thanh Luong, H. V.; Liu, J. C., Flotation separation of gallium from aqueous solution – Effects of chemical speciation and solubility. *Separation and Purification Technology* **2014,** *132*, 115-19.

80.   Fani, M.; André, J. P.; Maecke, H. R., 68Ga-PET: a powerful generator-based alternative to cyclotron-based PET radiopharmaceuticals. *Contrast Media & Molecular Imaging* **2008,** *3* (2), 53-63.

81.   Boros, E.; Ferreira, C. L.; Cawthray, J. F.; Price, E. W.; Patrick, B. O.; Wester, D. W.; Adam, M. J.; Orvig, C., Acyclic chelate with ideal properties for (68)Ga PET imaging agent elaboration. *J Am Chem Soc* **2010,** *132* (44), 15726-33.

82.   Boros, E.; Ferreira, C. L.; Yapp, D. T.; Gill, R. K.; Price, E. W.; Adam, M. J.; Orvig, C., RGD conjugates of the H2dedpa scaffold: synthesis, labeling and imaging with 68Ga. *Nucl Med Biol* **2012,** *39* (6), 785-94.

83.   Lifa, T.; Tieu, W.; Hocking, R. K.; Codd, R., Forward and Reverse (Retro) Iron(III) or Gallium(III) Desferrioxamine E and Ring-Expanded Analogues Prepared Using Metal-Templated Synthesis from endo-Hydroxamic Acid Monomers. *Inorg Chem* **2015,** *54* (7), 3573-83.

84.   Pascal, R.; Sola, R., Preservation of the Fmoc protective group under alkaline conditions by using CaCl2. Applications in peptide synthesis. *Tetrahedron Letters* **1998,** *39* (28), 5031-34.

85.   Berthet, M.; Davanier, F.; Dujardin, G.; Martinez, J.; Parrot, I., MgI2 -mediated chemoselective cleavage of protecting groups: an alternative to conventional deprotection methodologies. *Chemistry* **2015,** *21* (31), 11014-6.

86.   Sun, Y. Synthesis of peptides with hydroxamic acid side chain appendages. University of Louisville, Louisville, KY, 2003.

87.   Stark, H.; Sadek, B.; Krause, M.; Huels, A.; Lingneau, X.; Ganellin, C. R.; Arrang, J.; Schwartz, J.; Schunack, W., Novel Histamine H3-Receptor Antagonists with Carbonyl-Substituted 4-(3(Phenoxy)propyl)-1H-imidazole Structures like Ciproxifan and Related Compounds. *J. Med. Chem.* **2000,** *43*, 3988-94.

88.   Kaiser, E.; Bossinger, C. D.; Colescott, R. L.; Olsen, D. B., Color test for terminal prolyl residues in the solid-phase synthesis of peptides. *Analytica Chimica Acta* **1980,** *118* (1), 149-51.

89.   Fulmer, G. R.; Miller, A. J. M.; Sherden, N. H.; Gottlieb, H. E.; Nudelman, A.; Stoltz, B. M.; Bercaw, J. E.; Goldberg, K. I., NMR Chemical Shifts of Trace Impurities: Common Laboratory Solvents, Organics, and Gases in Deuterated Solvents Relevant to the Organometallic Chemist. *Organometallics* **2010,** *29* (9), 2176-79.

90.   Holland, J. P.; Vasdev, N., Charting the mechanism and reactivity of zirconium oxalate with hydroxamate ligands using density functional theory: implications in new chelate design. *Dalton Trans* **2014,** *43* (26), 9872-84.

91.   Michels, T.; Dölling, R.; Haberkorn, U.; Mier, W., Acid-Mediated Prevention of Aspartimide Formation in Solid Phase Peptide Synthesis. *Organic Letters* **2012,** *14* (20), 5218-21.